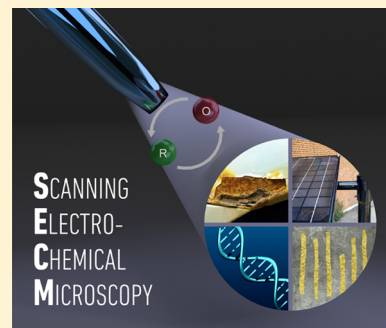


## Scanning Electrochemical Microscopy: A Comprehensive Review of Experimental Parameters from 1989 to 2015

David Polcari, Philippe Dauphin-Ducharme, and Janine Mauzeroll\*

Department of Chemistry, McGill University, 801 Sherbrooke Street West, Montreal, Quebec Canada, H3A 0B8

**ABSTRACT:** Scanning electrochemical microscopy (SECM) is an electroanalytical scanning probe technique capable of imaging substrate topography and local reactivity with high resolution. Since its inception in 1989, it has expanded into a wide variety of research areas including biology, corrosion, energy, kinetics, instrumental development, and surface modification. In the past 25 years, over 1800 peer-reviewed publications have focused on SECM, including several topical reviews. However, these reviews often omit key details, forcing readers to search the literature. In this review, we provide a comprehensive summary of the experimental parameters (e.g., solvents, probes, and mediators) used in all SECM publications since 1989, irrespective of the application. It can be used to rapidly assess experimental possibilities and make an informed decision about experimental design. In other words, it is a practical guide to SECM.



### CONTENTS

1. Introduction	13234
2. Principles of SECM	13234
2.1. Instrumentation	13234
2.2. Modes of Operation	13235
2.2.1. Feedback Mode	13236
2.2.2. Generation/Collection Modes	13236
2.2.3. Redox Competition Mode	13237
2.2.4. Direct Mode	13237
2.2.5. Potentiometric Mode	13237
3. Experimental Design	13237
3.1. Mediators	13237
3.2. Solvents	13244
3.3. Probes	13246
3.3.1. Amperometric Probes	13247
3.3.2. Potentiometric Probes	13247
4. Applications	13247
4.1. Instrumental Development	13249
4.2. Biological	13251
4.3. Enzymes	13252
4.4. Living Cell Studies	13253
4.5. Corrosion	13256
4.6. Energy	13258
4.7. Surface Modification	13259
4.8. Kinetics	13262
5. Summary and Future Perspectives	13263
Author Information	13264
Corresponding Author	13264
Notes	13264
Biographies	13264
References	13264

### 1. INTRODUCTION

Scanning electrochemical microscopy (SECM) was first introduced in 1989 concurrently by the Bard<sup>1</sup> and Engstrom<sup>2</sup> research groups. Twenty-five years later, more than 1800 peer-reviewed articles involving SECM have been published, including several general reviews<sup>3–6</sup> and two monographs.<sup>7,8</sup>

In its simplest form, SECM is a scanning probe technique in which a small scale electrode is scanned across an immersed substrate while recording the current response. This response is dependent on both the surface topography and the electrochemical activity of the substrate. Consequently, using an array of operational modes, a wide variety of substrates and experimental systems can be characterized. The strength of SECM lies in its ability to quantify material flux from a surface with a high spatial and temporal resolution. As a result, it has been used in a variety of application fields (Figure 1).

In this review, we will first describe the fundamentals of SECM, including the required instrumentation and the principles of the most frequently used operational modes. Following this basic understanding of SECM principles, we then move toward a comprehensive summary of the critical parameters for any SECM experiment. More specifically, we will discuss in detail redox mediators, probes, and solvent systems that have been used in SECM experiments since 1989. Each of these parameters has been summarized in exhaustive tables for easy reference, and provide an ideal overview of the field. Finally, we will discuss recent applications of SECM, with an emphasis on the last five years (2009–2015).

**Received:** February 1, 2016

**Published:** October 13, 2016

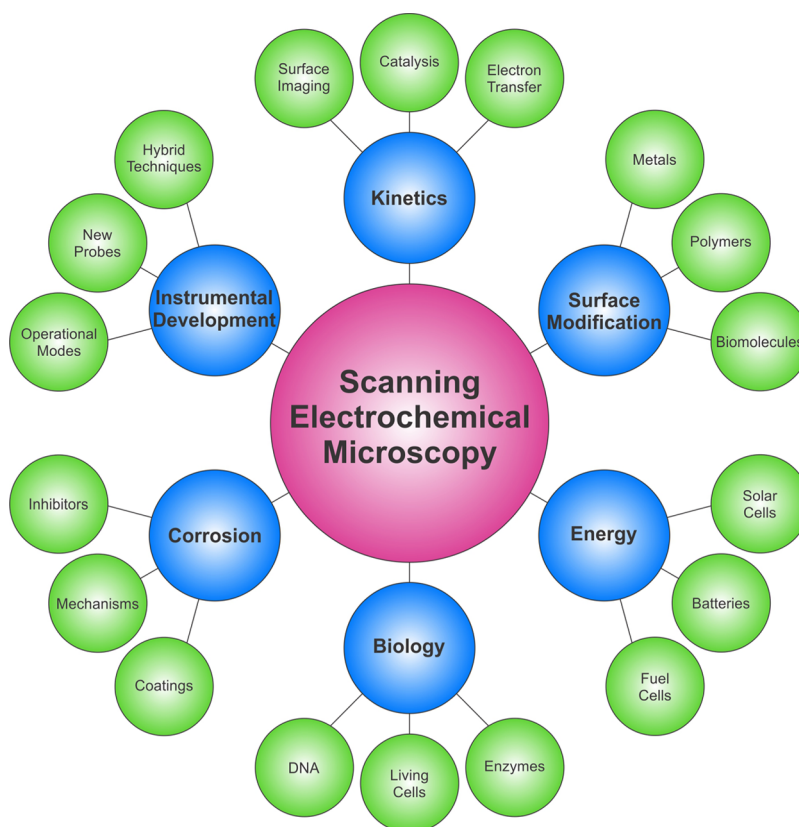


Figure 1. Experimental SECM applications.

## 2. PRINCIPLES OF SECM

### 2.1. Instrumentation

A typical scanning electrochemical microscope consists of four essential components (Figure 2). First, a low current bipotentiostat ( $\leq \text{pA}$ ) is used to precisely measure and control the current and potential at both a probe and a substrate. A high resolution three-dimensional (3D) positioning system allows for accurate movement of a probe and a substrate using an  $x$ ,  $y$ ,  $z$  stage with stepper and piezoelectric motors for coarse and finer

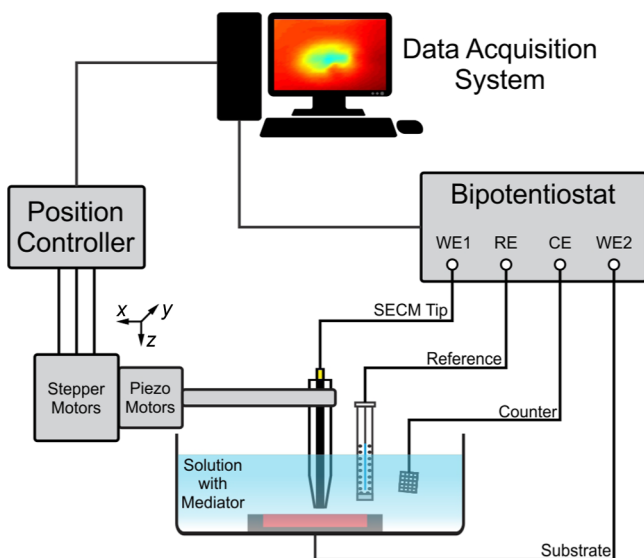


Figure 2. Schematic of a SECM instrument.

movements, respectively. The third component is a small scale probe with dimensions in the low micrometer to nanometer range, also referred to as a SECM tip. This critical component defines the resolution of an SECM measurement and will be described in detail in section 3.3. Finally, a data acquisition system (i.e., computer) is required to synchronize and coordinate each component to perform a successful measurement. Depending on the application, additional components can be added to a SECM instrument, including an inverted optical microscope for biological measurements involving live cells, a fluorescence detection system, or a constant distance unit. Although many research groups have opted to manufacture their own in-house SECM system, an increase in demand has caused several commercial systems to become available (e.g., BioLogic, CH Instruments, Heka Elektronik, Sensolytics, Uniscan Instruments).

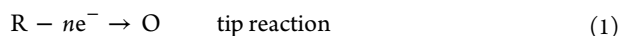
### 2.2. Modes of Operation

SECM measurements can be performed using different operational modes. Historically, feedback and generation/collection modes were the first to be introduced.<sup>1,2</sup> Since these initial reports in the early 1990s, a wide variety of new SECM modes have been developed in order to accommodate expanding applications. The principles of the most prevalent SECM modes, based on number of publications, will be discussed below. We will assume that the redox mediator (i.e., electroactive species) in solution is in its reduced form R.

It is important to note that, in the context of SECM data, lowercase  $i$  designates raw current, while an uppercase  $I$  designates normalized current. Current normalization is typically performed by dividing the measured tip current  $i_T$  with the steady-state current  $i_{T,\infty}$  (see eq 2). Distances are also reported as normalized distance  $L$ , whereby tip-to-substrate distance,  $d$ , is

normalized by the probe radius,  $a$ . These normalizations allow a comparison between measurements performed using different probe dimensions.

**2.2.1. Feedback Mode.** The most common operational mode used during SECM experiments is the feedback mode. Due to its great versatility, it has been used in virtually every SECM field of application. In feedback mode, a biased probe is approached toward a substrate of interest, and a redox mediator  $R$  is oxidized at the probe, according to the following reaction:



The faradaic current resulting from the electrochemical reaction of the mediator is recorded at the probe and depends on the topography and the electrochemical activity of the substrate.

When a probe is positioned at a tip-to-substrate distance greater than 10 times the radius of the electroactive core ( $d > 10a$ ), also known as bulk solution (Figure 3A), the measured

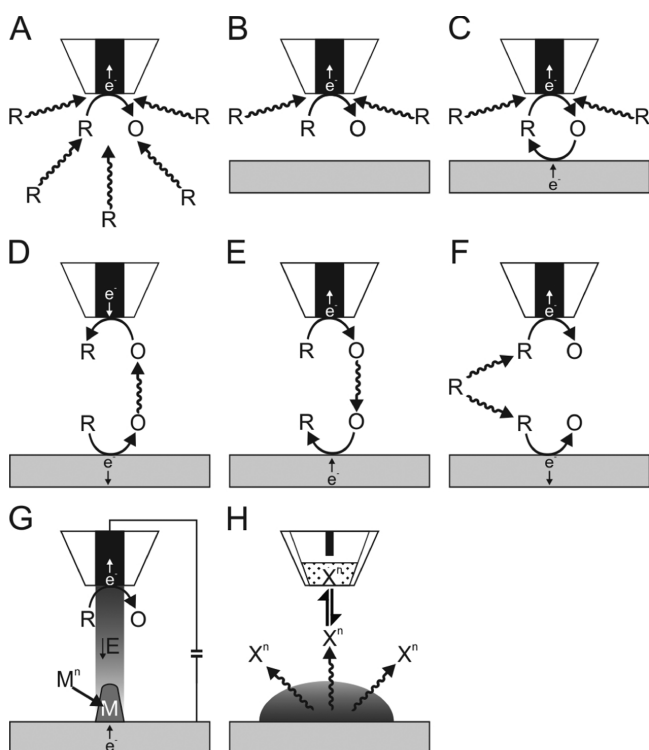


**Figure 3.** Schematic of SECM operational modes. (A) Steady-state behavior (diffusion-limited) in bulk solution. (B) Feedback mode over an inert substrate (negative feedback). (C) Feedback mode over a conducting substrate (positive feedback). (D) Substrate-Generation/Tip-Collection (SG/TC) mode. (E) Tip-Generation/Substrate-Collection (TG/SC) mode. (F) Redox competition (RC) mode. (G) Direct mode, where “M” is a metal precursor in solution with charge  $n$  ( $n$  = integer) and  $M$  is a solid metal. (H) Potentiometric mode with an ion-selective electrode, where “X” is an ion in solution with charge  $n$  ( $n$  = integer).

current,  $i_T$ , equals the diffusion limited current,  $i_{T,\infty}$  (i.e., steady-state current).<sup>9</sup> For a probe with disk geometry, the steady-state current is defined as

$$i_{T,\infty} = 4nFDC^*a\beta \quad (2)$$

where  $n$  is the number of electrons exchanged in the redox reaction,  $F$  is the Faraday constant ( $96\,485\text{ A s mol}^{-1}$ ),  $D$  is the diffusion coefficient of the redox species  $R$  in solution ( $\text{cm}^2\text{ s}^{-1}$ ),  $C^*$  is the concentration of the redox mediator in solution (mol

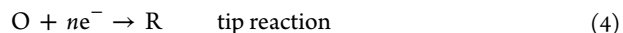
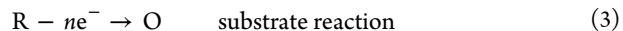
$\text{cm}^{-3}$ ),  $a$  is the radius of the electroactive surface of the electrode (cm), and  $\beta$  is a geometric coefficient.<sup>10</sup>

When a probe approaches an inert substrate, diffusion of redox species  $R$  to the probe tip is hindered by the physical presence of the substrate, resulting in a decrease in current relative to steady-state conditions ( $i_T < i_{T,\infty}$ ). This process, shown in Figure 3B, is referred to as a negative feedback response. As the probe approaches a conducting substrate such as a biased Pt electrode, the diffusion of species  $R$  to the tip is again hindered by the presence of the substrate. However, in this case, the conducting substrate allows for the reduction of species  $O$  back to  $R$ , resulting in an increased local flux of  $R$  and thus an increase in current relative to steady-state conditions ( $i_T > i_{T,\infty}$ ). This is called a positive feedback response and is shown in Figure 3C.

An important component of SECM feedback experiments is the measurement of current response with decreasing tip-to-substrate distance, which is called an approach curve (plot of  $i_T$  vs  $d$ ). The three behaviors described above, namely bulk, pure negative feedback, and pure positive feedback, are diffusion limiting cases, and usually an approach curve will fall somewhere in between positive and negative feedback behaviors. The current response recorded during these approach curve measurements, which is dependent on both tip-to-substrate distance and apparent kinetics, has been described using analytical approximations, and these equations are neatly summarized in a recent review.<sup>10</sup> It should be noted that, since the current response in feedback mode is highly dependent on tip-to-substrate distance, it is preferable to use as small a distance as possible (without crashing) to increase sensitivity.

**2.2.2. Generation/Collection Modes.** The term “generation/collection (GC) mode” is used to encompass a wide variety of experiments. These experiments can be performed in either amperometric mode, as discussed here, or in potentiometric mode, as discussed in section 2.2.5. The two main types of experiments are substrate generation/tip collection (SG/TC) and tip generation/substrate collection (TG/SC), with the main difference being the origin of the redox reaction, either at the substrate or at the tip.

In SG/TC mode (Figure 3D), an electroactive species is generated at a substrate and collected at a biased tip according to the following reactions (assuming only  $R$  is initially in solution):



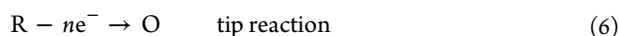
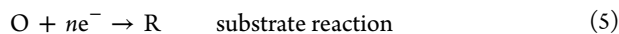
These reactions represent the simplest depiction of this mode, assuming that the system contains only  $R$ , without the possibility of other side reactions. Evidently, although the reduction of  $R$  at the substrate produces  $O$ , following electrochemical or chemical reactions can also occur to produce a completely different product.

Typically, SG/TC mode is used for the measurements of concentration profiles or chemical flux from a substrate. In order to obtain this information, currents are measured at both the tip and the substrate. The sizes of the substrate  $a_s$  and the tip  $a$  are an important consideration, and usually  $a_s/a \gg 1$  such that the diffusion layer of the substrate is much larger than that of the tip. This mode assumes no feedback contribution to the measured current, such that no current would be recorded at the tip prior to biasing of the substrate. However, SG/TC suffers from several disadvantages, including a low collection efficiency, interference between substrate and tip reactions, and a lack of steady state at



large substrate. Nevertheless, this mode has proven quite useful in both corrosion and enzymatic measurements.

In TG/SC mode (Figure 3E), the electroactive species is generated at the tip and subsequently collected by the substrate.



As with SG/TC mode, currents are measured at both the tip and the substrate. Immediately after biasing both working electrodes, substrate current,  $i_s$ , is close to zero as species R (generated at the tip reaction) has not yet been produced and/or had time to diffuse to the substrate. However, as time increases,  $i_s$  also increases and eventually, when a steady state is achieved, the difference between  $i_s$  and  $i_T$  becomes negligible. When the distance between the tip and the substrate is small ( $L \leq 2$ ), tip-generated species R will mainly diffuse to the substrate and a high collection efficiency ( $i_s/i_T > 0.99$ ) can be achieved.<sup>11</sup> TG/SC mode is predominantly used for the measurement of reaction kinetics and to perform modifications to the substrate.

**2.2.3. Redox Competition Mode.** The use of redox competition (RC) mode is less prominent than feedback and GC, but since its development by Schuhmann and co-workers,<sup>12</sup> it has found a niche in the measurement of surface catalytic activity and corrosion.<sup>12,13</sup> In this mode, the SECM tip and the substrate, which are in close proximity to each other, compete for the same redox species, as shown in Figure 3F. Similar to TG/SC mode, the use of a bipotentiostat is necessary in such experiments in order to apply potentials to both the substrate and the SECM tip. However, unlike TG/SC mode, the current is measured at the SECM tip and not the substrate, which means that the background current contribution is significantly decreased, resulting in an increased sensitivity toward the measurement of catalytic activity.

To avoid complete depletion of the redox mediator within the tip-to-substrate gap, the substrate is biased at a reduction potential, while a reductive potential pulse is applied to the SECM tip. When scanning over an inactive region of the substrate, the reductive current measured at the SECM tip remains constant. Over an active region of the substrate where the reduction process occurs, i.e. the catalytic spot, the redox species is consumed at both the SECM tip and the substrate, leading to a decrease in measured current at the SECM tip. This decrease in current can then be correlated with substrate activity.

**2.2.4. Direct Mode.** Direct mode is a specific subset of SECM in which the electrochemical cell configuration is reversed such that the microelectrode tip is used as the counter electrode and the substrate is used as the working electrode, as illustrated in Figure 3G. When a potential is applied, the electric field is localized between the tip and the substrate (shown by the shaded area in Figure 3G). Consequently, small tip-to-substrate distances allow for higher patterning resolution. In the SECM community, direct mode has been mainly used in the context of surface modification, particularly for semiconductor etching, enzyme deposition, and micropatterning.<sup>14–16</sup>

**2.2.5. Potentiometric Mode.** The one common point between the modes described above is that they all involve an amperometric measurement. In potentiometric mode SECM, the measured signal is a potential and not a current. The use of this mode provides several advantages, including high selectivity and measurement of nonelectroactive species or electroactive species with standard reduction potentials outside the solvent window. Furthermore, since no faradaic reaction is occurring or

required, the concentration and oxidation state of the analyte species is unchanged during the measurement.

In this mode, the potential is measured between an ion-selective electrode (ISE) and an external reference electrode. Specific examples will be discussed in Table 5, but typically an ISE used in SECM is composed of an internal reference electrode, inserted into a glass capillary filled with a constant activity solution of the ion of interest and an ion-selective membrane at the tip. When the ISE is immersed in a sample solution containing the ion of interest, chemical recognition of the analyte at the ion-selective membrane causes the formation of a junction potential. The difference in chemical activity between the internal and external solutions creates a junction potential which can then be measured at the internal reference electrode. The measured potential is linearly dependent on the activity of the ion of interest. As such, the tip-to-substrate bears no influence on the measured signal and is less important than in other operational modes (e.g., feedback mode).

Potentiometric probes are not limited to the use of an ion-selective membrane, but still require the presence of a component capable of differentiating species. For instance, oxide films deposited on a microelectrode core have shown great capabilities to monitor local variations in pH.<sup>17</sup>

### 3. EXPERIMENTAL DESIGN

Designing a SECM experiment is not trivial, and requires the careful consideration of several important factors including the following:

- mediator and/or substrate being investigated
- solvent in which the electrochemical reaction(s) will occur
- probe that should be used

The success of an experiment relies on the identification of the right combination of these three parameters. In this section, mediators, solvents, and probes will be discussed in the context of a SECM experiment. An exhaustive list of the parameters used in the literature since 1989 is also tabulated for each section.

#### 3.1. Mediators

A redox mediator is an electroactive molecule/atom that can be oxidized or reduced. A direct redox mediator is defined as a molecule that is already present in solution (e.g.,  $\text{O}_2$ ), while an indirect mediator designates a molecule that has been added to solution prior to the experiment (e.g., FcMeOH). Although no strict rules exist in terms of which mediator should be employed with a specific operational mode, most experiments have common properties which can be used for the selection of an ideal mediator for a specific application.

The selection of a given mediator for a SECM experiment greatly depends on the nature of the sample studied and the mode of SECM used. The mediator will typically need to be chemically stable in the solvent environment and inert in the presence of the working, counter, and reference electrodes. The charge, hydro-/lipophilicity, size, permeability coefficient, standard redox potential, and pH dependent behaviors are also important factors that can alter the observed SECM measurements.<sup>18,19</sup> Additional requirements such as photostability, toxicity, thermal stability, and solubility may also apply.

In addition to the nature of the mediator, its concentration needs to be carefully considered based on the reaction rates at the sample. If we consider self-assembled monolayer films<sup>20–22</sup> or conductive polymer films,<sup>23</sup> the observed feedback response could be a combination of the diffusion flux in solution and the



Table 1. Redox Mediators Used in Feedback Mode SECM<sup>a</sup>

abbrev	mediator	redox reaction	solvent	$E^0$ (V vs NHE)	application
A	adenosine	$A^{*+} + e^- \rightarrow A$	aqueous	1.722 <sup>26</sup>	kinetics <sup>26</sup>
AA/DHAA	ascorbic acid/dehydroascorbic acid	$DHAA + 2H^+ + 2e^- \rightarrow AA$	aqueous	0.713 <sup>b27</sup>	kinetics <sup>27,28</sup>
AB	azobenzene	$AB + e^- \rightarrow AB^{*-}$	DMF	1.059 <sup>29</sup>	kinetics <sup>29,30</sup>
			MeCN	-1.378 <sup>30</sup>	SM <sup>31,32</sup>
ABTS	2,2'-azino-bis(3-ethylbenzothiazoline-6-sulfonate)	$ABTS + e^- \rightarrow ABTS^{*-}$	aqueous	1.113 <sup>33</sup>	ITIES <sup>33</sup>
		$ABTS^{*-} + e^- \rightarrow ABTS^{2-}$		0.703 <sup>33</sup>	
ADPA	1,4-amino-diphenylamine	$ADPA^+ + e^- \rightarrow ADPA$	MeCN	0.522 <sup>34</sup>	energy <sup>34</sup>
		$ADPA^{2+} + e^- \rightarrow ADPA^+$		0.972 <sup>34</sup>	
An	anthracene	$An + e^- \rightarrow An^{*-}$	DMF	-1.659 <sup>35</sup>	kinetics <sup>36,37</sup>
			[Et <sub>3</sub> BuN][TFSI]	-2.350 <sup>d36</sup>	SM <sup>31,35</sup>
BN	benzonitrile	$BN + e^- \rightarrow BN^{*-}$	DMF	-2.019 <sup>35</sup>	SM <sup>35</sup>
BQ/HQ	benzoquinone/hydroquinone	$BQ + 2H^+ + 2e^- \rightarrow HQ$	aqueous	0.102 <sup>38</sup>	enzymes <sup>40,41</sup>
		$BQ + e^- \rightarrow BQ^{*-}$	MeCN	-0.278 <sup>30</sup>	living cell <sup>18</sup>
		$BQ^{*-} + e^- \rightarrow BQ^{2-}$	PC	-1.000 <sup>b39</sup>	SM <sup>39,42</sup>
Br	bromine	$Br_2 + 2e^- \rightarrow 2Br^-$	aqueous	1.082 <sup>43</sup>	corrosion <sup>43</sup>
		$Br_3^- + 2e^- \rightarrow 3Br^-$	MeCN	1.293 <sup>44</sup>	kinetics <sup>45-48</sup>
		$3Br_2 + 2e^- \rightarrow 2Br_3^-$	MeCN	1.663 <sup>44</sup>	SM <sup>49,50</sup>
B12	vitamin B12	$B12^{2+} + e^- \rightarrow B12^+$	aqueous	-0.518 <sup>51</sup>	ITIES <sup>51</sup>
C60	C60	$C60 + e^- \rightarrow C60^{*-}$	DCB	-1.100 <sup>c52</sup>	kinetics <sup>52,54</sup>
			PhCN	-1.100 <sup>d52</sup>	
			MeCN	-0.410 <sup>53</sup>	
C70	C70	$C70 + e^- \rightarrow C70^{*-}$	PhCl	-0.409 to -1.856 (4e <sup>-</sup> ) <sup>54</sup>	kinetics <sup>54</sup>
Cl	chlorine	$Cl_2 + 2e^- \rightarrow 2Cl^-$	aqueous	1.367 <sup>55</sup>	corrosion <sup>56,57</sup>
Co(bpy) <sub>3</sub>	tris(4,4'-bipyridine)cobalt(II) chloride	$[Co(bpy)_3]^{3+} + e^- \rightarrow [Co(bpy)_3]^{2+}$	aqueous	0.300 <sup>58</sup>	biological <sup>59</sup>
					energy <sup>60,61</sup>
					SM <sup>58</sup>
Co(dapa) <sub>2</sub>	(2,6-bis[1-(phenylimino)-ethyl]pyridine)cobalt	$[Co(dapa)_2]^{3+} + e^- \rightarrow [Co(dapa)_2]^{2+}$	DMF	0.562 <sup>62</sup>	kinetics <sup>62</sup>
		$[Co(dapa)_2]^{2+} + e^- \rightarrow [Co(dapa)_2]^+$	DMF	-0.318 <sup>62</sup>	kinetics <sup>62</sup>
Co(phen) <sub>3</sub>	tris(1,10-phenanthroline)cobalt(II)	$[Co(phen)_3]^{3+} + e^- \rightarrow [Co(phen)_3]^{2+}$	aqueous	0.588 <sup>b63</sup>	kinetics <sup>63</sup>
Co(sep)	cobalt(III) sepulchrate trichloride	$[Co(sep)]^{3+} + e^- \rightarrow [Co(sep)]^{2+}$	aqueous	-0.315 <sup>64</sup>	ITIES <sup>65,66</sup>
					kinetics <sup>62,64</sup>
DA/DOQ	dopamine/dopamine- <i>o</i> -quinone	$DOQ + 2H^+ + 2e^- \rightarrow DA$	aqueous	1.087 <sup>67</sup>	kinetics <sup>67</sup>
DBDMB	2,5-di- <i>tert</i> -butyl-1,4-dimethoxybenzene	$DBDMB^+ + e^- \rightarrow DBDMB$	EC	0.875 <sup>69</sup>	ITIES <sup>68</sup>
DcMeFc	decamethylferrocene	$[DcMeFc]^+ + e^- \rightarrow DcMeFc$	MeCN	0.031 <sup>70</sup>	energy <sup>69</sup>
			DCM	0.091 <sup>71</sup>	ITIES <sup>72,76</sup>
			DCE	0.261 <sup>72</sup>	
			NPOE	0.368 <sup>73</sup>	
			TFT	0.222 <sup>74</sup>	
			nitrobenzene	0.113 <sup>75</sup>	
DEA	diethoxyanthracene	$DEA + e^- \rightarrow DEA^{*-}$	DMF	-1.669 <sup>32</sup>	kinetics <sup>31</sup>
					SM <sup>32</sup>
DiMeFc	dimethylferrocene	$[DiMeFc]^+ + e^- \rightarrow DiMeFc$	MeCN	0.561 <sup>77</sup>	corrosion <sup>79</sup>
			DCE	0.742 <sup>78</sup>	
			DCM	0.521 <sup>71</sup>	ITIES <sup>78,80</sup>
DF	dimethyl fumarate	$DF + e^- \rightarrow DF^{*-}$	DMF	-1.100 <sup>c11</sup>	kinetics <sup>11</sup>
DMAMFc	dimethylamino-methylferrocene	$[DMAMFc]^+ + e^- \rightarrow DMAMFc$	aqueous	0.551 <sup>81</sup>	corrosion <sup>81-83</sup>
					enzymes <sup>84</sup>
DMPPD	<i>N,N</i> -dimethyl- <i>p</i> -phenylenediamine	$DMPPD^+ + H^+ + 2e^- \rightarrow DMPPD$	aqueous	0.297 <sup>85</sup>	kinetics <sup>86</sup>
DP	2,2'-dipyridyl	$DP + e^- \rightarrow DP^{*-}$	DMF	-1.959 <sup>29</sup>	kinetics <sup>29,35</sup>
DP	2,4'-dipyridyl	$DP + e^- \rightarrow DP^{*-}$	DMF	-1.709 <sup>35</sup>	kinetics <sup>35</sup>

Table 1. continued

abbrev	mediator	redox reaction	solvent	$E^0$ (V vs NHE)	application
DP	4,4'-dipyridyl	$DP + e^- \rightarrow DP^{*-}$	DMF	$-1.659^{29}$	kinetics <sup>29</sup>
DPA	diphenylanthracene	$DPA + e^- \rightarrow DPA^{*-}$	MeCN	$-2.159^{87}$	SM <sup>87</sup>
EtnyFc	ethynylferrocene	$[EtnyFc]^+ + e^- \rightarrow EtnyFc$	MeCN	$0.831^{37}$	kinetics <sup>37,71</sup>
			DCM	$0.811^{71}$	kinetics <sup>37,71</sup>
EV	ethylviologen	$EV^{2+} + e^- \rightarrow EV^+$	MeCN	$-0.250^{c88}$	energy <sup>89</sup>
		$EV^+ + e^- \rightarrow EV$	MeCN	$-0.653^{62}$	kinetics <sup>62</sup>
		$EV^{2+} + e^- \rightarrow EV^+$	PC	$-0.852^{b89}$	
Fc	ferrocene	$Fc^+ + e^- \rightarrow Fc$	MeCN	$0.665^{90}$	ITIES <sup>94,95</sup>
			DCM	$0.651^{71}$	
			DMF	$0.691^{91}$	energy <sup>96,97</sup>
			PC	$0.175^{92}$	enzymes <sup>98</sup>
			ChCl TFA	$0.522^{93}$	kinetics <sup>99,100</sup>
FcCOOH	ferrocenecarboxylic acid	$[FcCOOH]^+ + e^- \rightarrow FcCOOH$	aqueous	$0.541^{101}$	biological <sup>102,103</sup>
					corrosion <sup>104,105</sup>
					enzymes <sup>106,107</sup>
					ITIES <sup>108</sup>
					kinetics <sup>109,110</sup>
					living cell <sup>18,111</sup>
					SM <sup>112,113</sup>
Fc(COOH) <sub>2</sub>	ferrocenedicarboxylic acid	$[Fc(COOH)_2]^+ + e^- \rightarrow Fc(COOH)_2$	aqueous	$0.649^{18}$	living cell <sup>18</sup>
FcEmiTFSI	1-(ferrocenylmethyl)-3-methylimidazolium bis (trifluoromethanesulfonyl) amide	$[FcEmiTFSI]^+ + e^- \rightarrow FcEmiTFSI$	[Emi][TFSI]	$0.200^{d114}$	kinetics <sup>114</sup>
FcMeOH	ferrocenemethanol	$[FcMeOH]^+ + e^- \rightarrow FcMeOH$	aqueous	$0.500^{115}$	
			DMF	$0.661^{116}$	corrosion <sup>64,119</sup>
			MeCN	$0.672^{117}$	enzymes <sup>120,121</sup>
			DCM	$0.691^{116}$	kinetics <sup>122–125</sup>
			ethylene glycol	$0.280^{c118}$	living cell <sup>126,127</sup>
Fc(MeOH) <sub>2</sub>	ferrocenedimethanol	$[Fc(MeOH)_2]^+ + e^- \rightarrow Fc(MeOH)_2$	aqueous	$0.457^{128}$	biological <sup>129</sup>
					kinetics <sup>63,73,103</sup>
Fc-Naph-Fc	ferrocenyl naphthalene diimide	$[Fc-Naph-Fc]^+ + e^- \rightarrow Fc-Naph-Fc$	aqueous	$0.988^{130}$	kinetics <sup>130</sup>
FcTMA	ferrocenylmethyl trimethylammonium	$[FcTMA]^+ + e^- \rightarrow FcTMA$	aqueous	$0.652^{131}$	biological <sup>132,133</sup>
					kinetics <sup>134</sup>
Fe	iron	$Fe^{3+} + e^- \rightarrow Fe^{2+}$	aqueous	$0.772^{135}$	SM <sup>136</sup>
					ITIES <sup>65</sup>
					kinetics <sup>137</sup>
Fe(bpy) <sub>3</sub>	iron(III) tris(bipyridine)	$[Fe(bpy)_3]^{3+} + e^- \rightarrow [Fe(bpy)_3]^{2+}$	aqueous	$1.022^{138}$	SM <sup>53,138</sup>
Fe(CN) <sub>6</sub>	hexacyanoferrate(III)	$[Fe(CN)_6]^{4+} + e^- \rightarrow [Fe(CN)_6]^{3+}$	aqueous	$0.491^{139}$	biological <sup>103,140</sup>
					catalysis <sup>141</sup>
					corrosion <sup>142–144</sup>
					energy <sup>41</sup>
					enzymes <sup>145</sup>
					ITIES <sup>146,147</sup>
					kinetics <sup>100,148</sup>
					living cell <sup>149,150</sup>
					SM <sup>151,152</sup>
Fe(EDTA)	iron(III) ethylenediamine tetraacetic acid	$[Fe(EDTA)]^- + e^- \rightarrow [Fe(EDTA)]^{2-}$	aqueous	$0.120^{153}$	kinetics <sup>147,154</sup>
Fe(phen) <sub>3</sub>	iron(II) tris(1,10-phenanthroline)	$[Fe(phen)_3]^{3+} + e^- \rightarrow [Fe(phen)_3]^{2+}$	aqueous	$1.241^{155}$	kinetics <sup>156</sup>
					SM <sup>155</sup>
FeTTP	iron porphyrin	$[FeTTP]^{3+} + e^- \rightarrow [FeTTP]^{2+}$	nitrobenzene	$1.163^{157}$	ITIES <sup>157</sup>
FN	fumaronitrile	$FN + e^- \rightarrow FN^{*-}$	DMF	$-1.100^{c11}$	kinetics <sup>11</sup>
G	guanosine	$G^+ + e^- \rightarrow G$	aqueous	$1.392^{26}$	kinetics <sup>26,158</sup>
			DMF	$1.590^{158}$	
H	hydrogen	$2H^+ + 2e^- \rightarrow H_2$	aqueous	$0.000^{159}$	biological <sup>160</sup>

Table 1. continued

abbrev	mediator	redox reaction	solvent	$E^0$ (V vs NHE)	application
$\text{H}_2\text{O}_2$	hydrogen peroxide	$\text{O}_2 + 2\text{H}^+ + 2\text{e}^- \rightarrow \text{H}_2\text{O}_2$	aqueous	0.670 <sup>165</sup>	catalysis <sup>159</sup> energy <sup>161</sup> kinetics <sup>162–164</sup> biological <sup>166</sup> energy <sup>167,168</sup> enzymes <sup>165</sup> ITIES <sup>169</sup> kinetics <sup>170</sup> living cell <sup>171</sup> kinetics <sup>172</sup>
$\text{H}_2\text{PO}_4^-$	dihydrogen orthophosphate	$2\text{H}_2\text{PO}_4^- + 2\text{e}^- \rightarrow 2\text{HPO}_4^{2-} + \text{H}_2$	aqueous	−0.592 <sup>172</sup>	
HV	heptylviologen	$\text{HV}^{2+} + \text{e}^- \rightarrow \text{HV}^+$	MeCN	−0.728 <sup>62</sup>	kinetics <sup>62</sup>
I	iodide	$\text{I}_3^- + 2\text{e}^- \rightarrow 3\text{I}^-$	aqueous	0.963 <sup>173</sup>	corrosion <sup>175,176</sup> energy <sup>174,177</sup> kinetics <sup>178</sup> living cell <sup>179</sup> kinetics <sup>180</sup>
$\text{I}_2$		$\text{I}_2 + 2\text{e}^- \rightarrow 2\text{I}^-$	MeCN	0.180 <sup>174</sup>	
$\text{InCl}_3$	indium chloride	$\text{In}^{3+} + 2\text{e}^- \rightarrow \text{In}^+$	aqueous	−0.400 <sup>180</sup>	kinetics <sup>180</sup>
$\text{IrCl}_6$	iridium chloride	$[\text{IrCl}_6]^{2-} + \text{e}^- \rightarrow [\text{IrCl}_6]^{3-}$	aqueous	0.870 <sup>181</sup>	biological <sup>59,182</sup> corrosion <sup>64</sup> ITIES <sup>94,183</sup> kinetics <sup>184–186</sup> living cell <sup>187</sup> kinetics <sup>188</sup>
$\text{Ir}(\text{CN})_6$	hexacyanoiridate(III)	$[\text{Ir}(\text{CN})_6]^{2-} + \text{e}^- \rightarrow [\text{Ir}(\text{CN})_6]^{3-}$	aqueous	0.950 <sup>188</sup>	
LV	laurylviologen	$\text{LV}^{2+} + \text{e}^- \rightarrow \text{LV}^+$	MeCN	−0.678 <sup>62</sup>	kinetics <sup>62</sup>
MB	meldola blue	$\text{MB}^+ + 2\text{H}^+ + 2\text{e}^- \rightarrow \text{MBH}_2$	aqueous	0.118 <sup>189</sup>	kinetics <sup>189</sup>
MeB	methylene blue	$\text{MeB}^+ + 2\text{H}^+ + 2\text{e}^- \rightarrow \text{MeBH}_2$	aqueous	−0.079 <sup>190</sup>	kinetics <sup>190</sup>
MD/MDH	menadione/menadiol	$\text{MD} + 2\text{H}^+ + 2\text{e}^- \rightarrow \text{MDH}$	aqueous	−0.047 <sup>191</sup>	biological <sup>19</sup> living cell <sup>18,179</sup> catalysis <sup>189</sup>
M-NMP <sup>+</sup>	1-methoxy-5-methyl phenazine methosulfate	$\text{M-NMP}^+ + \text{H}^+ + 2\text{e}^- \rightarrow \text{M-NMPH}$	aqueous	0.098 <sup>189</sup>	
MNP	2-methyl-2-nitropropane	$\text{MNP} + \text{e}^- \rightarrow \text{MNP}^{\bullet-}$	$[\text{Et}_3\text{BuN}][\text{TFSI}]$	−2.020 <sup>d36</sup>	kinetics <sup>36</sup>
$\text{Mo}(\text{CN})_8$	octacyanomolybdate(IV)	$[\text{Mo}(\text{CN})_8]^{3-} + \text{e}^- \rightarrow [\text{Mo}(\text{CN})_8]^{4-}$	aqueous	0.757 <sup>62</sup>	ITIES <sup>65,147</sup> kinetics <sup>62</sup> biological <sup>193</sup> catalysis <sup>194</sup> enzymes <sup>145,195</sup> kinetics <sup>139,159</sup>
MV	methylviologen	$\text{MV}^{2+} + \text{e}^- \rightarrow \text{MV}^+$	aqueous	−0.446 <sup>159</sup>	
		$\text{MV}^+ + \text{e}^- \rightarrow \text{MV}$		−0.663 <sup>192</sup>	
N	naphthalene	$\text{N} + \text{e}^- \rightarrow \text{N}^{\bullet-}$	DMF	−2.159 <sup>29</sup>	kinetics <sup>29</sup>
NB	nitrobenzene	$\text{NB} + \text{e}^- \rightarrow \text{NB}^{\bullet-}$	DMF	−0.759 <sup>29</sup>	kinetics <sup>29,196</sup>
4NB	4-nitrobenzonitrile	$4\text{NB} + \text{e}^- \rightarrow 4\text{NB}^{\bullet-}$	DMF	0.659 <sup>31</sup>	kinetics <sup>31</sup> SM <sup>32</sup> kinetics <sup>36</sup>
NM	2-nitromesitylene	$\text{NM} + \text{e}^- \rightarrow \text{NM}^{\bullet-}$	$[\text{Pyr}][\text{TFSI}]$ $[\text{BMIM}][\text{TFSI}]$ $[\text{Et}_3\text{BuN}][\text{TFSI}]$	−1.680 <sup>d36</sup> −1.550 <sup>d36</sup> −1.760 <sup>d36</sup>	
NMP <sup>+</sup>	N-methyl phenazine methosulfate	$\text{NMP}^+ + \text{H}^+ + 2\text{e}^- \rightarrow \text{NMPH}$	aqueous	0.113 <sup>189</sup>	catalysis <sup>189</sup>
NO	nitric oxide	$\text{NO} + \text{e}^- \rightarrow \text{NO}^{\bullet-}$	aqueous	0.972 <sup>b197</sup>	living cell <sup>197,198</sup>
NQ	1,2-naphthoquinone	$\text{NQ} + 2\text{H}^+ + 2\text{e}^- \rightarrow \text{NQH}$	aqueous	0.077 <sup>18</sup>	living cell <sup>149,199</sup>
NQ	1,4-naphthoquinone	$\text{NQ} + 2\text{H}^+ + 2\text{e}^- \rightarrow \text{NQH}$	aqueous	−0.045 <sup>18</sup>	living cell <sup>18</sup>
NT	4-nitrotoluene	$\text{NT} + \text{e}^- \rightarrow \text{NT}^{\bullet-}$	$[\text{Pyr}][\text{TFSI}]$ $[\text{BMIM}][\text{TFSI}]$ $[\text{Et}_3\text{BuN}][\text{TFSI}]$	−1.460 <sup>d36</sup> −1.370 <sup>d36</sup> −1.530 <sup>d36</sup>	kinetics <sup>36</sup>
NX	3- <i>o</i> -nitroxylen	$\text{NX} + \text{e}^- \rightarrow \text{NX}^{\bullet-}$	DMF	−0.999 <sup>200</sup>	kinetics <sup>200</sup>
$\text{O}_2$	oxygen	$\text{O}_2 + 2\text{H}^+ + 2\text{e}^- \rightarrow \text{H}_2\text{O}_2$	aqueous	−0.387 <sup>201</sup>	biological <sup>205,206</sup>
		$\text{O}_2 + 4\text{H}^+ + 4\text{e}^- \rightarrow 2\text{H}_2\text{O}$	aqueous	−0.243 <sup>111</sup>	
		$\text{O}_2 + \text{e}^- \rightarrow \text{O}_2^{\bullet-}$	DMSO	−0.498 <sup>202</sup>	corrosion <sup>207</sup>
			DMF	−0.097 <sup>203</sup>	ITIES <sup>208</sup>
			IL	−0.659 <sup>204</sup>	living cell <sup>201,209</sup>



Table 1. continued

abbrev	mediator	redox reaction	solvent	$E^0$ (V vs NHE)	application
Os(bpy) <sub>3</sub>	Os(bpy) <sub>3</sub>	$[\text{Os}(\text{bpy})_3]^{3+} + e^- \rightarrow [\text{Os}(\text{bpy})_3]^{2+}$	aqueous	0.834 <sup>182</sup>	biological <sup>182,210</sup>
					kinetics <sup>62,211</sup>
Os(bpy) <sub>2</sub> fpy	Os(2,2'-bipyridine)-2-(4-formylpyridine)	$[\text{Os}(\text{bpy})_2\text{fpy}]^{2+} + e^- \rightarrow [\text{Os}(\text{bpy})_2\text{fpy}]^+$	MeCN	0.452 <sup>62</sup>	SM <sup>155</sup>
			aqueous	0.763 <sup>107</sup>	biological <sup>107</sup>
P	phenanthridine	$\text{P} + e^- \rightarrow \text{P}^{\bullet-}$	DMF	-1.789 <sup>35</sup>	SM <sup>35</sup>
PN	phthalonitrile	$\text{PN} + e^- \rightarrow \text{PN}^{\bullet-}$	DMF	-1.349 <sup>35</sup>	SM <sup>35</sup>
PP	4-phenylpyridine	$\text{PP} + e^- \rightarrow \text{PP}^{\bullet-}$	DMF	-1.909 <sup>35</sup>	SM <sup>35</sup>
PTN	<i>p</i> -tolunitrile	$\text{PTN} + e^- \rightarrow \text{PTN}^{\bullet-}$	DMF	-2.119 <sup>212</sup>	SM <sup>212</sup>
PYO	pyocyanin	$\text{PYO}^+ + 2\text{H}^+ + 2e^- \rightarrow \text{PYO}$	aqueous	0.040 <sup>213</sup>	living cell <sup>213</sup>
Re(dmpe) <sub>3</sub>	tris(1,2-bis-dimethyl-phosphino ethane) rhenium(I)	$[\text{Re}(\text{dmpe})_3]^{2+} + e^- \rightarrow [\text{Re}(\text{dmpe})_3]^+$	aqueous	0.037 <sup>6214</sup>	kinetics <sup>214</sup>
R-NO	4-(3-nitrosophenyl)-2,6-dimethyl-3,5-diisopropiloxycarbonyl-1,4-dihydropyridine	$\text{R-NO} + 2\text{H}^+ + 2e^- \rightarrow \text{RNHOH}$	aqueous	0.162 <sup>215</sup>	kinetics <sup>215</sup>
Ru(bpy) <sub>3</sub>	tris(2,2'-bipyridine) ruthenium(II)	$[\text{Ru}(\text{bpy})_3]^{3+} + e^- \rightarrow [\text{Ru}(\text{bpy})_3]^{2+}$	MeCN	1.556 <sup>216</sup>	biological <sup>133</sup>
			aqueous	1.501 <sup>217</sup>	ITIES <sup>108,218</sup>
					kinetics <sup>219</sup>
Ru(CN) <sub>6</sub>	hexacyanoruthenate(II)	$[\text{Ru}(\text{CN})_6]^{3-} + e^- \rightarrow [\text{Ru}(\text{CN})_6]^{4-}$	aqueous	0.907 <sup>62</sup>	biological <sup>205</sup>
					ITIES <sup>76,220</sup>
					kinetics <sup>62,221</sup>
					living cell <sup>18</sup>
Ru(NH <sub>3</sub> ) <sub>6</sub>	hexaammineruthenium(II)	$[\text{Ru}(\text{NH}_3)_6]^{3+} + e^- \rightarrow [\text{Ru}(\text{NH}_3)_6]^{2+}$	aqueous	-0.059 <sup>222</sup>	biological <sup>107,223</sup>
					corrosion <sup>64,224,225</sup>
					ITIES <sup>226</sup>
					kinetics <sup>162</sup>
					living cell <sup>111,149</sup>
Ru(phen) <sub>3</sub>	tris(1,10-phenanthroline) ruthenium(II)	$[\text{Ru}(\text{phen})_3]^{3+} + e^- \rightarrow [\text{Ru}(\text{phen})_3]^{2+}$	aqueous	1.270 <sup>227</sup>	SM <sup>227</sup>
Ru(phen) <sub>2</sub> dppz	bis(1,10-phenanthroline) dipyrdo[3,2- <i>a</i> :2',3'- <i>c</i> ] phenazine ruthenium(II)	$[\text{Ru}(\text{phen})_2\text{dppz}]^{3+} + e^- \rightarrow [\text{Ru}(\text{phen})_2\text{dppz}]^{2+}$	aqueous	1.518 <sup>228</sup>	catalysis <sup>228</sup>
SV	stearylviologen	$\text{SV}^{2+} + e^- \rightarrow \text{SV}^+$	MeCN	-0.708 <sup>62</sup>	kinetics <sup>62</sup>
T	1-methy-1 <i>H</i> -tetrazole-5-thiolate	$\text{T}_2 + 2e^- \rightarrow 2\text{T}^{\bullet-}$	MeCN	-0.457 <sup>60</sup>	energy <sup>60,229</sup>
TBNB	2,4,6-tri- <i>tert</i> -butylnitrobenzene	$\text{TBNB} + e^- \rightarrow \text{TBNB}^{\bullet-}$	[BMIM][TFSI]	-0.165 <sup>d36</sup>	kinetics <sup>36</sup>
			[Pyr][TFSI]	-1.740 <sup>d36</sup>	
			[Et <sub>3</sub> BuN][TFSI]	-1.830 <sup>d36</sup>	
TCNQ	tetracyanoquinodimethane	$\text{TCNQ} + e^- \rightarrow \text{TCNQ}^{\bullet-}$	aqueous	0.356 <sup>230</sup>	
			DCE	0.502 <sup>146</sup>	ITIES <sup>66,76</sup>
			MeCN	0.322 <sup>30</sup>	
			nitrobenzene	0.100 <sup>c231</sup>	kinetics <sup>232</sup>
		$\text{TCNQ}^{\bullet-} + e^- \rightarrow \text{TCNQ}^{2-}$	DMF	0.541 <sup>32</sup>	
TEMPO	2,2,6,6-tetramethylpiperidine 1-oxyl	$\text{TEMPO}^{++} + e^- \rightarrow \text{TEMPO}$	aqueous	0.666 <sup>18</sup>	kinetics <sup>232</sup>
					living cell <sup>18</sup>
Th	thianthrene	$\text{Th}^+ + e^- \rightarrow \text{Th}$	MeCN	1.352 <sup>34</sup>	energy <sup>34</sup>
TMB/TMBD	tetramethylbenzidine/tetramethylbenzidine diimine	$\text{TMBD} + 2\text{H}^+ + 2e^- \rightarrow \text{TMB}$	aqueous	0.422 <sup>b233</sup>	enzymes <sup>233</sup>
TMPD	tetramethyl- <i>p</i> -phenylenediamine	$\text{TMPD}^{2+} + e^- \rightarrow \text{TMPD}^+$	aqueous	0.668 <sup>179</sup>	
		$\text{TMPD}^+ + e^- \rightarrow \text{TMPD}$	aqueous	0.258 <sup>179</sup>	
			MeCN	0.341 <sup>100</sup>	kinetics <sup>11,100</sup>
			MeOH	0.341 <sup>100</sup>	living cell <sup>199,234</sup>
			DMF	0.543 <sup>11</sup>	
			DMSO	0.482 <sup>202</sup>	
TPA	tri- <i>p</i> -tolylamine	$\text{TPA}^+ + e^- \rightarrow \text{TPA}$	MeCN	1.041 <sup>37</sup>	kinetics <sup>37,71</sup>
			DCM	1.001 <sup>71</sup>	
TPN	terephthalonitrile	$\text{TPN} + e^- \rightarrow \text{TPN}^{\bullet-}$	DMF	-1.259 <sup>212</sup>	SM <sup>212</sup>
TTF	tetrathiafulvalene	$\text{TTF}^{2+} + e^- \rightarrow \text{TTF}^+$	MeCN	0.593 <sup>90</sup>	kinetics <sup>90,91,235</sup>
		$\text{TTF}^+ + e^- \rightarrow \text{TTF}$	MeCN	0.943 <sup>90</sup>	
			DMF	0.661 <sup>91</sup>	
V	vanadium	$\text{V}^{3+} + e^- \rightarrow \text{V}^{2+}$	aqueous	0.065 <sup>b236</sup>	ITIES <sup>65,66</sup>
					SM <sup>236</sup>

Table 1. continued

abbrev	mediator	redox reaction	solvent	$E^0$ (V vs NHE)	application
$W(CN)_8$	octacyanotungstate(IV)	$[W(CN)_8]^{3-} + e^- \rightarrow [W(CN)_8]^{4-}$	aqueous	0.608 <sup>66</sup>	ITIES <sup>66</sup>
ZnPor	5,10,15,20-tetraphenyl 21H,23H-porphyrin zinc	$ZnPor^+ + e^- \rightarrow ZnPor$	DCE	1.172 <sup>237</sup>	ITIES <sup>147,220</sup>
			benzene	1.072 <sup>220</sup>	
			nitrobenzene	1.172 <sup>76</sup>	
		$ZnPor^{2+} + e^- \rightarrow ZnPor^+$	DCE	1.572 <sup>237</sup>	
			benzene	1.342 <sup>220</sup>	
			nitrobenzene	1.572 <sup>76</sup>	

<sup>a</sup>Abbreviations used: dimethylformamide (DMF), acetonitrile (MeCN), butyltriethylammonium bis(trifluoromethylsulfonyl)amide ( $[Et_3BuN][TFSI]$ ), propylene carbonate (PC), dichlorobenzene (DCB), benzonitrile (PhCN), chlorobenzene (PhCl), ethylene carbonate (EC), dichloromethane (DCM), dichloroethane (DCE), *o*-nitrophenyloctyl ether (NPOE), trifluorotoluene (TFT), choline chloride tetrafluoroacetamide (ChCl TFA), 1-ethyl-3-methylimidazolium bis(trifluoromethylsulfonyl)imide ( $[Emi][TFSI]$ ), *N*-methyl-*N*-butylpyrrolidinium bis[(trifluoromethylsulfonyl)amide] ( $[Pyr][TFSI]$ ), 1-butyl-3-methylimidazolium bis(trifluoromethylsulfonyl)amide ( $[BMIM][TFSI]$ ), dimethyl sulfoxide (DMSO), and butyltriethylammonium bis(trifluoromethylsulfonyl)amide  $[Et_3BuN][NTf_2]$ . <sup>b</sup> $E_{tip}$  (potential applied at the tip). <sup>c</sup>Potential vs QRE. <sup>d</sup>Potential vs Fc/Fc<sup>+</sup>.

lateral electron transfer in the film. To specifically observe this lateral transport, the concentration of mediator in solution has to be reduced considerably. This is also the case when substrate reactions exhibit an equilibrium involving the mediator used in the SECM measurement.<sup>24</sup> Overall, the establishment of a concentration cell in the tip-to-substrate gap drives the lateral charge transport and interfacial reactions of the substrate.<sup>5</sup>

Finally, to investigate a complex sample with SECM, probes of different sizes should be used as they address different ranges of lateral resolution<sup>25</sup> and heterogeneous constants (Table 3 in ref 5). For example, as the electrode area shrinks, the mass transport from the solution becomes more efficient, increasing the background signal, and effectively competing with the reactant flux from the substrate, thereby decreasing the achievable contrast.

Since its inception, 133 molecules have been used or investigated with amperometric detection in SECM (molecules detected potentiometrically will be described in section 3.3.2). Several molecules have been used in more than one operational mode. Feedback mode has been used with the most mediators (102 mediators), followed by GC modes (45 mediators), and RC mode (7 mediators). Readers should note that the following descriptions should be used as a guideline and do not necessarily consist of universal statements that can be applied to all systems.

In feedback mode, a redox mediator should be a molecule or ion that undergoes oxidation and reduction reversibly (or quasi-reversibly). Furthermore, in order to investigate the reactivity of a substrate, the mediator being used should have fast heterogeneous kinetics at the SECM tip, such that substrate kinetics are rate limiting. In most cases, the tip reaction occurs through a one-electron process (>80% for feedback mode). The majority of molecules used in feedback mode are indirect redox mediators, since they are species that have been added to the solution. In summary, ideal mediator properties in feedback mode include electrochemical reversibility, fast heterogeneous kinetics at the SECM tip, and a one-electron reaction.

Feedback and GC share 17 mediators which have been used in both modes. Unlike feedback mode, more than half of the GC mode mediator electrochemical reactions involve two or more electrons. Species measured in GC mode can be produced by several different pathways:

- homogeneous chemical reactions with other molecules in solution (e.g.,  $A + B \rightarrow C$ )

- homogeneous chemical reactions at a substrate (e.g., enzymatic reactions)
- heterogeneous electrochemical reactions at a substrate

As for RC mode, the limited number of redox mediators (7) have also all been used in GC mode. Consequently, the properties they share are identical.

Tables 1–4 present an exhaustive compilation of all the molecules/atoms that have been used or investigated in SECM experiments from 1989 to 2015. They have been divided according to the SECM mode in which they were employed, with several molecules being used in multiple modes. Tables have been ordered alphabetically in terms of mediator abbreviations. For each molecule, the associated electrochemical reactions, the standard redox potential in specific solvents, and SECM applications are given.

Potentials have been adjusted from the original publication, considering reference electrode type and electrolyte concentrations, in order to be reported versus a normal hydrogen electrode (NHE). However, in certain cases this was not possible, and some redox potentials are given versus a quasi-reference electrode or the ferrocene/ferrocenium ( $Fc/Fc^+$ ) standard couple, and readers should refer to the original publication for exact experimental conditions. Furthermore, if the standard redox potential was unavailable or undefined, the potential applied at the tip during experimentation ( $E_{tip}$ ) is given. Also, in cases where pH sensitivity is pertinent, readers should assume that all potentials are reported for measurement at pH 7.

The last column of each table describes all the applications in which each mediator has been used. These include the following possible classifications: biological, catalysis, kinetics, corrosion, energy, enzymes, interface between two immiscible electrolyte solutions (ITIES), living cell, and surface modification (SM). Although some of these categories are related, we believe that it is much more useful to show specific terms such as “living cell” instead of simply “biological”. Representative references are also provided for each application.

The choice of redox mediator for the investigation of a specific system can affect the local electrochemistry of the substrate. By answering the following questions, the choice of possible mediator begins to narrow:

- Which SECM mode will be used for measurement?
- Must an indirect redox mediator be added into the solution or can a direct mediator be used?
- Does the application have specific restrictions?

Table 2. Redox Mediators Used in Generation-Collection Mode SECM<sup>a</sup>

abbrev	mediator	redox reaction	solvent	$E^0$ (V vs NHE)	application
A	anethole	$A + e^- \rightarrow A^{*-}$	MeCN	1.641 <sup>238</sup>	kinetics <sup>238</sup>
ABTS	2,2'-azino-bis(3-ethylbenzothiazoline-6-sulfonate)	$ABTS + e^- \rightarrow ABTS^{*-}$ $ABTS^{*-} + e^- \rightarrow ABTS^{2*-}$	aqueous	1.113 <sup>33</sup> 0.703 <sup>33</sup>	enzymes <sup>33,239</sup>
AQDS/AHQDS	anthraquinone-2,6-disulfonate	$AQDS + 2H^+ + 2e^- \rightarrow AHQDS$	aqueous	0.252 <sup>240</sup>	corrosion <sup>240</sup>
AQS/AHQs	anthraquinone-2-sulfonate	$AQS + 2H^+ + 2e^- \rightarrow AHQS$	aqueous	0.212 <sup>240</sup>	corrosion <sup>240</sup>
ArO	4-nitrophenolate	$ArO^* + e^- \rightarrow ArO^-$	MeCN	0.990 <sup>241</sup>	kinetics <sup>241</sup>
BH <sub>4</sub> <sup>-</sup>	borohydride	$BH_4^- + 8OH^- \rightarrow BO_2^- + 6H_2O + 8e^-$	aqueous	-0.087 <sup>242</sup>	kinetics <sup>242</sup>
BQ/HQ	benzoquinone/hydroquinone	$BQ + 2H^+ + 2e^- \rightarrow HQ$ $BQ + e^- \rightarrow BQ^{*-}$ $BQ^{*-} + e^- \rightarrow BQ^{2*-}$	aqueous MeCN PC	0.102 <sup>38</sup> -0.278 <sup>30</sup> -1.000 <sup>639</sup>	biological <sup>243-245</sup> enzymes <sup>243,246</sup>
BQSA/HQSA	benzoquinone sulfonic acid/hydroquinone sulfonic acid	$BQSA + 2H^+ + 2e^- \rightarrow HQSA$	aqueous	0.812 <sup>240</sup>	corrosion <sup>240</sup>
Br	bromine	$Br_2 + 2e^- \rightarrow 2Br^-$ $Br_3^- + 2e^- \rightarrow 3Br^-$ $3Br_2 + 2e^- \rightarrow 2Br_3^-$	aqueous MeCN MeCN	1.082 <sup>43</sup> 1.293 <sup>44</sup> 1.663 <sup>44</sup>	corrosion <sup>247</sup> kinetics <sup>43,45</sup>
Cl	chlorine	$Cl_2 + 2e^- \rightarrow 2Cl^-$	aqueous	1.367 <sup>55</sup>	catalysis <sup>248</sup>
CO <sub>2</sub>	carbon dioxide	$CO_2 + 2H^+ + 2e^- \rightarrow HCOOH$	aqueous	-0.278 <sup>249</sup>	catalysis <sup>249</sup>
Cu	copper	$Cu^{2+} + e^- \rightarrow Cu^+$ $Cu^{2+} + 2e^- \rightarrow Cu$ $Cu^+ + e^- \rightarrow Cu$	aqueous	0.773 <sup>250</sup> 0.953 <sup>250</sup> 1.133 <sup>250</sup>	SM <sup>251,252</sup>
DA/DOQ	dopamine/dopamine- <i>o</i> -quinone	$DOQ + 2H^+ + 2e^- \rightarrow DA$	aqueous	1.087 <sup>67</sup>	kinetics <sup>253</sup>
DF	dimethyl fumarate	$DF + e^- \rightarrow DF^{*-}$	DMF	-1.100 <sup>c11</sup>	kinetics <sup>11</sup>
DHBA	2,3-dihydroxybenzoic acid	$DHBA_{[-2H^+]} + 2H^+ + 2e^- \rightarrow DHBA$	aqueous	0.872 <sup>253</sup>	kinetics <sup>253</sup>
DMA	<i>N,N</i> -dimethylaniline	$DMA^{*+} + e^- \rightarrow DMA$	MeCN	0.920 <sup>b88</sup>	kinetics <sup>88</sup>
DMPPD	<i>N,N</i> -dimethyl- <i>p</i> -phenylenediamine	$DMPPD^+ + H^+ + 2e^- \rightarrow DMPPD$	aqueous	0.297 <sup>85</sup>	kinetics <sup>254</sup>
DTBN	di- <i>tert</i> -butyl nitroxide	$DTBN^{*+} + e^- \rightarrow DTBN$	MeCN	0.550 <sup>c255</sup>	kinetics <sup>255</sup>
EP/EPQ	epinephrine/epinephrinequinone	$EPQ + 2H^+ + 2e^- \rightarrow EP$	aqueous	0.341 <sup>256</sup>	kinetics <sup>256,257</sup>
Fc	ferrocene	$Fc^+ + e^- \rightarrow Fc$	MeCN DCM DMF PC ChCl TFA	0.665 <sup>90</sup> 0.651 <sup>71</sup> 0.691 <sup>91</sup> 0.175 <sup>92</sup> 0.522 <sup>93</sup>	kinetics <sup>258</sup>
FcCOOH	ferrocenecarboxylic acid	$[FcCOOH]^+ + e^- \rightarrow FcCOOH$	aqueous	0.541 <sup>101</sup>	enzymes <sup>259</sup>
FcMeOH	ferrocenemethanol	$[FcMeOH]^+ + e^- \rightarrow FcMeOH$	aqueous DMF MeCN DCM ethylene glycol	0.500 <sup>115</sup> 0.661 <sup>116</sup> 0.672 <sup>117</sup> 0.691 <sup>116</sup> 0.280 <sup>c118</sup>	biological <sup>260,261</sup> enzymes <sup>262,263</sup> kinetics <sup>115,117</sup> living cell <sup>264</sup>
FcTMA	ferrocenylmethyl-trimethylammonium	$[FcTMA]^+ + e^- \rightarrow FcTMA$	aqueous	0.652 <sup>131</sup>	kinetics <sup>265</sup>
Fe	iron	$Fe^{3+} + e^- \rightarrow Fe^{2+}$ $Fe^{2+} + 2e^- \rightarrow Fe$	aqueous	0.772 <sup>135</sup> -0.447 <sup>266</sup>	corrosion <sup>267,268</sup> SM <sup>136,266,269</sup>
Fe(CN) <sub>6</sub>	hexacyanoferrate(III)	$[Fe(CN)_6]^{4+} + e^- \rightarrow [Fe(CN)_6]^{3+}$	aqueous	0.491 <sup>139</sup>	catalysis <sup>141</sup>
Fe(phen) <sub>3</sub>	iron(II) tris(1,10-phenanthroline)	$[Fe(phen)_3]^{3+} + e^- \rightarrow [Fe(phen)_3]^{2+}$	aqueous	1.241 <sup>155</sup>	kinetics <sup>258</sup> kinetics <sup>270</sup>
FN	fumaronitrile	$FN + e^- \rightarrow FN^{*-}$	DMF	-1.100 <sup>c11</sup>	kinetics <sup>11</sup>
H	hydrogen	$2H^+ + 2e^- \rightarrow H_2$	aqueous	0.000 <sup>159</sup>	SM <sup>16</sup> corrosion <sup>271,272</sup> kinetics <sup>273</sup>
HAuCl <sub>4</sub>	chloroauric acid	$AuCl_4^- + 3e^- \rightarrow Au + 4Cl^-$	aqueous	1.308 <sup>274</sup>	SM <sup>274-276</sup>
H <sub>2</sub> O <sub>2</sub>	hydrogen peroxide	$O_2 + 2H^+ + 2e^- \rightarrow H_2O_2$	aqueous	0.670 <sup>165</sup>	corrosion <sup>135</sup> energy <sup>167</sup> enzymes <sup>14,277</sup> kinetics <sup>278,279</sup>
I	iodide	$I_3^- + 2e^- \rightarrow 3I^-$ $I_2 + 2e^- \rightarrow 2I^-$	aqueous MeCN aqueous	0.963 <sup>173</sup> 0.180 <sup>c174</sup> 0.532 <sup>43</sup>	corrosion <sup>43,173</sup>
Li	lithium	$Li^+ + e^- \rightarrow Li(Hg)$	PC	-2.032 <sup>89</sup>	energy <sup>89,280</sup>



Table 2. continued

abbrev	mediator	redox reaction	solvent	$E^0$ (V vs NHE)	application
MD/MDH <sub>2</sub>	menadione/menadiol	$\text{MD} + 2\text{H}^+ + 2\text{e}^- \rightarrow \text{MDH}_2$	aqueous	$-0.047^{191}$	kinetics <sup>281</sup> living cell <sup>191,282</sup>
MNZ	metronidazole	$\text{MNZ} + 2\text{H}^+ + 2\text{e}^- \rightarrow \text{MNZH}_2$	DMSO	$-0.848^{283}$	kinetics <sup>283</sup>
$\text{NO}_2^-$	nitrite	$\text{NO}_3^- + 2\text{H}^+ + 2\text{e}^- \rightarrow \text{NO}_2^- + \text{H}_2\text{O}$	aqueous	$1.400^{c266}$	SM <sup>266</sup>
$\text{O}_2$	oxygen	$\text{O}_2 + 2\text{H}^+ + 2\text{e}^- \rightarrow \text{H}_2\text{O}_2$	aqueous	$-0.387^{201}$	corrosion <sup>207,267</sup>
		$\text{O}_2 + 4\text{H}^+ + 4\text{e}^- \rightarrow 2\text{H}_2\text{O}$	aqueous	$-0.243^{111}$	energy <sup>284</sup>
		$\text{O}_2 + \text{e}^- \rightarrow \text{O}_2^{\bullet-}$	DMSO	$-0.498^{202}$	enzymes <sup>285</sup>
			DMF	$-0.097^{203}$	kinetics <sup>286</sup>
			IL	$-0.659^{204}$	living cell <sup>287</sup>
PAP/PQI	<i>p</i> -aminophenol/ <i>p</i> -quinone imine	$\text{PQI} + 2\text{H}^+ + 2\text{e}^- \rightarrow \text{PAP}$	aqueous	$0.493^{288}$	enzymes <sup>289,290</sup> kinetics <sup>288</sup> living cell <sup>291,292</sup>
Pa824	protemanid	$\text{Pa824} + \text{e}^- \rightarrow \text{Pa824}^{\bullet-}$	DMSO	$-0.978^{283}$	kinetics <sup>283</sup>
PYO	pyocyanin	$\text{PYO} + 2\text{H}^+ + 2\text{e}^- \rightarrow \text{PYOH}_2$	aqueous	$0.040^{213}$	biological <sup>213</sup>
RSSR/RSH	L-cystine/L-cysteine	$\text{RSSR} + 2\text{H}^+ + 2\text{e}^- \rightarrow \text{RSH}$	aqueous	$-1.30^{b293}$	catalysis <sup>293</sup>
Sn	tin	$\text{Sn}^{2+} + 2\text{e}^- \rightarrow \text{Sn}$	aqueous	$0.072^{294}$	kinetics <sup>294</sup>
		$\text{Sn}^{4+} + 2\text{e}^- \rightarrow \text{Sn}^{2+}$		$0.472^{294}$	
TCNQ	tetracyanoquinodimethane	$\text{TCNQ} + \text{e}^- \rightarrow \text{TCNQ}^{\bullet-}$	aqueous	$0.356^{230}$	
			DCE	$0.502^{146}$	corrosion <sup>295</sup>
			MeCN	$0.322^{30}$	kinetics <sup>230</sup>
			nitrobenzene	$0.100^{c231}$	
		$\text{TCNQ}^{\bullet-} + \text{e}^- \rightarrow \text{TCNQ}^{2-}$	DMF	$0.541^{32}$	
Th	thiodione	$\text{Th}^+ + \text{e}^- \rightarrow \text{Th}$	aqueous	$0.713^{b296}$	living cell <sup>191,297</sup>
Tl	thallium	$\text{Tl}^+ + \text{e}^- \rightarrow \text{Tl}(\text{Hg})$	aqueous	$-0.347^{298}$	kinetics <sup>298</sup>
TMPD	tetramethyl- <i>p</i> -phenylenediamine	$\text{TMPD}^{2+} + \text{e}^- \rightarrow \text{TMPD}^{\bullet+}$	aqueous	$0.668^{179}$	
		$\text{TMPD}^{\bullet+} + \text{e}^- \rightarrow \text{TMPD}$	aqueous	$0.258^{179}$	
			MeCN	$0.341^{100}$	kinetics <sup>11</sup>
			MeOH	$0.341^{100}$	
			DMF	$0.543^{11}$	
			DMSO	$0.482^{202}$	

Table 3. Redox Mediators Used in Redox Competition Mode SECM<sup>a</sup>

abbrev	mediator	redox reaction	solvent	$E^0$ (V vs NHE)	application
ABTS	2,2'-azino-bis(3-ethylbenzothiazoline-6-sulfonate)	$\text{ABTS} + \text{e}^- \rightarrow \text{ABTS}^{\bullet-}$ $\text{ABTS}^{\bullet-} + \text{e}^- \rightarrow \text{ABTS}^{2-}$	aqueous	$1.113^{33}$ $0.703^{33}$	enzymes <sup>33,239</sup>
Cl	chlorine	$\text{Cl}_2 + 2\text{e}^- \rightarrow 2\text{Cl}^-$	aqueous	$1.367^{55}$	catalysis <sup>248</sup>
Fe	iron	$\text{Fe}^{3+} + \text{e}^- \rightarrow \text{Fe}^{2+}$	aqueous	$0.772^{135}$	kinetics <sup>299</sup>
$\text{Fe}(\text{CN})_6$	hexacyanoferrate(III)	$[\text{Fe}(\text{CN})_6]^{4+} + \text{e}^- \rightarrow [\text{Fe}(\text{CN})_6]^{3+}$	aqueous	$0.491^{139}$	energy <sup>299</sup> catalysis <sup>300</sup>
H	hydrogen	$2\text{H}^+ + 2\text{e}^- \rightarrow \text{H}_2$	aqueous	$0.000^{159}$	corrosion <sup>301</sup>
$\text{H}_2\text{O}_2$	hydrogen peroxide	$\text{O}_2 + 2\text{H}^+ + 2\text{e}^- \rightarrow \text{H}_2\text{O}_2$	aqueous	$0.670^{165}$	energy <sup>167</sup>
$\text{O}_2$	oxygen	$\text{O}_2 + 2\text{H}^+ + 2\text{e}^- \rightarrow \text{H}_2\text{O}_2$	aqueous	$-0.387^{201}$	
		$\text{O}_2 + 4\text{H}^+ + 4\text{e}^- \rightarrow 2\text{H}_2\text{O}$	aqueous	$-0.243^{111}$	corrosion <sup>302,303</sup>
		$\text{O}_2 + \text{e}^- \rightarrow \text{O}_2^{\bullet-}$	DMSO	$-0.498^{202}$	energy <sup>304</sup>
			DMF	$-0.097^{203}$	kinetics <sup>12,305</sup>
			IL	$-0.659^{204}$	living cell <sup>287</sup>

<sup>a</sup>Abbreviations used: dimethylformamide (DMF), butyltriethylammonium bis(trifluoromethylsulfonyl)amide (IL).

- Can the mediator produce other side reactions at the substrate or at the tip (pH changes, phase changes, etc.)?

For example, using feedback mode limits the choice to mediators that display electrochemical reversibility. Next, the experimental system will determine whether a direct mediator (e.g., oxygen) is present in solution. It will also dictate whether electrochemically produced species can react with other solution components (homogeneous reactions) at the tip. Finally, the

application will determine if specific mediators can be used (e.g., nontoxic mediators must be used for live cells). In this capacity, Tables 1–4 provide a guide to which mediators have been used for a specific application, and can be used as an excellent starting point for experimental design.

### 3.2. Solvents

In any electrochemical experiment, including SECM, selection of the proper combination of a solvent and a supporting electrolyte,

Table 4. Redox Mediators Used in Other SECM Modes<sup>a</sup>

abbrev	mediator	redox reaction	solvent	$E^0$ (V vs NHE)	mode	application
Ag	silver	$\text{Ag}^+ + \text{e}^- \rightarrow \text{Ag}$	aqueous	0.611 <sup>306</sup>	ASV-SECM	biological <sup>307</sup>
APAP	<i>N</i> -acetyl- <i>p</i> -aminophenol (acetaminophen)	$[\text{APAP}]_{\text{ox}} + 2\text{H}^+ + 2\text{e}^- \rightarrow \text{APAP}$	aqueous	0.722 <sup>308</sup>	FSCV-SECM	biological <sup>85,309</sup>
Cd	cadmium	$\text{Cd}^{2+} + 2\text{e}^- \rightarrow \text{Cd}(\text{Hg})$	aqueous	-0.352 <sup>310</sup>	ASV-SECM	kinetics <sup>310–312</sup>
DMPPD	<i>N,N</i> -dimethyl- <i>p</i> -phenylenediamine	$\text{DMPPD}^+ + \text{H}^+ + 2\text{e}^- \rightarrow \text{DMPPD}$	aqueous	0.297 <sup>254</sup>	FSCV-SECM	kinetics <sup>86</sup>
FA	formic acid	$\text{FA}^+ + \text{e}^- \rightarrow \text{FA}$	aqueous	0.300 <sup>313</sup>	MD/SC	kinetics <sup>313</sup>
$\text{Fc}(\text{MeOH})_2$	ferrocenedimethanol	$[\text{Fc}(\text{MeOH})_2]^+ + \text{e}^- \rightarrow \text{Fc}(\text{MeOH})_2$	aqueous	0.442 <sup>128</sup>	SI-SECM	catalysis <sup>128</sup> kinetics <sup>314</sup>
Fe	iron	$\text{Fe}^{3+} + \text{e}^- \rightarrow \text{Fe}^{2+}$	aqueous	0.772 <sup>135</sup>	direct	kinetics <sup>315,316</sup>
Fe(EDTA)	iron(III) ethylenediaminetetraacetic acid	$[\text{Fe}(\text{EDTA})]^- + \text{e}^- \rightarrow [\text{Fe}(\text{EDTA})]^{2-}$	aqueous	0.120 <sup>153</sup>	SI-SECM	kinetics <sup>153</sup>
H	hydrogen	$2\text{H}^+ + 2\text{e}^- \rightarrow \text{H}_2$	aqueous	0.000 <sup>159</sup>	induced desorption	kinetics <sup>317</sup>
$\text{IrCl}_6$	iridium chloride	$[\text{IrCl}_6]^{2-} + \text{e}^- \rightarrow [\text{IrCl}_6]^{3-}$	aqueous	0.870 <sup>181</sup>	SI-SECM	energy <sup>181,318</sup> kinetics <sup>128</sup>
Li	lithium	$\text{Li}^+ + \text{e}^- \rightarrow \text{Li}(\text{Hg})$	PC	-2.032 <sup>89</sup>	ASV-SECM	energy <sup>89,280</sup>
Hg	mercury	$\text{Hg}_2^{2+} + 2\text{e}^- \rightarrow 2\text{Hg}$	aqueous	0.722 <sup>319</sup>	ASV-SECM	kinetics <sup>319</sup>
MV	methylviologen	$\text{MV}^{2+} + \text{e}^- \rightarrow \text{MV}^+$ $\text{MV}^+ + \text{e}^- \rightarrow \text{MV}$	aqueous	-0.446 <sup>159</sup> -0.663 <sup>192</sup>	induced transfer	biological <sup>320</sup>
Ni	nickel	$\text{Ni}^{2+} + 2\text{e}^- \rightarrow \text{Ni}(\text{Hg})$	aqueous	0.338 <sup>321</sup>	ASV-SECM	corrosion <sup>321</sup>
Pb	lead	$\text{Pb}^{2+} + 2\text{e}^- \rightarrow \text{Pb}(\text{Hg})$	aqueous	-0.121 <sup>310</sup>	ASV-SECM	kinetics <sup>310,322</sup>
$\text{Ru}(\text{bpy})_3$	tris(2,2'-bipyridine)ruthenium(II)	$[\text{Ru}(\text{bpy})_3]^{3+} + \text{e}^- \rightarrow [\text{Ru}(\text{bpy})_3]^{2+}$	MeCN	1.556 <sup>216</sup>	ECL-SECM	kinetics <sup>216,217</sup>
			aqueous	1.501 <sup>217</sup>		
TMPD	tetramethyl- <i>p</i> -phenylenediamine	$\text{TMPD}^{2+} + \text{e}^- \rightarrow \text{TMPD}^+$ $\text{TMPD}^+ + \text{e}^- \rightarrow \text{TMPD}$	aqueous	0.668 <sup>179</sup>	SI-SECM	kinetics <sup>323</sup>
			aqueous	0.258 <sup>179</sup>		
			MeCN	0.341 <sup>100</sup>		
			MeOH	0.341 <sup>100</sup>		
			DMF	0.543 <sup>11</sup>		
			DMSO	0.482 <sup>202</sup>		
TEMPO	2,2,6,6-tetramethylpiperidine 1-oxyl	$\text{TEMPO}^{*+} + \text{e}^- \rightarrow \text{TEMPO}$	aqueous	0.666 <sup>18</sup>	FSCV-SECM	kinetics <sup>324</sup>
Zn	zinc	$\text{Zn}^{2+} + 2\text{e}^- \rightarrow \text{Zn}(\text{Hg})$	aqueous	-0.578 <sup>325</sup>	ASV-SECM	corrosion <sup>312,325</sup>

<sup>a</sup>Abbreviations used: anodic stripping voltammetry (ASV), fast scan cyclic voltammetry (FSCV), micropipet-delivery/substrate-collection (MD/SC), surface interrogation (SI), propylene carbonate (PC), acetonitrile (MeCN), electrogenerated chemiluminescence (ECL), and dimethylformamide (DMF).

defined here as the solvent system, is important. While an in-depth discussion of electrochemical solvent system properties is beyond the scope of this review, it is useful to briefly consider several aspects during experimental design, especially in the context of SECM measurements.

The first important parameter, conductivity of the solvent system (inversely referred to as solution resistance), relies on the addition of excess amounts of a supporting electrolyte (typically dissolved salts, e.g. KCl). The role of this supporting electrolyte is particularly important, since it supports current flow between electrodes by minimizing solution resistance and effectively eliminates the contribution of migration during treatment of SECM data. From Tables 1–4, >99% of all SECM experiments were carried out in >0.1 mM electrolyte concentration.<sup>326</sup>

It should be noted that significant changes in the concentration of the supporting electrolyte can cause variations in solution conductivity and result in misinterpretation of data. Evidently, the ability of the solvent to dissolve both the supporting electrolyte and the redox mediator (i.e., solubility) should also be considered, especially when significant changes in concentration could occur during the experiment (e.g., SG/TC). The reactivity or stability of the solvent system is perhaps the most important parameter in terms of SECM measurements. This reactivity is often interpreted in terms of the potential window, defined as the potential range in which the experimental system remains electrochemically inert. SECM measurement should be

performed within this potential window. Outside these three parameters, the choice of solvent system is often restricted by the application, such as biological measurements involving live cells.

Predictably, most SECM experiments are performed in aqueous solution (~91%), albeit with varying electrolytes and pH. However, limitations such as a relatively small potential window have resulted in the use of several organic solvents such as acetonitrile (MeCN; ~5%), dichloroethane (DCE; ~3.7%), and dimethylformamide (DMF; ~2.3%). Investigation of electron and ion transfer processes in biphasic systems (i.e., ITIES measurements) have also used even less conventional solvents, including benzene,<sup>147</sup> DMSO,<sup>122</sup> and heptane.<sup>327</sup> Furthermore, the use of ionic liquids as solvents in SECM has also been explored (~12 publications) and recently reviewed.<sup>328</sup>

In total, 23 different solvents have been used in SECM experiments (considering different aqueous combinations as a single solvent). Figure 4 illustrates the useful potential window for most of these solvents (data was not available for decane,<sup>329</sup> dichlorohexane,<sup>330</sup> heptane,<sup>327</sup> and methanol<sup>79</sup>). The potentials are reported with respect to a specific electrode material, noted in parentheses, and with a particular supporting electrolyte. In the case where full potential windows are not described or are not available, experimental parameters are given from a specific publication in SECM literature. Consequently, the actual potential window may be wider than reported. Readers should

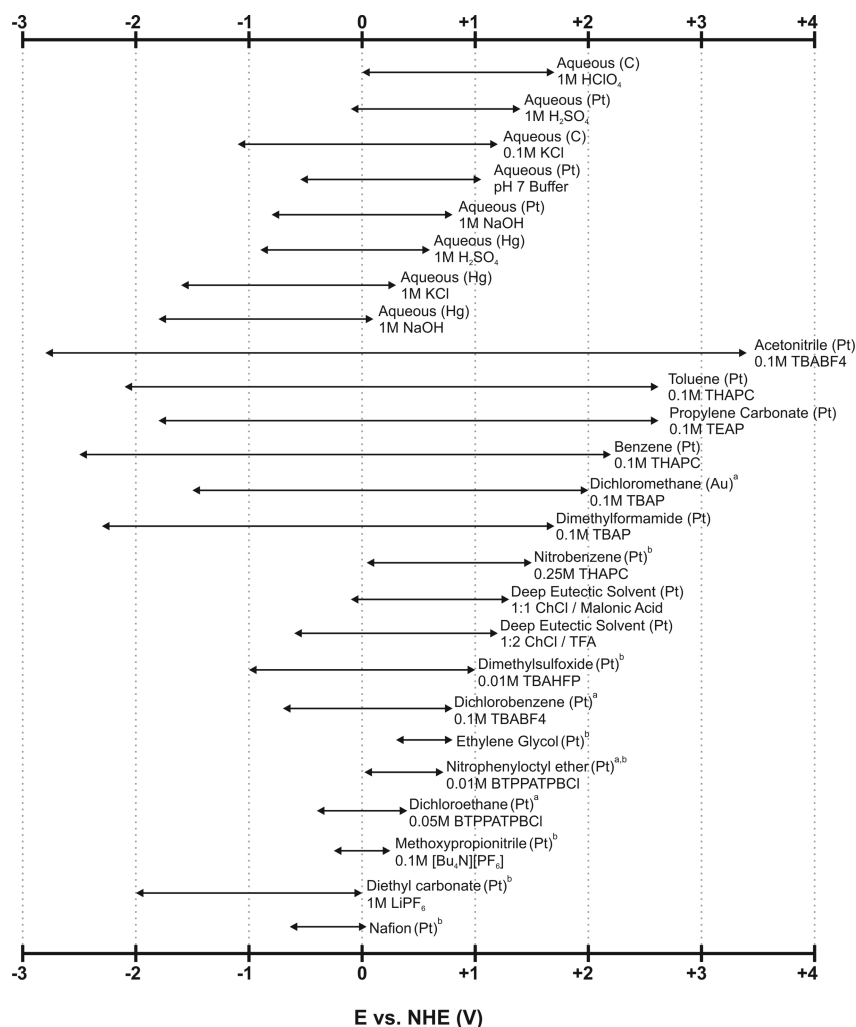


**Figure 4.** Potential windows for all solvent systems used in SECM measurements from 1989 to 2015. The active material of the working electrode is indicated in brackets. <sup>a</sup>Potential vs quasi-reference electrode. <sup>b</sup>Potential range used during experiment; full window may be wider. Abbreviations used: TBABF<sub>4</sub>, tetra-*n*-butylammonium tetrafluoroborate; THAPC, tetrahexylammonium perchlorate; TEAP, tetraethylammonium perchlorate; TBAP, tetrabutylammonium perchlorate; ChCl, choline chloride; TFA, trifluoroacetic acid; TBAHFP, tetrabutylammonium hexafluorophosphate; BTPPATPBCl, bis(triphenylphosphoranylidene)ammonium tetrakis(4-chlorophenyl)borate.

also note that a change in electrolyte and probe could result in a change of the potential window.

### 3.3. Probes

The last important parameter to consider for the design of a successful SECM experiment is the probe. The spatial resolution of a SECM measurement is strongly dependent on the dimensions of the probe, and consequently, a significant amount of SECM literature has focused on the design and fabrication of sophisticated small scale tips with sizes in the low micrometer to nanometer range. Fabrication protocols and characterization techniques have been the subject of several reviews.<sup>331,332</sup> The small size of SECM tips also provides several other advantages including fast steady-state response and low *iR* drop. Readers should note that the term “ultramicroelectrode” is commonly used in SECM literature, and it is defined as an electrode with at least one dimension smaller than 25  $\mu\text{m}$ .<sup>333</sup>

SECM tips can generally be divided into two different types: amperometric and potentiometric. Each type has its own strengths and weaknesses, but the vast majority of SECM measurements have been performed with amperometric probes (>99%), compared to their potentiometric counterparts (<1%).

Amperometric probes have many advantages, including high robustness (i.e., they can function for several years if properly manipulated), fast response times ( $\sim$ nanoseconds to milliseconds), and relative ease in probe positioning. However, this type of probe suffers from low selectivity, such that the measured signal can be a convolution of several different faradaic processes. In this context, potentiometric probes provide the significant advantage of high selectivity toward a specific analyte. Additionally, the analyte concentration and oxidation state remain unchanged during measurement, allowing minimal disturbance to the experimental system. However, unlike amperometric tips, potentiometric probes suffer from relatively slow response times ( $\sim$ milliseconds to seconds), small lifetimes (i.e., probe function degrades within a few weeks), and difficult probe positioning.

After a significant effort in the miniaturization of SECM tips (i.e., nanometer-sized electrodes down to 3 nm),<sup>123,334,335</sup> recent years have seen an increase in the development of combined probes, such as those used for scanning ion conductance microscopy (SICM-SECM) and atomic force microscopy (AFM-SECM). Advancements in the fabrication of these combined probes have been recently reviewed and will thus only be minimally discussed here.<sup>336</sup> Nevertheless, a general



overview of all the probes that have been used in SECM will be given.

**3.3.1. Amperometric Probes.** As the name implies, the recorded signal with an amperometric probe is a current, produced by a faradaic reaction occurring at the SECM tip. These probes typically consist of an electroactive core surrounded by an insulating sheath (e.g., glass). The size of these tips can vary over the low micrometer ( $\leq 25\ \mu\text{m}$ ) to nanometer scale. Several different geometries have been elucidated over the years, including conical,<sup>337</sup> hemispherical,<sup>338</sup> ring,<sup>339</sup> and ring-disk.<sup>27</sup> However, the most common geometry is definitely disk microelectrodes.<sup>340</sup>

Perhaps the most important component of SECM tip geometry is the ratio between the insulating sheath (e.g., glass) and the electroactive core, defined as the RG. A smaller RG decreases the risk of tip crashing during experimentation and controls the amount of back diffusion. For example, at  $L = 0.1$  over an insulating surface, the current at a microelectrode with an  $\text{RG} = 2$  is 91% higher than with an  $\text{RG} = 10$ , which demonstrates a tremendous difference that back diffusion has on the recorded current.<sup>341,342</sup> For this reason, although early SECM experiments used microelectrodes with an  $\text{RG} = 10$  (obtained through extensive manual polishing), recent literature shows an increase in the use of small RG electrodes ( $\text{RG} < 3$ ).

Although the RG is a dominant geometrical parameter for microdisk tips, other geometries (hemispherical, conical, beveled) can be strongly influenced by additional parameters such as recession/protrusion, bluntness, aspect ratio, insulation angle, off-center positioning of the metal wire, uneven insulation, insulation gaps, and cracks. Their weighted impact on the tip response is best deconvoluted using numerical simulations. For example, Denuault and co-workers demonstrated that, in the case of conical tips, the importance of the above-mentioned parameters varied greatly with the aspect ratio and that generally the relative differences became larger as the dimensions of the tips became smaller.<sup>342</sup> They found that bluntness, insulation defects/cracks, and uneven insulation had significant impact because they lead to an increase in the electroactive area, whereas off-centering of the metal wire had minimal effect. For microdisks, off-centering and insulation angle variations can have detrimental effects during the quantitative high-speed SECM measurements.<sup>25,343</sup>

Some examples of frequently used SECM tip geometries are shown in Figure 5. The electroactive material can vary, but the most popular electrode cores are platinum (74%), carbon (10.8%), gold (9.5%), mercury (2.1%), and silver (1.7%). Disk microelectrodes composed of these materials can be fabricated in-house using relatively simple protocols, but they are also commercially available (excluding Hg) from several sources (e.g., CH Instruments, Heka Elektronik, Metrohm, and Sensolytics), with prices between US\$140 and 400 per probe.<sup>340</sup>

The use of some less-common cores has also been reported. For example, cobalt and tungsten microelectrodes were used for surface patterning applications,<sup>16,136</sup> whereas aluminum was used to study corrosion processes.<sup>347</sup> Gallium was also used as the amperometric component in a combined amperometric–potentiometric probe,<sup>348</sup> and a manganese microelectrode was used to investigate multireactional electrochemical interfaces.<sup>349</sup>

Despite extensive use of SECM to study the enzymatic activity of a substrate, only a limited number of reports describe the use of amperometric biosensors, whereby an enzyme is immobilized onto the surface of an electrode. This most likely is the result of relatively slow response times and difficulty in achieving

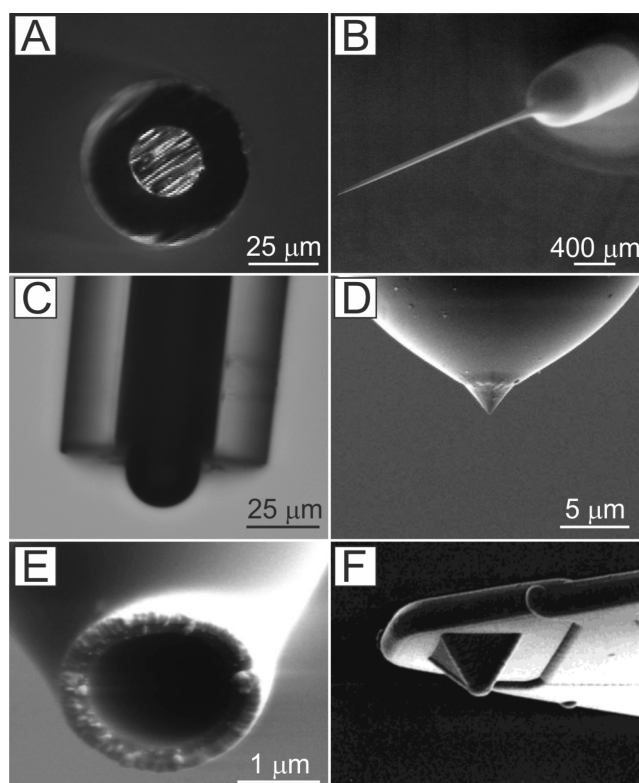


**Figure 5.** Examples of SECM tip geometries. (A) 25  $\mu\text{m}$  Pt disk microelectrode. (B) 200 nm Pt disk nanoelectrode. (C) 25  $\mu\text{m}$  Hg hemispherical microelectrode. (D) Au conical microelectrode. (E) 0.7  $\mu\text{m}$  Au ring microelectrode. (F) AFM-SECM tip with 100 nm Au layer. (A and C) Reprinted from ref 340. Copyright 2015 American Chemical Society. (B) Reprinted with permission from ref 334. Copyright 2002 John Wiley & Sons, Ltd. (D) Reprinted with permission from ref 344. Copyright 2004 Elsevier Ltd. (E) Reprinted from ref 345. Copyright 2005 American Chemical Society. (F) Reprinted from ref 346. Copyright 2001 American Chemical Society.

reproducible enzyme deposition. Nevertheless, glucose oxidase has been immobilized on carbon,<sup>350</sup> gold,<sup>351</sup> and platinum microelectrodes.<sup>165</sup> Glucose and lactate concentration profiles above living cells (fibroblasts) were imaged using enzymatic biosensors.<sup>352</sup> Using a dual probe containing both glucose oxidase and hexokinase, the release of adenosine-5'-triphosphate (ATP) was measured above bone cells. Therefore, although the number of reports is limited, enzymatic amperometric probes (i.e., biosensors) can also be used in the context of SECM.

**3.3.2. Potentiometric Probes.** The second category of SECM probes is potentiometric. These types of probes have predominantly been used in either corrosion,<sup>353,354</sup> kinetics,<sup>348,355</sup> or biological measurements.<sup>356,357</sup> In more than 50% of potentiometric mode publications, they are used for localized pH measurements. Table 5 shows all the potentiometric probes that have been reported in SECM literature, classified according to the ion of interest. The ion-selective component, the response time (when available), and example references for each type of probe are also provided.

## 4. APPLICATIONS

The versatility of SECM has allowed it to expand into a wide variety of applications, which were summarized in Figure 1. In the last five years, approximately 100 manuscripts per year have been published focusing on SECM. Areas such as corrosion and

Table 5. Probes Used in Potentiometric Mode SECM

ion of interest	ion-selective component	response time <sup>a</sup>	ref
ammonium (NH <sub>4</sub> <sup>+</sup> )	nonactin	300 ms ( $\tau_{100}$ )	358
calcium (Ca <sup>2+</sup> )	ETH1001	N/A	357
	ETH129	N/A	359
carbon dioxide (CO <sub>2</sub> )	antimony	N/A	360
chloride (Cl <sup>-</sup> )	chloride ionophore I	710 ms ( $\tau_{95}$ )	354
	ETH9009	710 ms ( $\tau_{95}$ )	
copper (Cu <sup>2+</sup> )	AgCl	1 s ( $\tau_{95}$ )	361
	tetraethylthiuram disulfide	16 s ( $\tau_{90}$ )	355
hydrogen (H <sup>+</sup> )	antimony	N/A	362
	ETH1907	1 s ( $\tau_{90}$ )	363
	IrOx	10 s ( $\tau_{90}$ )	17
	PtOx	30 ms	364
magnesium (Mg <sup>2+</sup> )	bis- <i>N,N</i> -dicyclohexyl-malonamide	27.7 s ( $\tau_{95}$ )	365
potassium (K <sup>+</sup> )	BME 44	300 ms ( $\tau_{100}$ )	358
	valinomycin	N/A	356
	DB18C6	N/A	366
silver (Ag <sup>+</sup> )	AgI	N/A	367
sodium (Na <sup>+</sup> )	ETH157		
	bis[(12-crown-4) methyl] dodecylmethylmalonate		
	bis[(12-crown-4) methyl] 2,2-didodecylmalonate	640 ms ( $\tau_{95}$ )	354
	4- <i>tert</i> -butylcalix[4]arene-tetraacetic acid tetraethylester		
zinc (Zn <sup>2+</sup> )	<i>N,N'</i> -dicyclohexylbisamide	300 ms ( $\tau_{100}$ )	358
	<i>N</i> -phenyliminodiacetic acid bis- <i>N,N'</i> -dicyclohexylamide	N/A	353

<sup>a</sup>Response time ( $\tau$ ) is defined as the time needed to attain a certain percentage of the peak signal. The reporting method varies in each publication such that the peak percentage used is shown in parentheses. For example,  $\tau_{90}$  corresponds to time required to attain 90% of the peak signal. N/A is shown when data was not available in the original publication.

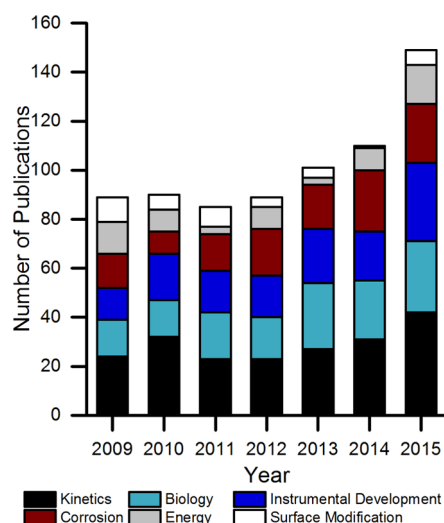


Figure 6. Experimental SECM publications from 2009 to 2015, divided by application.

energy have showed increasing interest as they gain public attention, while surface modification using SECM is declining. Instrumental development remains a significant focus, particularly in terms of hyphenated techniques. Recent trends in SECM research have shifted more toward applications, but a significant amount of fundamental investigations are still being pursued. Figure 6 illustrates SECM publications over the last five years and provides a breakdown based on the application, with only experimental SECM manuscripts being considered. In the following sections, the various applications of SECM from 2009 to 2015 will be discussed, with pertinent application-specific reviews being provided. Additional information about the breadth of SECM applications can also be obtained in the SECM monograph.<sup>8</sup>

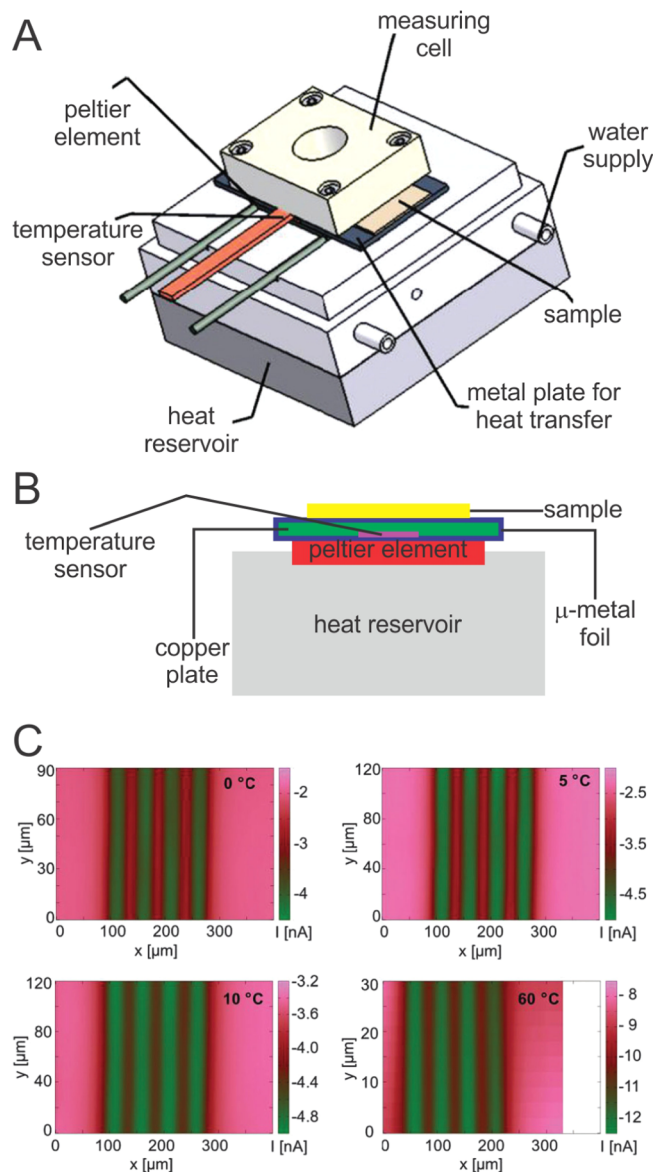
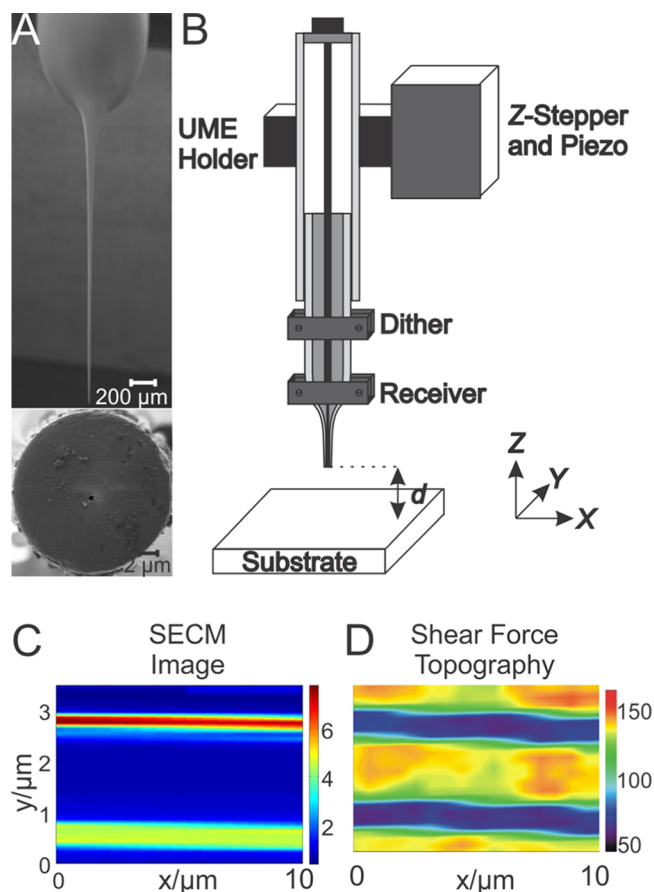


Figure 7. Schematic view of the temperature-controlled measuring cell (A) and its cross section (B). (C) Feedback-mode images of band electrodes at different temperatures (10  $\mu$ m Pt disk electrode, 5 mM Ru(NH<sub>3</sub>)<sub>6</sub><sup>3+</sup>, -350 mV vs Ag/AgCl,  $d = 6 \mu$ m). Reprinted with permission from ref 368. Copyright 2013 Royal Society of Chemistry.



**Figure 8.** (A) SEM images of the nanoelectrode tip from a side and perpendicular view to the electrode. (B) Scheme of the holder by which the piezoelectric plates are mechanically mounted to the nanoelectrode. The holder is attached to the Z-stepper motor of the SECM setup. (C) SECM image of a  $10\ \mu\text{m} \times 3.5\ \mu\text{m}$  portion of CD surface obtained with a 47 nm radius Pt microelectrode ( $RG = 5$ ). The scale bar represents current in nanoamperes. (D) Shear force topography image. The scale bar represents tip-to-substrate distance in nanometers. Reprinted with permission from ref 335. Copyright 2014 Elsevier Ltd.

#### 4.1. Instrumental Development

Perhaps the most important application of SECM has been the continuing effort in instrumental development. This consists of the establishment of additional operational modes, the fabrication of smaller and more sensitive probes, and, last but not least, the combination of SECM with complementary techniques. The former was described in section 3.3 and will thus only be minimally discussed here. In the last five years, instrumental development has comprised 19.6% of all SECM reports.

One variable that is often overlooked in SECM experiments is the temperature during measurement, which is assumed to simply be “room temperature”. Interestingly, Schuhmann and co-workers recently reported the development of a SECM system with a precise temperature control unit.<sup>368</sup> As shown by the schemes in Figure 7A,B, they integrated a heat reservoir, a Peltier element, a temperature sensor, and a water supply into their SECM system, allowing for controlled temperatures between 0 and  $100^\circ\text{C}$ . Using this experimental setup, the authors measured the electrochemical activity of Pt band electrodes at four different temperatures between 0 and  $60^\circ\text{C}$  (Figure 7C). Lower temperatures (0 and  $5^\circ\text{C}$ ) increased spatial

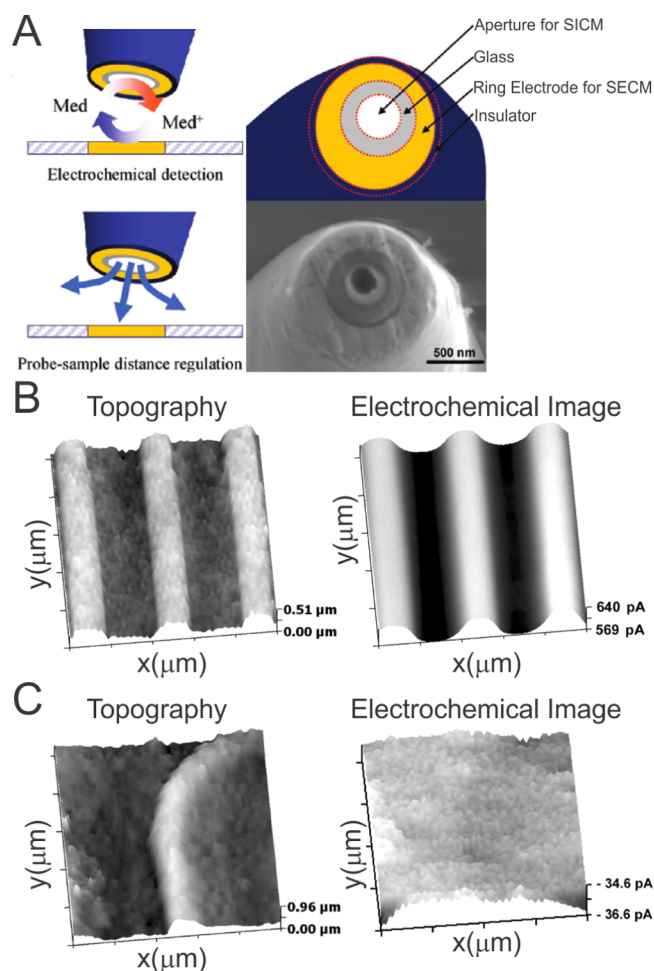


**Figure 9.** (A) Schematic illustration of the SECM-SICM system and probe with SEM micrograph of probe tip. (B) Topographic (left) and electrochemical (right) images of a Pt band microarray in  $0.50\ \text{mM}$  FcMeOH +  $0.1\ \text{M}$  KCl. The SECM nanoring and SICM nanopipet electrodes were held at 500 and 300 mV vs Ag/AgCl, respectively. Scan range was  $50\ \mu\text{m} \times 50\ \mu\text{m}$ . (C) Topographic (left) and electrochemical (right) images of a portion of the HRP spot immobilized on a glass substrate before adding  $0.5\ \text{mM}$   $\text{H}_2\text{O}_2$  in  $0.50\ \text{mM}$  FcMeOH and PBS. The SECM nanoring and SICM nanopipet electrodes were held at 50 and 300 mV vs Ag/AgCl, respectively. Scan range was  $50\ \mu\text{m} \times 50\ \mu\text{m}$ . Reprinted from ref 261. Copyright 2010 American Chemical Society.

resolution due to the decreased diffusion coefficient of the redox mediator. They also noted that future studies were necessary to evaluate the effect of natural and forced convection on image resolution. Although their study did not explicitly describe a new SECM operational mode, it did demonstrate the importance of temperature control, a concept which could be universally applied to all SECM experiments.

A significant portion of instrumental advancements have focused on the development of current decoupling methodologies in order to independently measure surface topography and electrochemical reactivity during SECM measurements, and this topic has recently been reviewed.<sup>369</sup> Several possibilities have been proposed, including but not limited to intermittent-contact SECM (IC-SECM),<sup>370</sup> hopping-intermittent-contact SECM (HIC-SECM),<sup>371</sup> and alternating-current SECM (AC-SECM).<sup>372,373</sup> However, the most prominent approach has been the utilization of shear-force SECM (SF-SECM),<sup>374–379</sup> developed by the Schuhmann research group.<sup>380,381</sup> In a recent



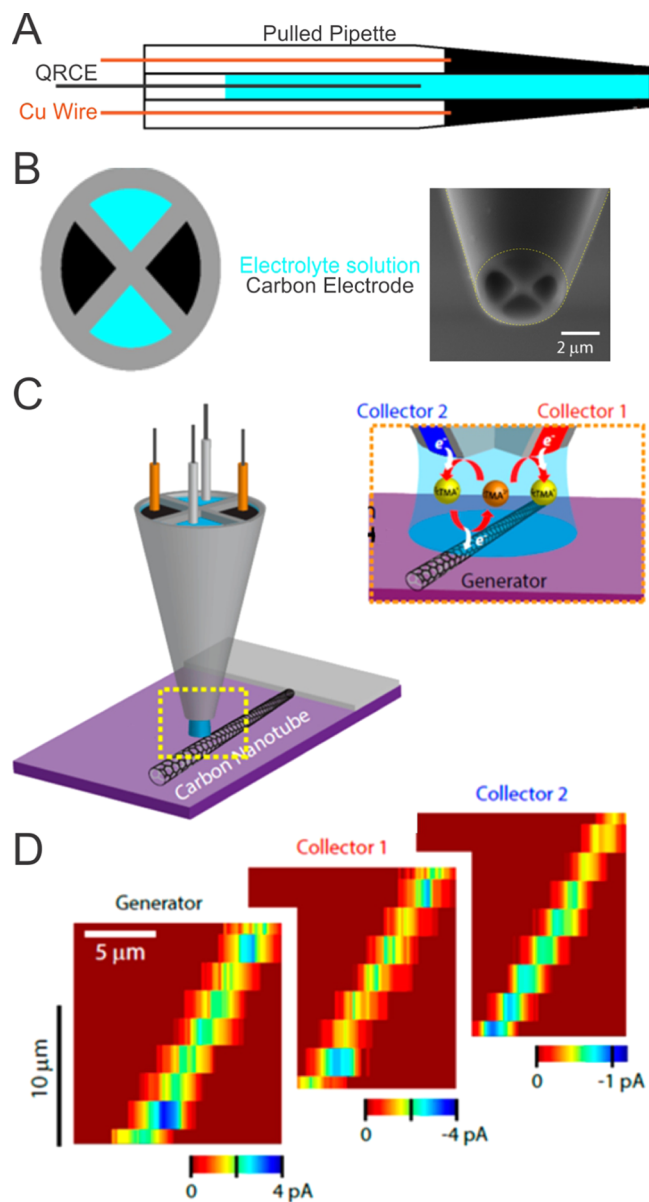


**Figure 10.** (A) Side view schematic of the fabricated quad probe with two open barrels filled with electrolyte, and AgCl coated Ag wire QRCEs. (B) Schematic top view of the fabricated quad probe with an SEM of a typical probe. (C) Schematic of imaging in surface generation/tip collection mode with a five-electrode configuration. The substrate (SWNT) was held at a potential that generated  $\text{FcTMA}^{2+}$ , while the two carbon electrodes in the probe were held at a potential to collect any  $\text{FcTMA}^{2+}$  produced. (D) Generator, Collector 1, and Collector 2 maps recorded on a SWNT. Adapted from ref 401. Copyright 2015 American Chemical Society.

example, Mauzeroll and co-workers demonstrated this concept by combining SF-SECM with disk nanoelectrodes to image surfaces with a constant distance between a probe and a substrate.<sup>335</sup> After fabrication of a Pt disk nanoelectrode (Figure 8A), they mounted two piezoelectric plates, one dither and one receiver, onto the shaft of the nanoelectrode, as shown in Figure 8B. A mechanical oscillation of known frequency was induced at the dither plate and detected at the receiver plate. Interaction between the nanoelectrode and a surface in close proximity dampens the oscillation. By varying the tip-to-substrate distance

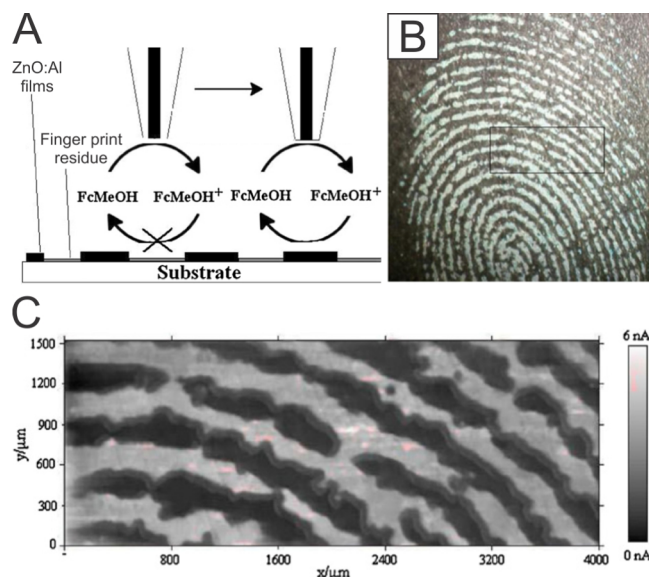


**Figure 11.** (A) Schematic (not to scale) diagram of SECM imaging of latent fingerprints. (B) Optical image of a ZAO-deposited fingerprint on glass. (C) High-resolution SECM image (4 mm × 1.5 mm) of sample with a scan rate of 320 μm s<sup>-1</sup>. The SECM image area corresponds approximately to the rectangular region marked in (B). The black and white lines correspond to the ridges and valleys, respectively. Measuring conditions: 25 μm Pt microelectrode, 2 mM  $\text{FcMeOH}$  in 0.1 M  $\text{KNO}_3$ ,  $E_{\text{probe}} = 0.3$  V vs Ag QRE, probe–substrate distance of approximately 10 μm. Total scan time takes ~40 min. Reprinted with permission from ref 411. Copyright 2012 Elsevier Ltd.

to maintain a specific oscillation frequency, independent images of surface topography and electrochemical activity were obtained, as shown in Figure 8C,D. Therefore, a significant improvement in SECM instrumentation has involved the integration of constant-distance hardware, such as shear-force units.

Another approach used for constant-distance measurements has been the combination of SECM with scanning ion conductance (i.e., SECM-SICM). Matsue and co-workers reported the fabrication of a nanopipet/nanoring probe allowing for simultaneous imaging of topography and electrochemical activity.<sup>261</sup> As shown in Figure 9A, this new probe consisted of a gold nanoring to be used as a SECM tip, while the nanoscale aperture was used for SICM distance regulation. Using this probe, the authors imaged the topography and electrochemical activity of Pt bands and HRP enzyme spots, as shown in Figure 9B,C. Interestingly, they demonstrated that if the image shown in Figure 9C would have been obtained using conventional GC mode with distance regulation, the response (caused here by topography) could have been misconceived to be due to enzymatic activity. Consequently, the authors demonstrated that their SECM-SICM methodology allowed them to obtain independent images of topography and electrochemical activity using a single probe.

Over the past several years, SECM instrumentation has been adapted and modified in order to be combined with several different techniques. Reported combinations include SECM with scanning force microscopy (SFM),<sup>25</sup> infrared attenuated total reflection spectroscopy,<sup>382,383</sup> scanning probe lithography (SPL),<sup>50</sup> impedance,<sup>384</sup> surface plasmon resonance (SPR),<sup>319,385</sup> scanning Kelvin probe (SKP),<sup>386,387</sup> scanning ion

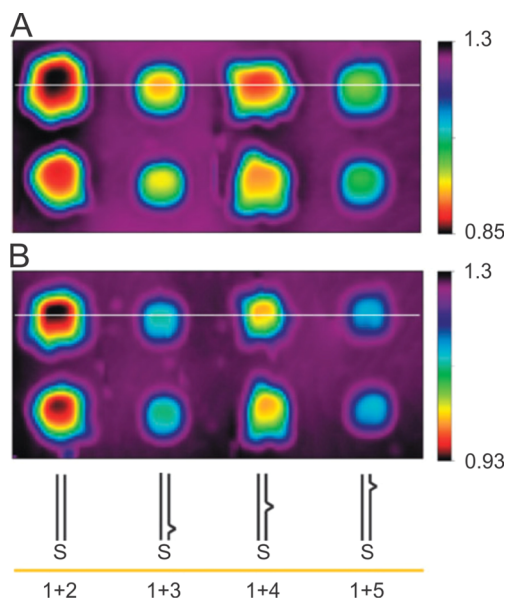


**Figure 12.** (A) Typical SECM image recorded over dsDNA microarray on Au substrate in the absence of  $\text{Zn}^{2+}$ . Each sample was spotted twice from left to right in the following order: 1 + 2, 1 + 3, 1 + 4, and 1 + 5. (B) Typical SECM image recorded above DNA microarray in the presence of  $\text{Zn}^{2+}$ . Data were obtained for the same sample as shown in (A) but after incubation in  $\text{Zn}(\text{ClO}_4)_2$  solution. Experiment carried out in 1 mM  $\text{K}_4\text{Fe}(\text{CN})_6$ , 50 mM  $\text{NaClO}_4$ , 20 mM Tris- $\text{ClO}_4$  (pH 8.6), with 25  $\mu\text{m}$  Pt tip,  $E_T = 0.5$  V vs Ag/AgCl. Adapted with permission from ref 419. Copyright 2009 The Royal Society of Chemistry.

conductance (SICM),<sup>388–391</sup> and fluorescence microscopy.<sup>392,393</sup> The most used combination has been SECM with atomic force microscopy (AFM).<sup>342,394–400</sup> As mentioned in section 3.3, the combination of these two techniques, particularly in terms of probe fabrication, has been recently reviewed and will thus not be discussed here.<sup>336</sup> On the other hand, Unwin and co-workers recently reported the fabrication of a “quad probe” in order to combine SECM with another technique, namely scanning electrochemical cell microscopy (SECCM).<sup>401</sup> As shown in Figure 10A,B, a four barrel pipet was pulled and cut using a focused ion beam (FIB). Two barrels were then filled

with carbon, acting as independent working electrodes, and the other two barrels were filled with electrolyte solution and Ag/AgCl QRCEs. The authors demonstrated the functionality of this newly developed probe by imaging the electrochemical activity of an individual single-walled carbon nanotube (SWNT) using a five-electrode configuration in a SECM-SECCM type measurement (Figure 10C). The images obtained for each working electrode are shown in Figure 10D, and demonstrate the feasibility of this combinatorial technique for high-resolution imaging of surfaces.

#### 4.2. Biological

Immediately after it was first reported, SECM was applied to a biological substrate to measure photosynthesis over a *Ligustrum sinensis* leaf (grass).<sup>140</sup> Since then, the application of SECM to the measurement of biological processes and systems has grown tremendously. A wide variety of biomolecules and substrates have been investigated including proteins (i.e., amino acids, peptides, and protein complexes), DNA, enzymes, and single cells. The latter two systems have been thoroughly explored and will be discussed in greater detail below (see sections 4.3 and 4.4). The importance of this application has not decreased within the past five years, and still represents 20.5% of SECM publications.

One emphasis of biological SECM measurements has been the characterization of proteins and their building blocks. Several different systems have been investigated in the past five years, including tryptophan (amino acid),<sup>402</sup> Tat(44–57) and melittin (peptides),<sup>403</sup> azurin (protein),<sup>404</sup> bacterial flagellin (protein),<sup>405</sup> cytochrome *c* (protein),<sup>406</sup> ovalbumin (protein),<sup>407</sup> and photosystem I (protein complex).<sup>193</sup> An interesting “real world” application involving proteins has been the analysis of latent fingerprints on various surfaces.<sup>408–410</sup> For example, Zhang and co-workers used direct current magnetron sputtering (based on vacuum metal deposition) to deposit a thin conductive film of Al-doped ZnO (ZAO) onto a surface containing a latent fingerprint.<sup>411</sup> The conductive ZAO film deposited only in the valleys of the fingerprint (i.e., bare surface), resulting in variations of conductivity. Using feedback mode (Figure 11A), they imaged a latent fingerprint with micrometer resolution (Figure 11B,C), demonstrating that areas with ZAO film displayed positive feedback behavior, while areas with fingerprint ridge residues

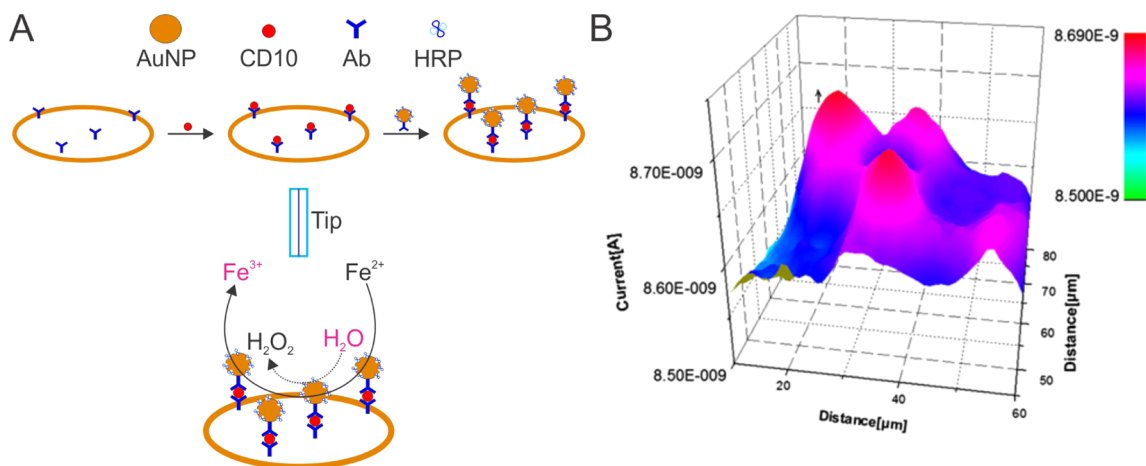


**Figure 13.** (A) Schematic of SECM imaging for binding reaction of CD10 and anti-CD10. (B) SECM SG/TC image displaying the reduction current collected for the modified electrode with CD10 antigen. The small arrows represent the binding of antigen and antibody, detected in a solution of 1 mM  $\text{H}_2\text{O}_2$ , PBS (0.01 M, pH 7.4) with 1.0 mM  $\text{Fe}(\text{CN})_6^{3-}$  and  $\text{Fe}(\text{CN})_6^{4-}$  containing 0.1 M KCl. Adapted with permission from ref 421. Copyright 2012 Elsevier Ltd.

displayed negative feedback behavior. The authors suggested that the use of SECM was advantageous when samples were under wet conditions or had a multicolor background. They did note that although their use of SECM for this measurement provided a higher sensitivity relative to optical microscopy, analysis time was unacceptably long. To remedy this limiting parameter, the authors proposed the use of linear microelectrode arrays to decrease total analysis time.

Immobilized DNA has been another major biological substrate investigated using SECM, and was first explored more than a decade ago.<sup>130,412</sup> More recently, the focus has been on the identification of mismatches in double-stranded DNA (dsDNA).<sup>413–418</sup> For example, Kraatz and co-workers demonstrated that the presence of  $\text{Zn}^{2+}$  ions allowed increased sensitivity for the detection of single-nucleotide mismatches along with their location in dsDNA.<sup>419</sup> They performed feedback approach curves and imaged an array of dsDNA spots with different mismatches, in the absence (Figure 12A) and presence of  $\text{Zn}^{2+}$  (Figure 12B). They showed that the presence of  $\text{Zn}^{2+}$  ions increased measured currents and suggested that this occurred because the ions reduced electrostatic repulsion between the phosphate backbone and the mediator, allowing for easier diffusion. Furthermore, they demonstrated that not only did the presence of a mismatch increase the heterogeneous rate constant, but the location of the mismatch within the dsDNA also had a significant effect, increasing the kinetic rate constant within higher mismatch positioning in the dsDNA.

The interaction between antigens and their antibodies has also been a focus for biological measurements.<sup>102,420</sup> Contrary to most reports using feedback mode to image a surface, Hu and co-workers used SG/TC mode to characterize the interaction of the CD10 antigen with its antibody (anti-CD10).<sup>421</sup> First, they attached anti-CD10 onto a gold electrode surface, followed by addition of CD10. They then exposed the modified electrode to a solution containing gold nanoparticles linked with more anti-CD10 and horseradish peroxidase (HRP), as shown in Figure 13A. By adding  $\text{Fe}(\text{CN})_6$  as an indirect redox mediator, the authors imaged a modified gold electrode surface without antigen and with antigen. The absence of antigen produced no current change over the entire surface, while an interaction with the antigen produced a large increase in current (Figure 13B), and it was concluded that binding was specific. Furthermore, by increasing the concentration of CD10 antigen, the current response increased linearly such that a dynamic range of 10–60 pM could be achieved. Therefore, the authors concluded that their sandwich immunoassay measured by SECM was useful for characterization of antibody interactions.

### 4.3. Enzymes

SECM has been extensively used to quantify the activity of various enzymes immobilized on several different surfaces.<sup>145,162</sup> Earlier work in this application has been thoroughly reviewed, dating back to 2001.<sup>422</sup> In that review, Wittstock describes in great detail the use of feedback and SG/TC modes for the measurement of enzymatic activity. Briefly, enzymatic activity determination using feedback mode is identical to the concept shown in Figure 3C. In this case, the conducting substrate is an immobilized enzyme, which allows for the regeneration of an indirect redox mediator. The magnitude of the positive feedback signal produced is correlated with the activity of the enzyme. Similarly, using SG/TC mode (see Figure 3D), the measurement of a local concentration profile can be correlated to the enzymatic activity. Although feedback mode provides a higher spatial

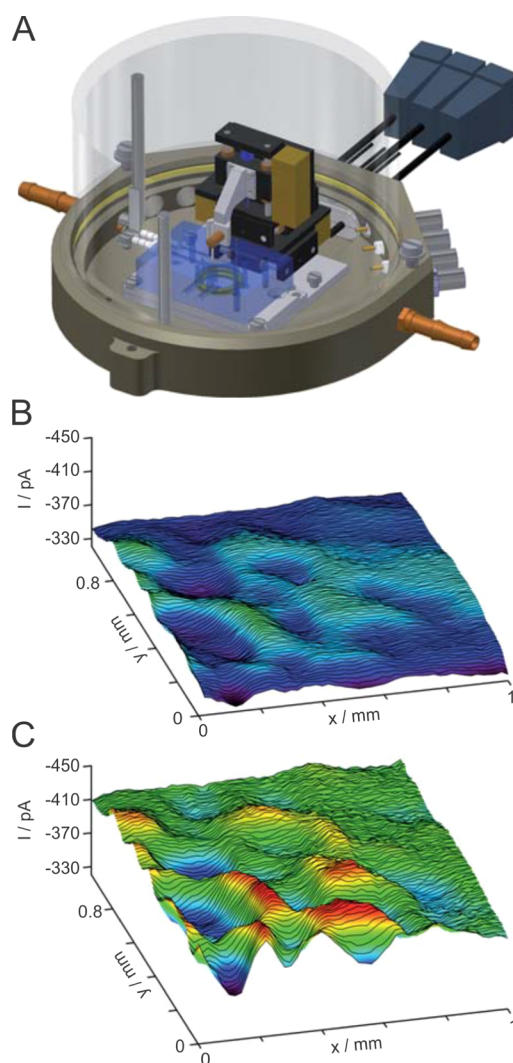


**Figure 14.** (A) SECM measurement head with controlled atmosphere. (B and C) SECM images of laccase–silicate film deposited on glass in 0.1 mM  $\text{K}_3\text{Fe}(\text{CN})_6$  in 0.1 M phosphate buffer, pH 4.8,  $E_T = 0$  V,  $a = 12.5$   $\mu\text{m}$ ,  $\text{RG} = 10$ ,  $\nu_T = 7.7$   $\mu\text{m s}^{-1}$ ,  $d = 20$   $\mu\text{m}$ : (B) Ar-saturated and (C)  $\text{O}_2$ -saturated solutions. Higher activity is shown as hills. Reprinted with permission from ref 41. Copyright 2010 The Royal Society of Chemistry.

resolution because the redox reactions only occur locally near the probe, SG/TC mode measurements allow for higher sensitivity since the background current is very low.<sup>422</sup>

In the past five years, the use of SECM for the study of enzymatic reactions has somewhat decreased, with only 23 investigations being reported ( $\sim 3.2\%$  of SECM reports). Following a more widespread use in its first two decades, where SECM studies were elaborated in order to demonstrate the applicability of the technique to various different enzymes, recent work has mostly focused on the use of SECM for optimization of enzymatic immobilization and bioassays, especially those involving glucose oxidase. For example, the robustness of a covalent immobilization protocol for glucose oxidase was investigated with the feedback mode of SECM. Using probe approach curves to extract Michaelis–Menten constants, Hapiot and co-workers demonstrated that the enzymatic activity of immobilized glucose oxidase remained comparable to enzyme in free solution even after their covalent



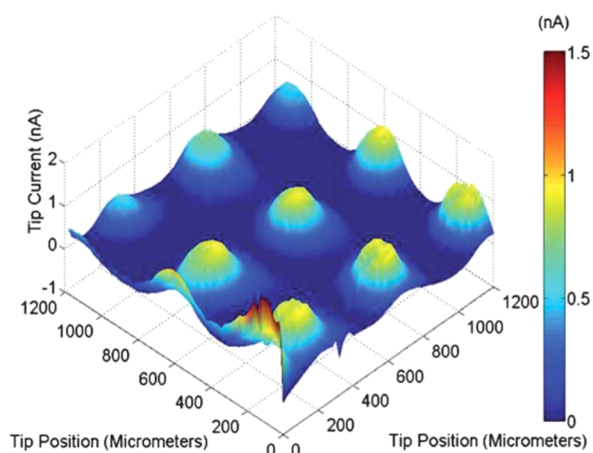


**Figure 15.** Background subtracted area scan over HRP modified array using pH 7.1 buffered solution containing 1 mM hydroquinone and 0.6 mM  $\text{H}_2\text{O}_2$ . Reprinted with permission from ref 246. Copyright 2011 The Royal Society of Chemistry.

immobilization protocol.<sup>423</sup> Similar uses of SECM for the characterization of the enzymatic activity have also been recently reported, namely for ceruloplasmin,<sup>424</sup> glucose oxidase,<sup>425</sup> horseradish peroxidase (HRP),<sup>426</sup> galactosidase,<sup>427</sup> and NADPH dehydrogenase.<sup>263</sup>

A particularly significant improvement on the use of SECM for enzymatic activity characterization was reported by Wittstock and co-workers.<sup>41</sup> As shown in Figure 14A, they developed an enclosed system such that the entire SECM measurement could be performed in a controlled atmosphere. Using feedback mode SECM with  $\text{Fe}(\text{CN})_6$  as an indirect redox mediator, they measured the enzymatic activity of laccase in oxygen-free (e.g., argon used) and oxygen-rich environments. As shown in Figure 14B,C, the presence of oxygen significantly increased the reductive current measured, demonstrating the role of oxygen in the enzymatic reaction of laccase. Additionally, the authors

used confocal laser scanning microscopy and SECM to compare the activities of codeposited laccase and bilirubin oxidase spots in solutions of varying pH, and determined that bilirubin oxidase was significantly more active than laccase at pH 7. The versatility of their methodology allows for improved characterization of the enzymatic behavior in various controlled environments.

Contrary to most recent reports describing enzymatic activity measurements, SECM has also been used for surface modification to produce arrays of enzymatic spots. Higson and co-workers used a 30  $\mu\text{m}$  diameter pulled microcapillary filled with HRP and a SECM system to deposit small enzyme droplets onto a silanized glass microscope slide in an array configuration.<sup>246</sup> Subsequently, the enzymatic activity of the immobilized enzyme spots was measured using SG/TC mode SECM, as shown in Figure 15. Using their deposition technique, the authors varied the concentration of enzyme in the microcapillary to investigate its effect on peak current signal, and determined that a plateau was reached at HRP concentrations greater than 1 mg/mL. Therefore, the authors were able to use SECM to both construct enzyme arrays and quantify enzymatic activity.

#### 4.4. Living Cell Studies

The application of SECM to the study of living cells, commonly referred to as Bio-SECM,<sup>428,429</sup> provides the extremely interesting advantage of high spatial resolution while being a relatively noninvasive technique. Initial reports investigated cellular respiration<sup>201,430</sup> and cancer cell redox activity.<sup>149</sup> Several reviews have focused on Bio-SECM investigations,<sup>9,431–435</sup> including a recent review in 2013 which looked at constant-distance methodologies for studying single cells.<sup>436</sup>

Over 70 studies focusing on Bio-SECM have been reported in the past five years, which represents  $\sim 10.2\%$  of SECM literature. A wide variety of experimental systems were investigated, including single cells (e.g., HeLa cells),<sup>437</sup> confluent cell monolayers,<sup>438</sup> and bacteria.<sup>439</sup> The source of the living cells has also not been limited to human species, and has also included

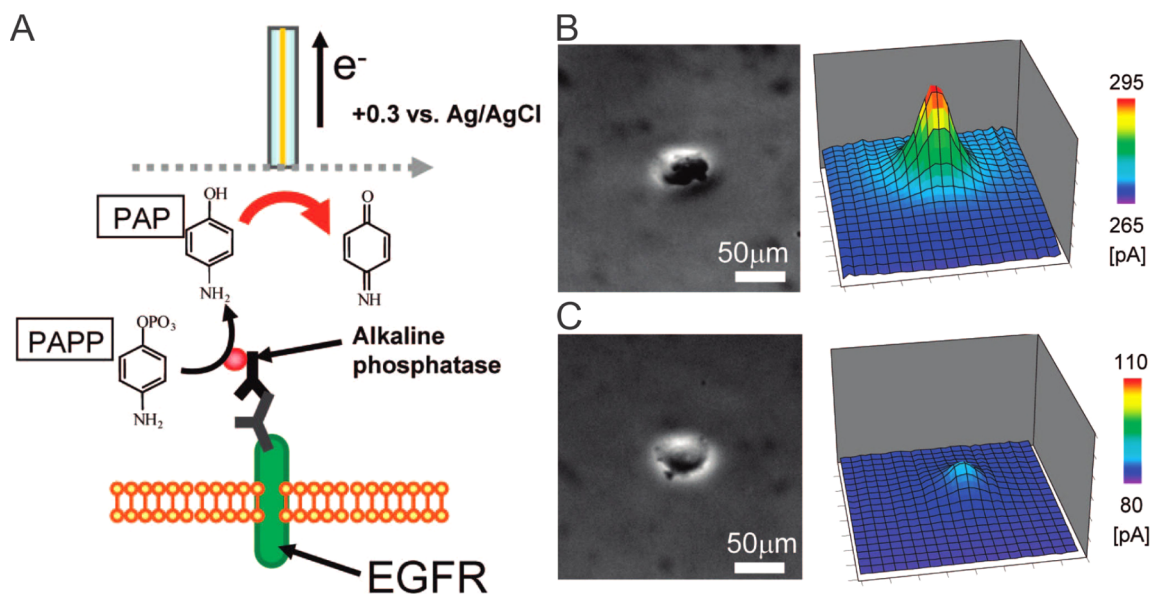


**Figure 16.** (A) Schematic diagrams of EGFR detection using generation-collection mode. SECM image in substrate generation/tip collection mode: (B) EGFR/CHO cell and (C) normal CHO cell. The electrode was set at 15  $\mu\text{m}$  above the substrate, and the scan rate was 5  $\mu\text{m s}^{-1}$ . The scan range was 200  $\mu\text{m} \times 200 \mu\text{m}$ , and the step size was 5  $\mu\text{m}$ . Reprinted from ref 292. Copyright 2009 American Chemical Society.

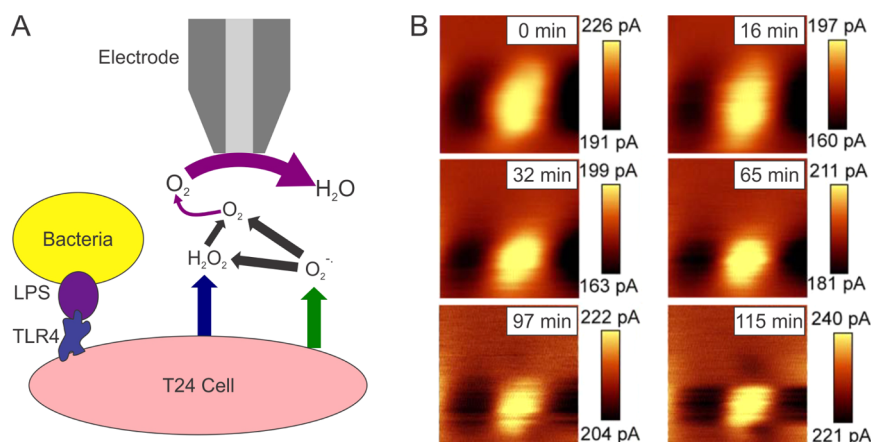


**Figure 17.** (A) Diagram of SECM setup along with a schematic showing the pathway of triggering the inflammatory and detection of reactive oxygen species. (B) Time-lapsed SECM images of a T24 cell (45  $\mu m \times 45 \mu m$ ) after the addition of heat-killed *E. coli* (hk-UPEC). Adapted with permission from ref 454. Copyright 2010 Elsevier Ltd.

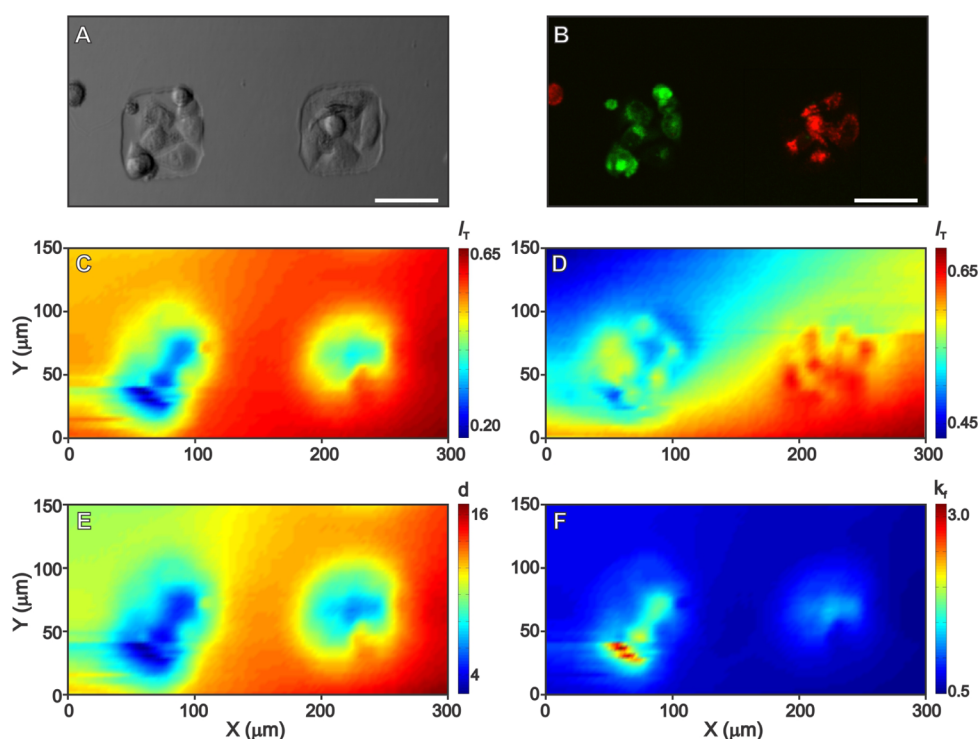


**Figure 18.** SECM imaging and decoupling of feedback response for HeLa and HeLa-R cell coculture substrate. (A) Optical micrograph of a coculture pattern containing seven HeLa-R cells (left) and six HeLa cells (right). (B) Fluorescence micrograph of the sample shown in (A), with HeLa-R cells stained green and HeLa cells stained red. (C and D) Normalized SECM currents recorded with the same sample at 12  $\mu m$  above the substrate in 1 mM  $[Ru(NH_3)_6]^{3+}$  (C) and 1 mM FcMeOH (D). (E) Extracted tip-to-substrate distance profile ( $\mu m$ ). (F) Profile of the extracted apparent heterogeneous rate constant ( $10^{-6} cm s^{-1}$ ) for the sample shown in (A). (Scale bar: 50  $\mu m$ .) Reprinted with permission from ref 455. Copyright 2013 National Academy of Sciences.

samples from boars,<sup>440</sup> dogs,<sup>441</sup> hamsters,<sup>292</sup> leeches,<sup>287</sup> mice,<sup>442</sup> plants,<sup>443</sup> and rats.<sup>444</sup>

Matsue's research group has focused heavily on the use of SECM for the measurement of cellular expression of proteins. For example, they measured the expression of secreted alkaline phosphatase (ALP) in HeLa cells,<sup>445</sup> MCF7 cells,<sup>446</sup> and mouse embryoid bodies.<sup>442</sup> In another recent report, Matsue and co-workers measured the expression of the epidermal growth factor receptor (EGFR), a membrane protein associated with cancer, on the surface of single Chinese hamster ovary (CHO) cells and

human epidermoid carcinoma (A431) cells.<sup>292</sup> As shown in Figure 16A, EGFR was labeled with an antibody containing alkaline phosphatase. Using SG/TC mode SECM and the indirect redox mediator *p*-aminophenylphosphate (PAPP), the presence of ALP-tagged EGFR on the cell membrane allowed for the enzyme-catalyzed hydrolysis of PAPP into *p*-aminophenol (PAP). PAP was subsequently oxidized at a 20  $\mu m$  Pt disk microelectrode to produce a current. Using this methodology, they measured the expression of EGFR at normal CHO cells (Figure 16C) and EGFR-overexpressing CHO cells (Figure



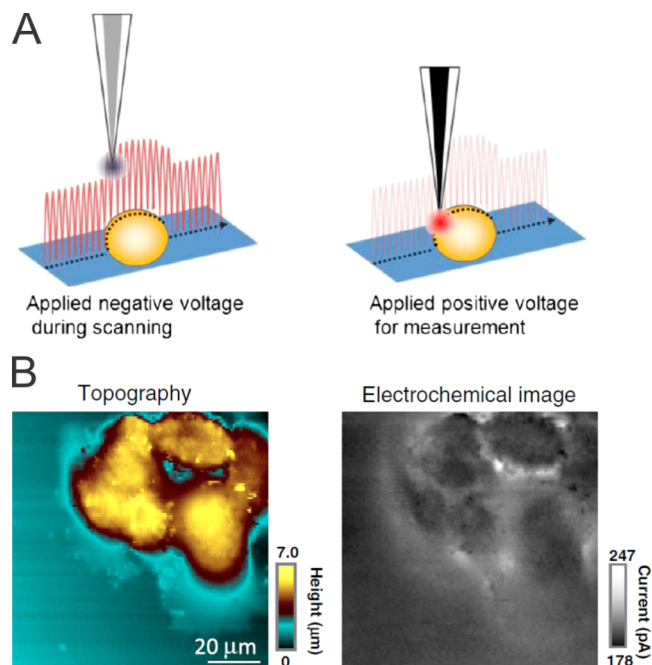


**Figure 19.** (A) Schematic illustration of voltage-switching mode SECM, in which a signal for the hindered diffusion of a mediator is implemented in hopping mode (probe approach at each pixel) to trace the topography of the surface (left) and at each set point (closest distance) an interfacial flux measurement (electrochemical activity) is made after switching the voltage (right). (B) Topography (left) and electrochemical (right) images of A431 cells. The carbon electrode was held at  $-500$  mV (topography) and  $350$  mV (electrochemical activity) vs Ag/AgCl in HEPES buffer containing  $10$  mM  $[\text{Ru}(\text{NH}_3)_6]^{3+}$  and  $4.7$  mM PAPP. The electrode radius is  $721.5$  nm. Reprinted with permission from ref 440. Copyright 2012 National Academy of Sciences.

16B), demonstrating a clear difference in expression levels. The authors state that their method is clearly advantageous since it is noninvasive and does not require detachment of the adherent cells prior to the expression measurement. Similar expression measurements have involved the transmembrane protein CD44<sup>447</sup> and green fluorescent protein.<sup>448</sup>

Bio-SECM has also been considerably employed in the study of cellular response to environmental stimuli. Cellular response is correlated to the release of reactive oxygen species (ROS) and/or by a change in cellular respiration (i.e., change in  $\text{O}_2$  levels around the cell), and is measured using SG/TC mode. Examples of stimuli used to induce cellular response include  $\text{Ag}^+$ ,<sup>449</sup> cadmium,<sup>450</sup> cisplatin,<sup>451</sup> ferrocenemethanol,<sup>437</sup> hydrogen peroxide,<sup>452</sup> Triton X-100,<sup>150</sup> and ZnO nanoparticles.<sup>453</sup> In a more specific example, Ding and co-workers exposed single human urinary bladder (T24) cells to heat-killed uropathogenic *Escherichia coli* GR-12 bacteria (hk-UPEC).<sup>454</sup> As shown in Figure 17A, using SG/TC mode, they measured cellular respiration and the release of reactive oxygen species from the cell (i.e., hydrogen peroxide and superoxide) in response to the bacteria's presence. After 115 min of exposure, a 45% increase in ROS production was observed. Additionally, the measured response (i.e., release of ROS) was localized to different areas of the cell: ROS release near the cell nuclei and mitochondria was higher and ROS release near the cell plasma was lower.

In addition to the measurement of protein expression at the cell surface, SECM has also been used to quantify the activity of transmembrane proteins. Recently, Mauzeroll and co-workers

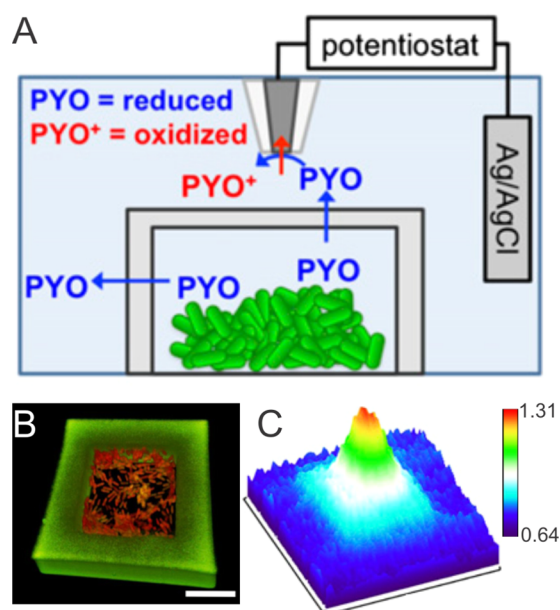


**Figure 20.** (A) Schematic of the microtrap-SECM system for measuring PYO in real time. (B) A 3D confocal reconstruction was used to count the number of cells ( $\sim 700$ ) in the microtrap. The walls appear green, and the bacteria appear red. (Scale bar:  $10$   $\mu\text{m}$ .) (C) A SECM reactive image for PYO collected above a microtrap containing WT *P. aeruginosa*. The SECM tip was biased at  $0$  V vs Ag/AgCl to oxidize PYO, and a 2D scan was acquired by moving the tip in the  $x$ - $y$  direction over the microtrap containing *P. aeruginosa* at a fixed height of  $2$   $\mu\text{m}$  above the roof. The change in the current response is highest (red) directly over the bacteria producing PYO ( $\sim 2.7$   $\mu\text{M}$ ) in the chamber. The scan area was  $65$   $\mu\text{m} \times 65$   $\mu\text{m}$ . Reprinted with permission from ref 439. Copyright 2014 National Academy of Sciences.

quantified the activity of multidrug resistance-associated protein 1 (MRP1), a protein associated with poor cancer prognosis, in normal HeLa cells and MRP1-overexpressing HeLa cells.<sup>455</sup> Using feedback mode over cocultured single cells (i.e., both cell lines patterned side-by-side on a single substrate; Figure 18A,B), they obtained one SECM image using the highly charged redox mediator  $[\text{Ru}(\text{NH}_3)_6]^{3+}$  (Figure 18C), and another image over exactly the same cells using the uncharged redox mediator FcMeOH (Figure 18D). The authors proposed that since  $[\text{Ru}(\text{NH}_3)_6]^{3+}$  was cell impermeable and thus had no interaction with the patterned cells, a topography profile of the cells could be extracted, as shown by the map of tip-to-substrate distance in Figure 18E. Using this topography map and both SECM images, an apparent heterogeneous rate constant profile was extracted (Figure 18F) and correlated back to the activity of the MRP1 protein. Therefore, the convoluted current signal in a constant-height feedback measurement, which is composed of both topography and electrochemical reactivity, was numerically decoupled into separated profiles and used to quantify the activity of a transmembrane protein.

Contrary to this approach, which involved a constant-height feedback measurement, Unwin, Matsue, and co-workers developed a new mode called voltage-switching mode SECM (VSM-SECM) to allow deconvolution of the current response using a constant-distance measurement.<sup>440</sup> This approach requires the presence of two distinct redox mediators in solution at the same time (e.g.,  $[\text{Ru}(\text{NH}_3)_6]^{3+}$  was used for topography and PAPP for electrochemical activity). First, a reductive potential is applied at a carbon disk nanoelectrode, which is

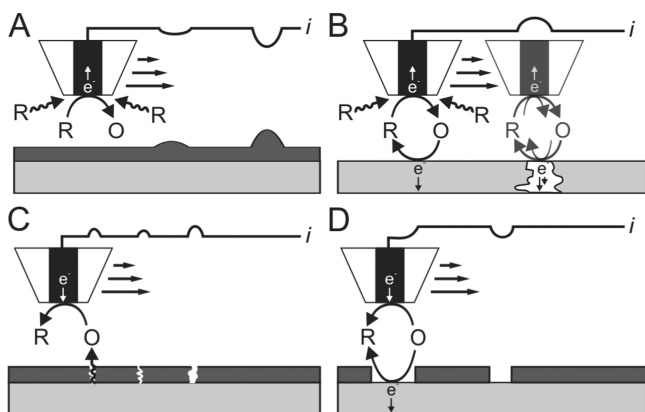


**Figure 21.** Different modes employed to monitor corrosion of a sample and their respective current responses measured at the microelectrode. (A) Negative feedback SECM measurement to record the changes in coating morphology using an indirect redox mediator. (B) Positive feedback measurement over a metal presenting heterogeneities in composition. (C) Substrate-generation/tip-collection measurement of ions/molecules generated from a coated/uncoated metal surface. (D) Pitting corrosion monitored using the redox-competition mode.

then moved closer/further to the surface to obtain a constant-current response, which is correlated with the surface topography (Figure 19A, left). Subsequently, the potential is rapidly switched to an oxidative potential, which then provides a measure of the electrochemical activity (Figure 19A, right). Using this methodology with antibody-labeled A431 cells, the authors imaged cell topography using  $[\text{Ru}(\text{NH}_3)_6]^{3+}$  as a mediator (Figure 19B, left) and then obtained an electrochemical image (Figure 19B, right) showing the expression levels of EGFR on the cell membrane (i.e., electrochemical activity) using PAPP. The authors point out that, although their approach is similar to constant-current imaging, it is more advantageous since it only requires the use of a single probe and can provide information on both topography and electrochemical activity, unlike other reports on constant-current imaging which only provide topography.<sup>186</sup>

Another very interesting advance in this application has been the combination of micro-3D printing with Bio-SECM measurements. Bard, Whiteley, and co-workers recently described the use of this platform to spatially arrange living bacterial populations (*Pseudomonas aeruginosa*) into small micro-3D printed cages and study communication between populations in separate cages (also known as quorum sensing).<sup>439</sup> As shown in Figure 20A, a microelectrode probe was positioned above a caged population of *P. aeruginosa* bacteria (Figure 20B) and the release of a quorum-sensing metabolite (i.e., pyocyanin) by these bacteria was measured. As shown by the SECM in Figure 20C, the authors successfully measured release of PYO using electrochemical oxidation at the SECM tip. They applied this technique to a varying number of bacterial aggregates to determine the minimum number of bacterial cells necessary to produce a measurable signal, which they determined was 500. The authors concluded that their methodology was very useful for investigating communication between bacterial aggregates, a subject that is essential to understanding infection and bacterial resistance.

#### 4.5. Corrosion

Corrosion is the result of a heterogeneous electron transfer between a metal and its surrounding environment, and depends

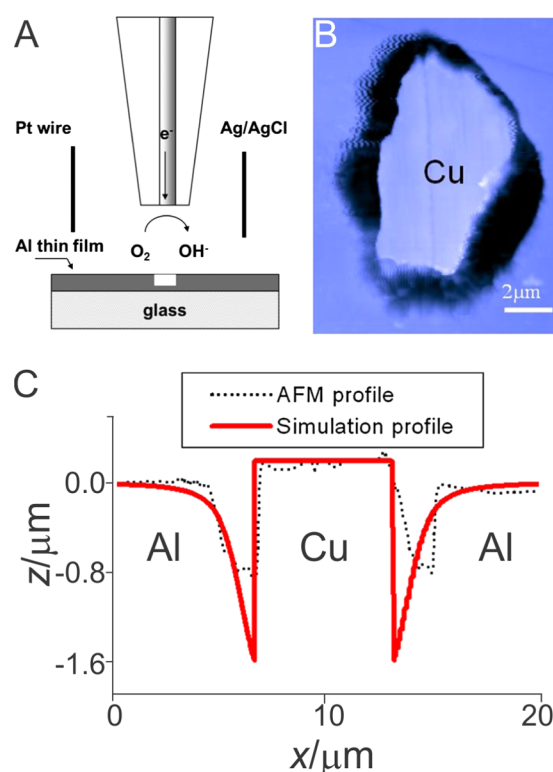


**Figure 22.** (A) Local alkalinization of the corroding media to induce the local dissolution of the Al thin film. (B) Atomic force microscopy 2D topographic mapping of copper particles embedded in a pure aluminum matrix after 15 min of polarization at  $-0.8$  V vs SCE in  $0.1$  M sulfate solution. (C) Atomic force microscopy 2D profile of the surface sample compared to simulated profile with  $2.5$   $\mu\text{m}$  radius particle. Reprinted with permission from ref 464. Copyright 2013 John Wiley & Sons, Ltd.

on the composition of a material (i.e., alloys) or the local environment. SECM has the ability to monitor this heterogeneous electron transfer with high spatial resolution, making it advantageous for the comprehension of corrosion mechanisms and corrosion mitigation strategies. For these reasons, the investigation of corrosion has seen growing interest since the initial reports,<sup>43,247,456,457</sup> and it has represented more than 17.4% of the SECM literature in the past five years, including several reviews.<sup>458–460</sup>

To probe the corrosion of a material, the feedback mode of SECM offers many possibilities (Figure 21A,B). For instance, due to the presence of heterogeneities in alloys, an indirect redox mediator was used to probe the difference in intrinsic reactivity of the various phases composing an alloy (Figure 21B).<sup>461</sup> Analytical approximations have been developed to extract the rate of regeneration of the indirect redox mediator.<sup>10</sup> Not only is the feedback mode capable of quantifying the intrinsic change in reactivity of the immersed sample, but it is also sensitive to small changes in the substrate topography. This property was employed to monitor the formation of blisters within coatings, as this process reduced the tip-to-substrate distance (Figure 21A).<sup>462</sup>

The GC modes of SECM are the most used to investigate corrosion properties, mainly due to their ability to probe a direct mediator (see Figure 21C,D). In most cases, upon immersion of a metal, the latter dissolves and produces ions/molecules that can be collected at a nearby microelectrode, as shown in Figure 21C. For example, the flux of iron ions or molecules such as oxygen

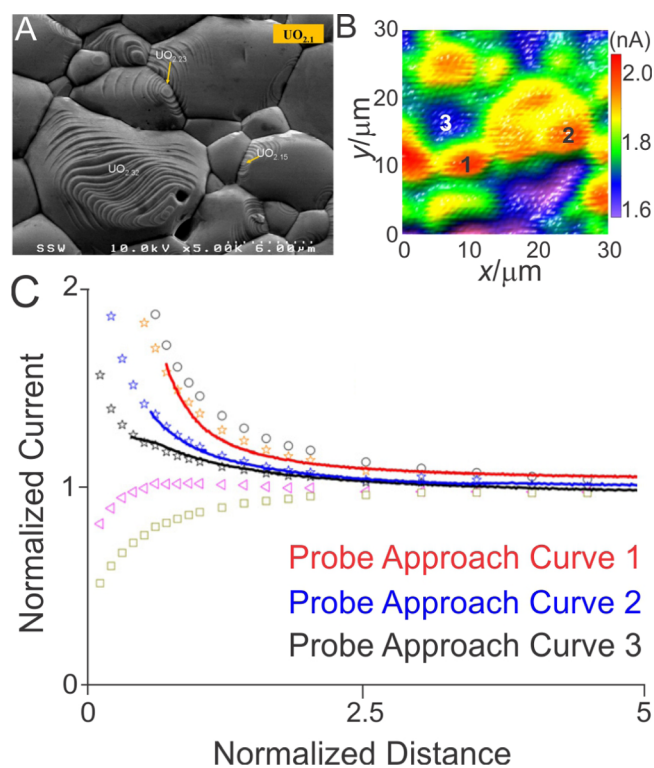


**Figure 23.** Characterization of various properties of the  $\text{UO}_{2.1}$  surface. (A) Electron micrograph of grain morphologies. (B) SECM image of the feedback current recorded under natural corrosion condition, and selected locations for the measurement of probe approach curves. (C) Determination of corrosion kinetics on selected grains obtained by fitting experimental approach curves (solid lines) to simulated curves (open symbols). Reprinted with permission from ref 119. Copyright 2010 Elsevier Ltd.

can be monitored upon immersion of a steel sample to characterize the local rates of corrosion.<sup>462</sup> In addition, by applying a significant anodic potential to the substrate of interest, pitting corrosion can be initiated locally and monitored through the collection of iron ions. A subset of the GC modes, described earlier as ASV-SECM, has also been employed to monitor ions that are reduced at very low potential (e.g., zinc) using a mercury hemisphere microelectrode.<sup>463</sup>

As mentioned in section 3.2, a limited solvent window (see Figure 4) can sometimes prevent the monitoring of certain ions produced during corrosion due to their low reduction potential. To circumvent this problem, potentiometric mode SECM has demonstrated the possibility of gaining local insights into the generation of certain ions produced at the metal surface, such as  $\text{Zn}^{2+}$ .<sup>353</sup> Determining the location and concentration of electrolytes over the metal substrate (e.g.,  $\text{Na}^+$  and  $\text{Cl}^-$ ) is also crucial to further understanding the corrosion mechanism. Potentiometric mode can also be used for this purpose, and an investigation of these fluxes over steel samples has been reported.<sup>354</sup>

The corrosion of steel also involves the presence of oxygen, which depending on its concentration can generate the formation of pits locally on the surface. The severity of such phenomenon was probed using RC mode SECM by monitoring oxygen as a mediator, as shown in Figure 21D.<sup>13</sup> This is achieved by biasing the microelectrode to reduce oxygen while a simultaneous collection of the mediator occurs at the steel surface without inducing the formation of a feedback loop.

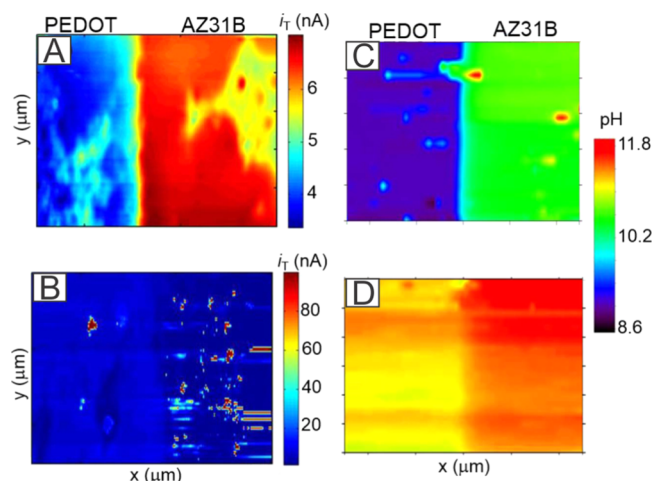


**Figure 24.** Detection of  $\text{H}_2$  evolution at the interface of uncoated and PEDOT-coated AZ31B. (A and B) SECM tip current images (A) after 30 min and (B) after 24 h immersion in 0.01 M NaCl aqueous solution. (C and D) pH maps measured with Pt/IrOx microprobe operated in potentiometric mode of SECM (C) after 30 min and (D) after 24 h immersion in 0.01 M NaCl. The scan area was  $500 \mu\text{m} \times 500 \mu\text{m}$ . Reprinted with permission from ref 467. Copyright 2015 The Electrochemical Society.

Higher currents (absolute values) are recorded over an area not experiencing any pitting corrosion in comparison to lower currents above an area competing for the mediator.

While these represent the usual strategies employed to investigate corrosion using SECM, over the past five years, SECM corrosion literature has focused on studying steel, aluminum, or magnesium in aqueous media with the objective of better understanding their respective corrosion mechanisms.

An example of the strengths of SECM to study corrosion was presented by Sorriano and co-workers, who investigated the microstructural corrosion of aluminum alloys and implemented a numerical finite element model to validate the results obtained by SECM.<sup>464</sup> The experiment consisted in using TG/SC mode, where oxygen is being reduced to hydroxyl ions capable of inducing the local dissolution of an Al thin film, as shown in Figure 22A. The authors were able to reproduce the damages that an aluminum alloy would suffer due to the presence of cathodic copper particles that are usually formed during alloy fabrication and were previously described as corrosion initiation sites (Figure 22B). Using the Nernst–Planck equation, local dissolution induced by the SECM tip was measured by atomic force microscopy and successfully corroborated (Figure 22C). Therefore, this approach would have the ability to simulate the corrosion of aluminum alloys at the micrometer level.

Less-common corroding materials, such as uranium, have also been studied using SECM. Shoesmith and co-workers investigated the hyperstoichiometry of uranium oxide (electron micrograph in Figure 23A) and its effect on the local reactivity of the material.<sup>119</sup> On top of performing Raman characterization of the sample to determine the local stoichiometry of the studied material, SECM current maps (Figure 23B) and probe approach curves (Figure 23C) were recorded when the uranium sample was immersed in a solution containing an indirect redox mediator, ferrocenemethanol. A nonlinear fitting of the analytical approximation to the experimental probe approach curves recorded over specific locations helped determine the rate of regeneration of the indirect redox mediator and thus that the highest stoichiometry possessed the highest reactivity.



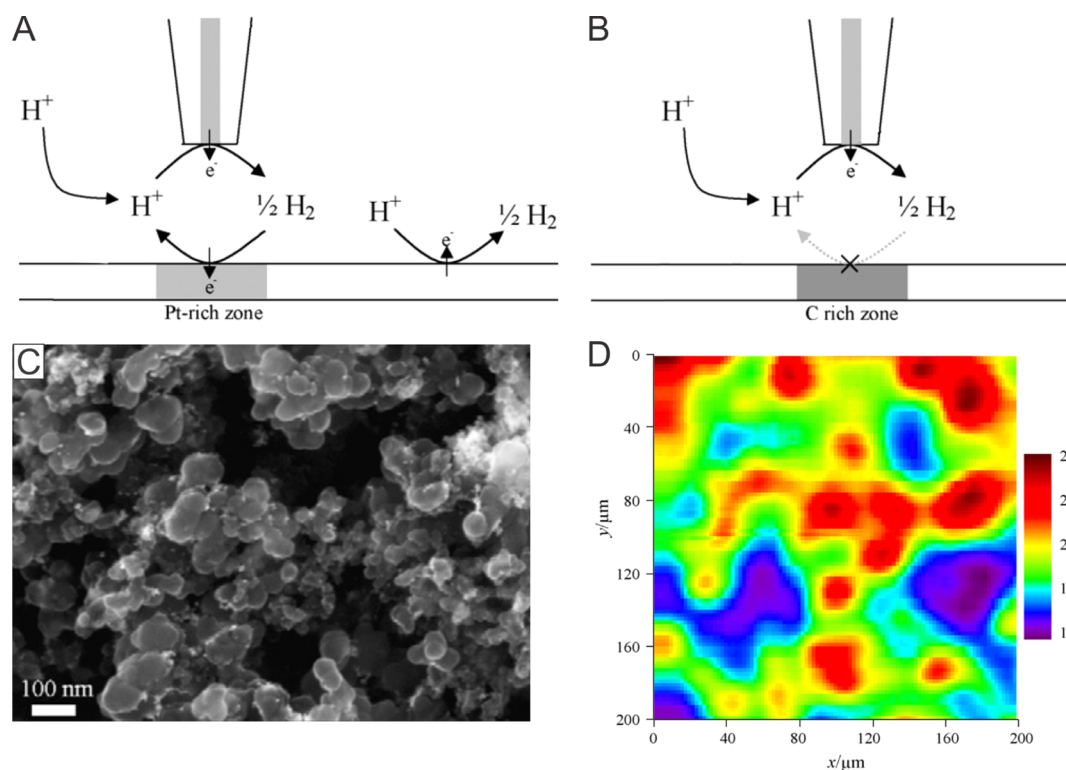


**Figure 25.** (A) An ultramicroelectrode (UME) tip is reducing protons at a diffusion-limited rate over a Pt-rich area of the film and the degree of positive feedback is due to both Pt content and differences in sample topography. (B) UME tip is reducing protons at a diffusion limited rate over a C-rich area of the film and the degree of negative feedback is due to differences in sample topography. (C) High magnification field-emission electron microscopy images of 6–4 Pt–C spin-cast ( $8 \text{ mg mL}^{-1}$ , 2000 rpm) films on silanized silicon substrates. (D) SECM map of a spin-cast ( $8 \text{ mg mL}^{-1}$ , 2000 rpm, 4 layers) 6–4 Pt–C film deposited on a HOPG substrate immersed in 10 mM sulfuric acid and 50 mM potassium sulfate. Proton reduction was driven at the UME tip ( $-0.8 \text{ V}$  vs Ag/AgCl). Tip radius and initial tip–substrate distance  $5 \mu\text{m}$ . Color scale corresponds to normalized current;  $i_{\text{bulk}} = 96 \text{ nA}$ . Scan speed  $15 \mu\text{m s}^{-1}$  and scan area  $200 \mu\text{m} \times 200 \mu\text{m}$ . Reprinted with permission from ref 161. Copyright 2009 Elsevier Ltd.

Although mechanistic investigations are important to better understand corrosion, an important task consists of the prevention of the reactions that take place on metals, as they will be used as structural components. While more than half of the corrosion SECM publications focused on investigating corrosion mechanisms, a large number studied corrosion mitigation strategies. Several strategies are routinely employed to prevent corrosion and have been studied using SECM and can be grouped as described below:

- (1) conversion coatings<sup>82</sup>
- (2) corrosion inhibitors<sup>465</sup>
- (3) polymer coatings<sup>462</sup>
- (4) surface treatments, i.e. mechanical stress<sup>466</sup>

Poly(3,4-ethylenedioxythiophene), a conductive polymer, has recently been electrodeposited on a magnesium alloy, AZ31B, using an ionic liquid solution.<sup>467</sup> The ability to prevent corrosion was then investigated using several electrochemical imaging techniques such as scanning vibrating electrode technique (SVET) and SECM operated in SG/TC and potentiometric modes. Mauzeroll and co-workers showed that the hydrogen evolution monitored using a Pt microelectrode was significantly higher over the uncoated side of the magnesium alloy, as shown in Figure 24A. The cathodic activity (also measured using SVET) recorded over the uncoated side of the material was corroborated by higher local pHs measured using a Pt–Ir oxide microelectrode operated under potentiometric control (Figure 24C). However, over longer immersion times, the conductive polymer was shown not to mitigate corrosion efficiently, as the pH and hydrogen

evolution started to increase significantly over the coated side of the sample (Figure 24B).

Although not considered as a coating, the presence of bacteria to mitigate corrosion was investigated over a low carbon steel material envisioned for high-level radioactive waste containers.<sup>468</sup> Using SG/TC mode, Vivier and co-workers investigated the evolution of hydrogen as carbon steel corroded, and this in a controlled anaerobic environment. The authors showed that 15% of the  $\text{H}_2$  evolved from the material was consumed by the presence of bacteria.

The examples presented above and in the current literature show that the development of more rapid screening approaches would benefit SECM investigations of corrosion. This could be achieved by developing multifunctional probes capable of monitoring simultaneously more than one flux at a time while recording the changes in topography of the surface which can be beneficial to better track the coating shapes. Moreover, the field is also devoted to developing multidisciplinary projects as more metals are being used daily in vivo. To grasp the complexity of these systems, the use of controlled environments will thus be mandatory and will have to be interfaced with SECM.

#### 4.6. Energy

In the growing search for new and more efficient materials, characterization of the electrochemical activity of a surface can provide valuable information. The use of SECM for this type of characterization has seen an increased interest, with the topic being reviewed in 2010.<sup>469</sup> Various types of materials and devices have been investigated, including batteries,<sup>300</sup> fuel cells,<sup>168</sup>

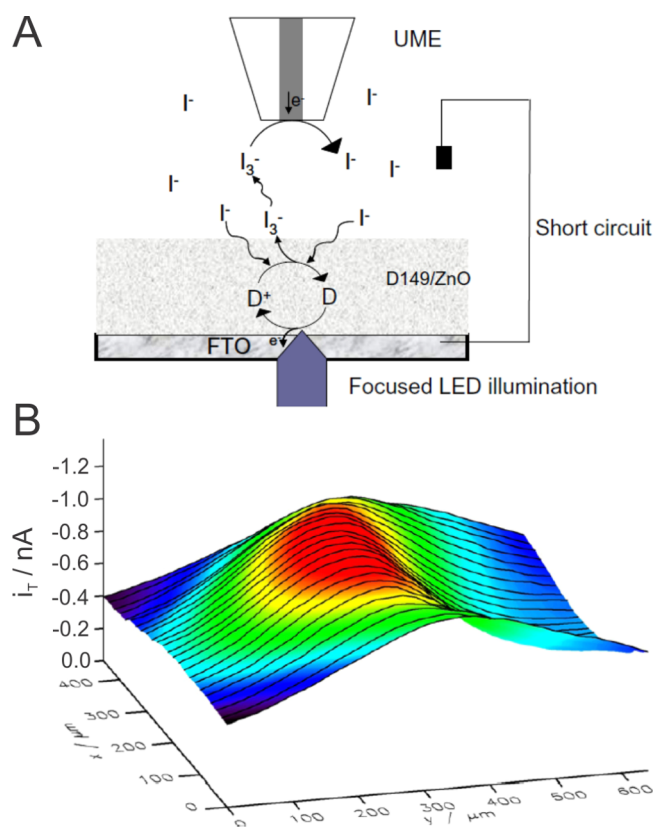


**Figure 26.** (A) Basic arrangement of SECM substrate-generation tip-collection mode experiment of DSSC. The light is focused on a small scale area on the sensitized electrode. (B) SECM SG/TC image of ZnO/D149 film electrode with  $I^-$  mediator obtained by scanning UME across a focused light illuminated area. The circular region at the middle of the image corresponds to the illuminated spot on the electrode.  $a = 12.5 \mu\text{m}$ ,  $v_T = 20 \mu\text{m/s}$ ,  $d = 30 \mu\text{m}$ ,  $E_T = -0.7 \text{ V}$ . Reprinted with permission from ref 480. Copyright 2010 Elsevier Ltd.

quantum dots,<sup>470</sup> solar cells,<sup>471</sup> and supercapacitors.<sup>472</sup> This application represented approximately 8.7% of SECM reports in the last five years.

One of the main focuses for SECM research in this application has been the development and characterization of fuel cells. This includes biofuel cells,<sup>473</sup> polymer electrolyte fuel cells,<sup>168,474,475</sup> and proton exchange membrane fuel cells (PEMFC).<sup>476</sup> Nicholson and co-workers recently reported the use of SECM for characterization of platinum-loaded carbon nanoparticle films in a PEMFC.<sup>161</sup> As shown by the schematics in Figure 25A,B, constant-height feedback mode scans were used to determine the electrocatalytic activity of a Pt–C spin-cast film toward hydrogen oxidation. The field-emission electron microscopy images (Figure 25C) demonstrated that the distribution of the film appeared to be heterogeneous, and this was confirmed by the obtained SECM image (Figure 25D), which showed variations in the electrocatalytic activity of the film. Consequently, the authors demonstrated that SECM imaging was well-suited to characterize heterogeneity in catalyst films. They did note that the use of nanoelectrodes would provide a much higher resolution and provide them with the ability to characterize individual nanoparticles.

Several research groups have used SECM to characterize the performance of solar cells, or more specifically dye-sensitized solar cells (DSSCs).<sup>471,477–479</sup> For example, Wittstock and co-workers investigated the dye (D149) regeneration kinetics in a

ZnO-based DSSC.<sup>480</sup> First, they used feedback approach curves with an indirect redox mediator ( $I_3^-$ ) to determine the dye regeneration rate constant under different illumination parameters (wavelength and intensity). Then, using SG/TC mode in the setup illustrated in Figure 26A, they imaged a DSSC that was illuminated with a focused LED (Figure 26B). Their results demonstrated that this mode could be used to image differences in electron transfer rates for an illuminated/nonilluminated DSSC. The authors noted that their methodology could be very useful for the identification and development of new redox couples to be used in DSSCs.

An interesting development in the characterization of battery materials has been the integration of SECM systems into a glovebox. The highly reactive nature of these materials necessitates measurements under complete anaerobic conditions, making the use of a glovebox essential. Several reports have described the use of this instrument configuration.<sup>89,92,481</sup> For example, Jung and co-workers investigated the transportation of  $Li^+$  ions at the interface of a charging  $LiCoO_2$  electrode in a glovebox.<sup>280</sup> Using SG/TC mode in anaerobic conditions, they scanned a Pt microelectrode over a  $LiCoO_2$  substrate biased at increased oxidative potentials, measuring the release of  $Li^+$  ions caused by dissociation of the substrate (Figure 27A). The SECM images (Figure 27B) showed that dissociation increased as the potential applied at the substrate (i.e., charging density) was increased. The authors concluded that SECM imaging allowed for the characterization of the dissociation ability, but also demonstrated the nonuniformity of the electrode surface. Therefore, the electrochemical activity and uniformity of  $Li^+$  ion battery materials could be analyzed using SECM under anaerobic conditions in a glovebox.

Evidently, feedback and GC modes have been the most popular for the characterization of energy-related materials. However, Bard and co-workers developed a new methodology, surface-interrogation mode (SI-SECM), which can be used to study adsorbed surface species on an electrode.<sup>181,482</sup> In SI-SECM, a reactive species A is adsorbed at a substrate electrode (Figure 28A). A SECM tip is used to generate a titrant R, produced by reduction of an indirect redox mediator O (Figure 28B). The titrant R reacts with A to regenerate O, producing positive feedback. As the adsorbed species A is depleted from the surface, the regeneration of the redox mediator decreases until negative feedback is detected. In this way, SI-SECM acts as a transient feedback mode, allowing for the quantification of adsorbed species on a surface. Using this concept, Bard and co-workers studied the photochemistry at a W and Mo doped  $BiVO_4$  semiconductor electrode.<sup>181</sup> After irradiation to cause water oxidation, hydroxyl radicals were generated and adsorbed on the surface of the W/Mo– $BiVO_4$  electrode. By measuring the regeneration of  $IrCl_6^{3-}$  (indirect redox mediator), represented by a positive feedback response, they determined the concentration of hydroxyl radicals formed at the surface under varying irradiation times (Figure 28E,F). They also determined that only 1% of absorbed photons were used for water oxidation. Consequently, the authors demonstrated that SI-SECM was useful for characterization of surface adsorption in energy-related materials.

#### 4.7. Surface Modification

The high spatial resolution afforded by SECM makes it ideal for surface modification, whether it be etching or deposition, and this principle has long been investigated since the initial reports by the Bard research group in 1989.<sup>155,275</sup> In the past five years,



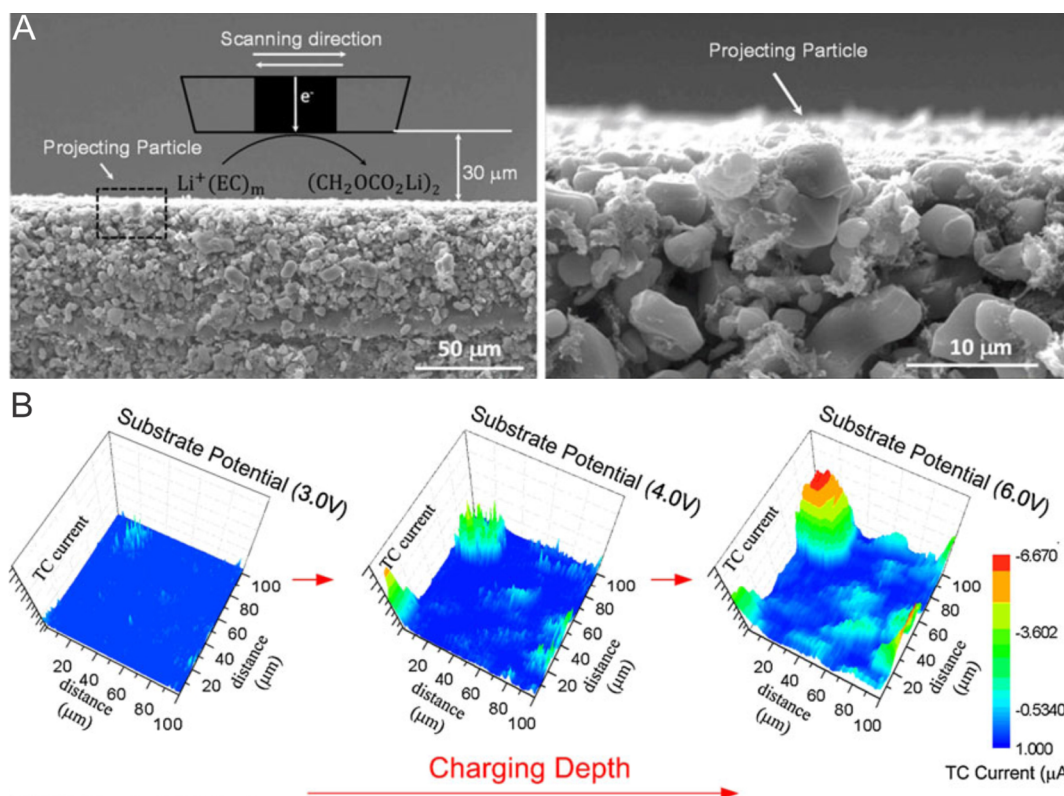


**Figure 27.** (A) SEM images of LiCoO<sub>2</sub> substrate to be studied in glovebox. (B) SECM images of LiCoO<sub>2</sub> substrate with increasing charging depth. The probe used was Pt, and Li metal was the reference electrode. Reprinted with permission from ref 280. Copyright 2011 Springer.

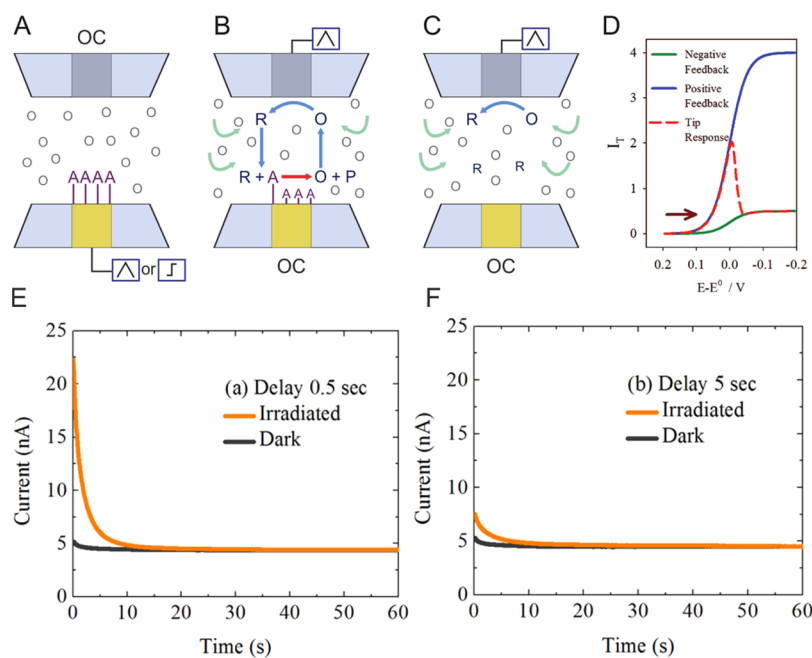


**Figure 28.** Schematic of the proposed mechanism for the surface interrogation. (A) Reactive species A is adsorbed at the substrate. (B) The SECM tip generates titrant R, which reacts at the surface of the substrate to produce positive feedback. (C) Depletion of the adsorbate causes negative feedback. (D) Tip response during SI-SECM. Reprinted from ref 482. Copyright 2008 American Chemical Society. (E and F) Chronoamperograms during SI-SECM using Au UME on the W/Mo–BiVO<sub>4</sub> electrode with different decay times of (E) 0.5 and (F) 5 s after UV–visible irradiation for 5 s (yellow). A scan without irradiation is shown as a black solid line.  $E_{\text{tip}} = 0.5$  V vs NHE, and  $E_{\text{substrate}} = 0.6$  V. Measurements were done in 1 mM K<sub>2</sub>IrCl<sub>6</sub> and 0.1 M Na<sub>2</sub>SO<sub>4</sub> aqueous solution.  $d = 12$   $\mu\text{m}$ . Reprinted from ref 181. Copyright 2013 American Chemical Society.

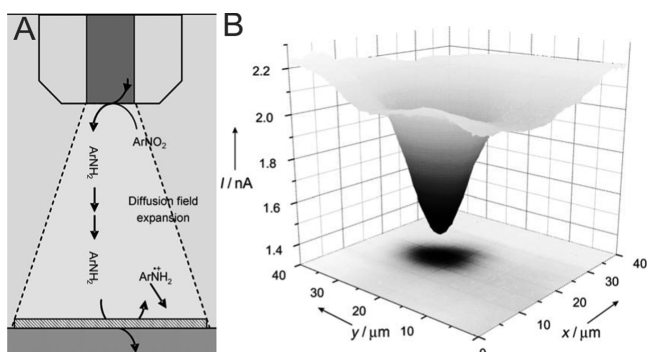


**Figure 29.** (A) Reaction system suitable for SECM patterning of surfaces in TG/SC mode based on oxidation of amine-containing compounds. (B) SECM image of a micropattern of organic moieties deposited on a gold sample by oxidation of an amine electrogenerated at the tip. Microstructure imaging conditions:  $E_T = 0.5$  V,  $E_S = -0.1$  V,  $d = 3$   $\mu\text{m}$ , translation speed =  $5$   $\mu\text{m s}^{-1}$ . Reprinted with permission from ref 494. Copyright 2009 John Wiley & Sons, Ltd.

and is oxidized, allowing for the deposition of an organic moiety. As shown by the SECM image in Figure 29B, the authors were able to selectively create a small micropattern (diameter  $\sim 15$   $\mu\text{m}$ ), and they suggested that their methodology could be used for complex organic micropatterning of surfaces.

On the theme of deposition of noble metals, Radtke and co-workers provided an example for the micropatterning of platinum on a nonconducting surface.<sup>495</sup> As shown in Figure 30A, a thin layer of platinum dichloride (i.e., metal precursor “p”) was deposited onto a surface. A biased SECM tip was then used to reduce the indirect redox mediator methylviologen. This reduced form of the mediator diffuses to the platinum dichloride surface, acting as a reducing agent and allowing for the formation of platinum metal. Figure 30B shows optical micrographs of several micropatterned platinum lines deposited on glass. Variations in line thickness were caused by increases in the scan speed of the SECM tip during precursor reduction. This surface was also characterized using SECM, as shown in Figure 30C. Consequently, the authors demonstrated that platinum

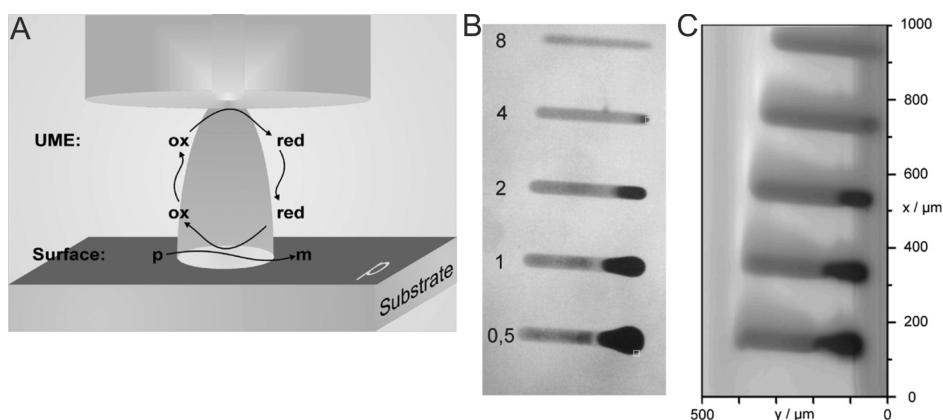


**Figure 30.** (A) Schematic SECM setup for the local reduction of a metal precursor (p) to the metal (m) by a reduced mediator generated at an ultramicroelectrode. (B and C) Line-shaped platinum microstructures on glass. (B) Light microscope image. Numbers indicate velocity in  $\mu\text{m s}^{-1}$ . (C) SECM-feedback mode image. Both images reveal different areas within the lines ascribable with different grades of reduction of the  $\text{PtCl}_2$ . Reprinted with permission from ref 495. Copyright 2009 Elsevier Ltd.

this application has represented 5.5% of reports using SECM. In terms of operational mode, feedback, TG/SC, and direct modes are the most commonly used methodologies for surface modification.

The number of SECM reports involving the etching of surfaces have diminished in recent years. Nevertheless, methodologies for the etching of several different materials have been reported, including copper,<sup>138,276</sup> silicon wafers,<sup>42</sup> polystyrene,<sup>483</sup> and ZnO films.<sup>484</sup> In contrast, most investigations involve the deposition or patterning of conducting and nonconducting surfaces. This includes the deposition of alumina films,<sup>485</sup> chitosan,<sup>486</sup> gold nanoparticles,<sup>276,487–489</sup> silver nanoparticles,<sup>306,488,490</sup> and vinyl monomers.<sup>491</sup>

Recently, there has been particular interest in the use of diazonium salts for surface modification.<sup>70,212,492,493</sup> One common approach involves the reduction of diazonium salts at a SECM tip in order to achieve deposition. However, this leads to tip passivation and consequently limited application. Belanger and co-workers avoided this problem by proposing a new methodology in which they use TG/SC mode to oxidize amine-containing compounds (Figure 29A).<sup>494</sup> Initially, a nitro-containing compound is reduced at a SECM tip to produce an amine. This amine then diffuses to the biased substrate surface

could be deposited with high resolution using SECM. Interestingly, they also noted that this methodology could be applied for the deposition of other metals such as palladium.

The use of SECM for living cell studies was discussed in section 4.4. In several examples, cells were arranged in a specific configuration in order to facilitate SECM measurements. In other words, patterned surfaces were used to encourage a particular cellular alignment. In most cases, these patterning schemes are created using some form of lithography. However, Wittstock and co-workers demonstrated that SECM could in fact be used for the fabrication of micropatterns on modified surfaces.<sup>50</sup> First, a gold surface was covered with self-assembled monolayers (SAMs) terminated with oligomers of ethylene glycol (OEG). OEG SAMs have been shown to minimize nonspecific adhesion of cells or proteins. A biased SECM tip was then used to electrochemically generate bromine and modify specific areas of the OEG SAMs, as shown in Figure 31A. The bromine cleaves the OEG part of the monolayer and consequently exposes the  $\text{CH}_3$ -terminated alkyl chain of the SAM, which is cell-adhesive. As shown in Figure 31B, circular micropatterns were successfully fabricated and imaged using SECM. These surfaces were then used for subsequent investigation of bacterial interaction. Therefore, the authors

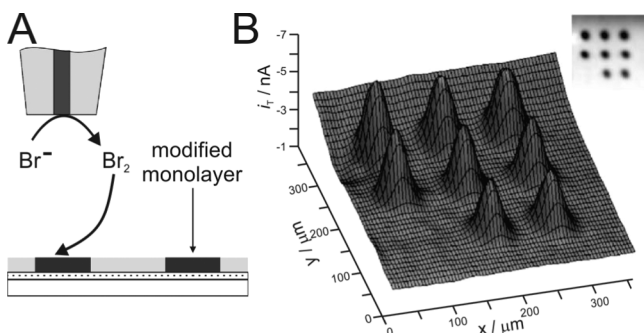


**Figure 31.** (A) SECM method for template-free micropatterning. The OEG SAM was locally modified by using electrochemically generated  $\text{Br}_2$ . (B) Characterization of the microfabricated OEG substrate for the micropatterning of bacteria using SECM. SECM feedback images of microfabricated patterns on the OEG SAM substrate. The images were recorded using  $\text{Ru}(\text{NH}_3)_6^{3+}$  as the electron-transfer mediator in 0.1 M PBS buffer (pH 7.4) after SECM microfabrication. The higher current (dark regions) in the images indicates a higher permeability of the monolayer.  $E_T = -400$  mV,  $a = 25$   $\mu\text{m}$ ,  $d = 5$   $\mu\text{m}$ , and translation speed =  $10$   $\mu\text{m s}^{-1}$ . Reprinted from ref 50. Copyright 2010 American Chemical Society.

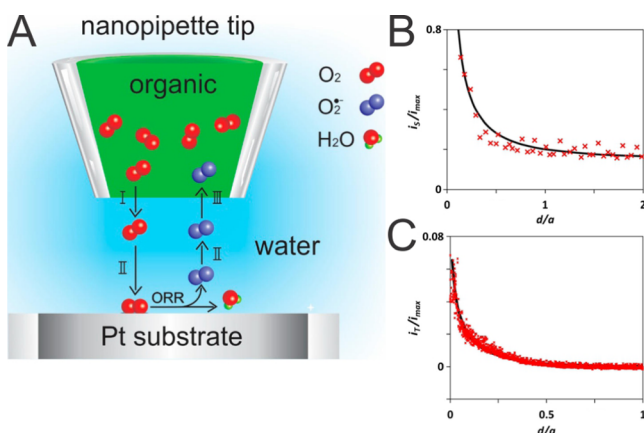


**Figure 32.** (A) Schematic representation of the detection of superoxide intermediate ( $\text{O}_2^{\bullet-}$ ) generated during ORR at the Pt substrate by ET/IT SECM technique: (I) oxygen partitioning from organic filling solution to the external aqueous phase; (II) diffusion; (III) transfer of  $\text{O}_2^{\bullet-}$  anion across the liquid/liquid nanointerface. (B and C) Experimental (symbols) and theoretical (solid lines) current–distance curves for oxygen delivery from the nanopipet to the Pt substrate and collection of the superoxide intermediate. The tip was a 69 nm radius pipet containing BTF solution (cell 1) saturated with  $\text{O}_2$ , and the substrate was a 25  $\mu\text{m}$  diameter Pt disk. Both the substrate (B) and tip (C) currents are normalized by the diffusion-limiting flux of oxygen from the nanopipet.  $E_T = 0.4$  V and  $E_S = -0.5$  V. The approach speed was 50 (B) and 1  $\text{nm s}^{-1}$  (C). Reprinted from ref 500. Copyright 2015 American Chemical Society.

demonstrated that SECM provided a useful tool to produce and manipulate micropatterns for fundamental studies.

#### 4.8. Kinetics

Above all else, SECM has been used to characterize reaction kinetics (i.e., electrochemical activity) at a substrate. Specific subsets have been discussed above (e.g., biological samples, energy-related materials, etc.), but the principles used remain the same. The measurement of surface kinetics, whether it be at a solid–liquid interface or a liquid–liquid interface, has represented over 28.3% of all SECM reports since 2009. This

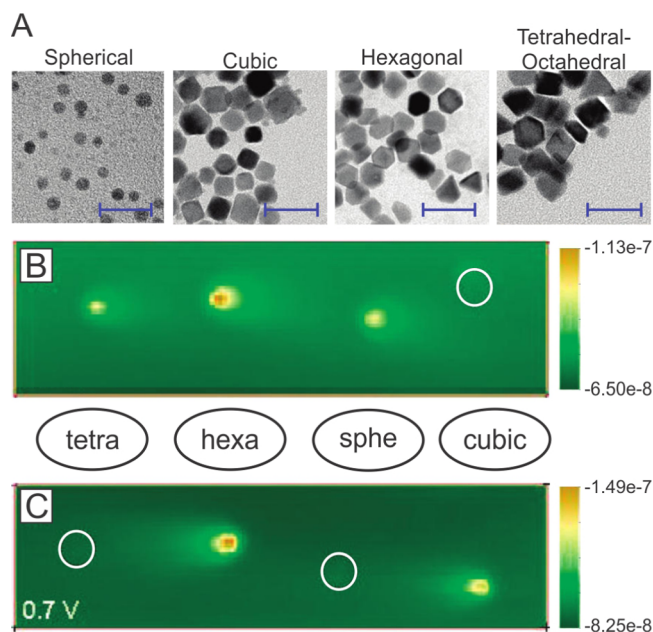


**Figure 33.** (A) TEM pictures of preferentially spherical, cubic, hexagonal, and tetrahedral–octahedral platinum NPs. Scale bars represent 20 nm. (B) SECM TG/SC image displaying the reduction current collected for ORR in 0.1 M  $\text{HClO}_4$  solution at a Pt NP array. (C) SECM TG/SC image displaying the reduction current collected for ORR in 0.5 M  $\text{H}_2\text{SO}_4$  solution at a Pt NP array. Scan rate =  $125$   $\mu\text{m s}^{-1}$ .  $E_S = 0.7$  V. Adapted from ref 505. Copyright 2010 American Chemical Society.

particular “application” is used to group measurements that do not fall within the context of other applications presented above. In general, it consists of measuring electron transfer rates for a wide variety of processes occurring at different substrates. Some particular subcategories include measurement of catalytic activity, surface imaging, and measurements at liquid interfaces.

In the vast majority of SECM experiments, the electrochemical process is occurring at a solid–liquid interface. However, a small portion of SECM literature has also focused on the study of kinetics at the liquid–liquid interface, also known as the interface between two immiscible electrolyte solutions (ITIES), and the topic has been summarized previously.<sup>496</sup> In the last five years, SECM research focusing on ITIES has decreased significantly, representing only 2.2% of reports. Nevertheless, several different behaviors have been investigated, including silver particle growth,<sup>306</sup> conductive gold nanoparticle mirror self-assembly,<sup>327</sup> metalloporphyrin species properties with different substituents,<sup>157</sup> and the diffusion of molecules through an ionic liquid–organic interface.<sup>497</sup> Particular interest has also been explored for the generation and measurements of hydrogen, hydrogen peroxide, oxygen, and superoxides at ITIES.<sup>74,169,498,499</sup> Mirkin and co-workers recently reported the detection of short-lived intermediates of electrocatalytic oxygen reduction at a nanoscale liquid–liquid interface.<sup>500</sup> As shown in Figure 32A, a nanopipet was filled with an organic solvent (benzotrifluoride) saturated with oxygen, and approached toward a catalytic substrate (e.g., platinum) in aqueous solvent. The oxygen diffused from the organic phase into the aqueous phase and was reduced at the platinum substrate, producing a superoxide intermediate, which subsequently diffused back into the nanopipet. By measuring the ion transfer current at potentials specific to the superoxide intermediate, the authors confirmed the formation of a short-



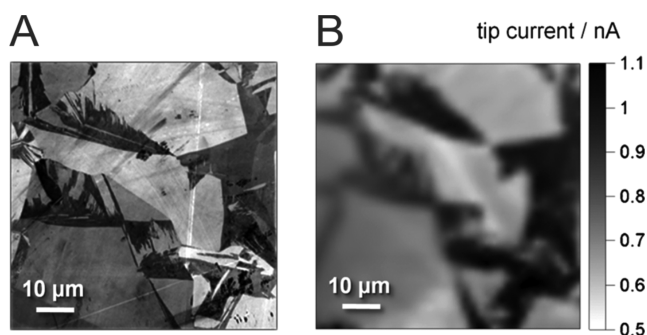


**Figure 34.** (A) Image ( $70\ \mu\text{m} \times 70\ \mu\text{m}$ ) of pBDD obtained using FE-SEM recorded with an in-lens detector at 2 kV. (B) IC-SECM SG/TC map for the collection of  $\text{Ru}(\text{NH}_3)_6^{2+}$  (by oxidation), electrogenerated at the surface of pBDD ( $\eta = -0.004\ \text{V}$ ). Reprinted with permission from ref 507. Copyright 2012 John Wiley & Sons, Ltd.

lived superoxide intermediate (see Figure 32B,C). They thus concluded that their newly developed methodology (electron transfer/ion transfer (ET/IT) SECM) could be very useful for the detection of charged reaction intermediates, including those with lifetimes on the order of nanoseconds.

In the context of heterogeneous electron transfer at solid–liquid interfaces, a particularly important role of SECM has been in the evaluation of the catalytic activities of different substrates. In the past five years, several different catalysts have been evaluated, including Au nanoparticles,<sup>273,501</sup> bimetallics (Pd–Co, Pt–Ag, Pd–W),<sup>305,474,476</sup> C–Pd and C–Au,<sup>502</sup> CoPi,<sup>128</sup> nanosheet  $\text{ZnCo}_2\text{O}_4$ /carbon nanotube composites,<sup>503</sup> and  $\text{RuO}_2$ .<sup>504</sup> Herrero and co-workers investigated the effect of shape of the catalytic activity of platinum nanoparticles.<sup>505</sup> As shown in Figure 33A, four different geometries of nanoparticles were synthesized (spherical, cubic, hexagonal, and tetrahedral–octahedral), with average sizes between 4.5 and 11.5 nm. Using TG/SC mode, the authors measured the oxygen reduction reaction (ORR) over arrays of different shaped Pt nanoparticles in two different acidic solutions (0.1 M  $\text{HClO}_4$  and 0.5 M  $\text{H}_2\text{SO}_4$ ). Interestingly, as shown in Figure 33B,C, the catalytic activity of each Pt nanoparticle was highly dependent on its shape. In both solvents, hexagonal nanoparticles displayed the highest catalytic activity. However, the SECM images also showed that, in the case of cubic and tetrahedral–octahedral nanoparticles, acid electrolyte composition was also significant, with a sharp decrease in catalytic activity in sulfuric acid. Nevertheless, the authors noted that SECM imaging was particularly useful for characterizing the electrochemical activity of catalysts.

The measurement of reaction kinetics using SECM has also proven useful in terms of so-called “surface imaging”. Ren and co-workers imaged the surface of graphene sheets with varying defect densities.<sup>506</sup> The resulting SECM images allowed them to establish a quantitative correlation between heterogeneous electron transfer rate and defect density. In another example, MacPherson, Unwin, and co-workers imaged the surface of polycrystalline boron-doped diamond (pBDD) electrodes (Figure 34A) with high spatial resolution using intermittent-contact SECM.<sup>507</sup> They demonstrated that electrochemical activity of pBDD was dependent on the region, either low-boron or high-boron facets. Furthermore, the SECM images (Figure 34B) showed that there was no enhanced electron transfer at the grain boundaries, which is a controversial topic in the literature.

## 5. SUMMARY AND FUTURE PERSPECTIVES

Following an overview of the principles of SECM, this review has provided a comprehensive summary of the experimental parameters used between 1989 and 2015, including all of the electrochemical redox mediators, solvents, and probes. We hope that the included compilation and discussion of these parameters can allow scientists to grasp the concepts and components necessary to integrate SECM measurements into their research, and be used as a practical guide to SECM.

More than 25 years after its inception, SECM has emerged from its infancy and matured into a versatile electroanalytical technique capable of characterizing substrates in a wide variety of applications (see Figure 1). This success stems from the exceptional spatial resolution provided by SECM, and its advancement as a characterization technique has relied mostly on the improvement of this aspect, as demonstrated by the vast amount of literature focusing on probe miniaturization.

Probe miniaturization down to the nanoelectrode level is attractive because it offers several benefits including the ability to carry out electrochemistry in small spaces (drops,<sup>508,509</sup> microemulsions,<sup>51</sup> vesicles,<sup>510</sup> single cells,<sup>127</sup> nucleus<sup>103,111</sup>) or resistive environments. The decreased electrical double layer capacitance results in decreased time constants allowing nanosecond time scale measurements. In scaling down to achieve single molecule electrochemistry, radial diffusion becomes the dominant form of mass transport and we are confronted with technical and fundamental challenges. For example, nanoelectrode characterization is particularly onerous regardless of the method of preparation since it requires knowledge of the electrode geometry, which leads to a significant investment in imaging, or the availability of a controlled geometry fabrication protocol, which currently are all serial in nature. Specific to SECM, the stability of the nanogaps required during imaging with nanoelectrodes is subject to severe thermal drifts (5–150 nm/min) that should be corrected using an isothermal chamber, a significant instrument modification.<sup>511</sup>

The fundamental behavior of nanoelectrodes also changes with decreasing size, which requires us to be even more careful in our choice of experimental conditions. For example, changes in supporting electrolyte concentrations can have drastic effects on the limiting current,<sup>512,513</sup> which are ascribed to promotion or inhibition of redox fluxes from migration. What causes the strong enhancement or inhibition remains unclear. Several possibilities, reviewed at length elsewhere,<sup>514</sup> have been put forth including decreased electron-transfer rate and the dynamic nature of the electrical double layer, which depends on the charge of redox species, the size of the electrode, and the dielectric properties of the double layer.

Whether the micro- or nanoelectrochemical sensors are electrode arrays, soft stylus probes, or multifunctional probes, there is a clear trend to multiplex and cross-correlate the signals obtained from different redox species involved in complex electrochemical systems within the same microenvironment at similar time points.<sup>515,516</sup> This strategy is critical to the more widespread adoption of SECM in a broader community since it promotes higher throughput, a multivariate analysis, and the possibility to develop quality control. For example, large-scale integration-based chips containing over 400 sensors in a single device<sup>517,518</sup> allow for increased imaging size, and also decrease overall imaging time. The system faces significant engineering problems related to the ideal spatial arrangement and geometry, which affects the achievable resolution,<sup>519</sup> the optimal method to

move/align/orient the supracatalytic assemblies and substrate,<sup>515</sup> and the ideal design morphology to limit recycling, cross-talk, and shielding.<sup>520</sup> Notwithstanding the engineering challenges, significant effort is needed to develop a generally usable plotting and data treatment software that can deal with the large data sets and image processing filters to remove recycling and cross-talk effects. It is difficult to see how a significant numerical simulation effort will not also be tied to a successful software development.

Despite these newly developed probes and devices, the main limitation of SECM remains the relatively slow imaging speeds. In several experimental systems, such as corrosion or live cell imaging, temporal resolution is crucial to tracking the process under investigation. Improvement of this temporal resolution aspect is certainly a direction for future progress in this field. For example, using a spiral scanning pattern (instead of conventional line scans) with SECCM, a scanning droplet technique, Unwin and co-workers recently reported electrochemical imaging at up to 1000 times faster than typical speeds used in SECM.<sup>521</sup> This significant improvement can allow for previously unattainable measurements to be completed, such as time-resolved corrosion progression at different potentials. A significant challenge with the development of high-speed SECM will be the availability of models or numerical simulations that include diffusion, convection, and fluid flow considerations.<sup>522,523</sup>

Finally, a most promising avenue for the advancement of SECM (and electrochemical imaging in general) lies within combinatorial analyses. Several examples were described above, but new developments are constantly being reported, including the integration of fluorescence microscopy systems, spectrometers (for example, SECM-ATR<sup>382</sup> and SECM-Raman<sup>524</sup>), and hyphenated techniques (SICM-SECM,<sup>388,389</sup> AFM-SECM,<sup>525</sup> SECM-SPR,<sup>526</sup> SKP-SECM,<sup>387</sup> photoinduced SECM<sup>527</sup>). These new integrated instruments and hyphenated techniques move us forward toward multifunctional analytical platforms suitable to study molecular processes in complex environments and a more widespread adoption by the materials science community.

## AUTHOR INFORMATION

### Corresponding Author

\*E-mail: [janine.mauzeroll@mcgill.ca](mailto:janine.mauzeroll@mcgill.ca). Tel.: 514-398-3898.

### Notes

The authors declare no competing financial interest.

### Biographies

David Polcari received a B.Sc. in chemistry from McGill University in 2011 and is currently completing a Ph.D. in analytical chemistry under the supervision of Janine Mauzeroll at McGill University. His research focuses on the development of a diagnostic tool for the detection of multidrug resistance in human cancer cells using scanning electrochemical microscopy. He has also worked on the development of electrochemical biosensors for the in vivo detection of neurotransmitters.

Philippe Dauphin-Ducharme received his B.Sc. from l'Université de Montréal in 2011 and pursued his graduate studies under the supervision of Janine Mauzeroll at McGill University. He completed his Ph.D. in 2015 in materials chemistry where he studied the corrosion of magnesium alloys using a wide variety of analytical surface methods, notably scanning electrochemical microscopy. He is an author of six and coauthor in seven peer-reviewed publications. Dauphin-Ducharme is currently a Fond de Recherche—Nature et Technologies postdoctoral fellow at the University of California in Santa Barbara under the

supervision of Kevin Plaxco where he is developing new electrochemical DNA sensors for point-of-care diagnostics.

Janine Mauzeroll completed a B.Sc. (1999) in chemistry at McGill University, followed by a Ph.D. (2004) in electrochemistry at the premier laboratory of Allen J. Bard at the University of Texas Austin. Following this, Mauzeroll undertook a PDF position at l'Université de Paris 7 in the theoretical electrochemistry group of Jean-Micheal Savéant under the guidance of D. Marchal. Her work consistently combines experimental and theoretical electrochemical methods applied to pressing biomedical and industrial problems such as multidrug resistance in human cancer cells and corrosion in magnesium-containing automobiles.

## REFERENCES

- (1) Bard, A. J.; Fan, F. R. F.; Kwak, J.; Lev, O. Scanning Electrochemical Microscopy. Introduction and Principles. *Anal. Chem.* **1989**, *61*, 132–138.
- (2) Engstrom, R. C.; Pharr, C. M. Scanning Electrochemical Microscopy. *Anal. Chem.* **1989**, *61*, 1099A–1104A.
- (3) Mirkin, M. V.; Horrocks, B. R. Electroanalytical Measurements Using the Scanning Electrochemical Microscope. *Anal. Chim. Acta* **2000**, *406*, 119–146.
- (4) Sun, P.; Laforge, F. O.; Mirkin, M. V. Scanning Electrochemical Microscopy in the 21st Century. *Phys. Chem. Chem. Phys.* **2007**, *9*, 802–823.
- (5) Wittstock, G.; Burchardt, M.; Pust, S. E.; Shen, Y.; Zhao, C. Scanning Electrochemical Microscopy for Direct Imaging of Reaction Rates. *Angew. Chem., Int. Ed.* **2007**, *46*, 1584–1617.
- (6) Amemiya, S.; Bard, A. J.; Fan, F. R. F.; Mirkin, M. V.; Unwin, P. R. Scanning Electrochemical Microscopy. *Annu. Rev. Anal. Chem.* **2008**, *1*, 95–131.
- (7) Bard, A.; Mirkin, M. *Scanning Electrochemical Microscopy*; Monographs in Electroanalytical Chemistry and Electrochemistry; CRC Press: New York, 2001.
- (8) Bard, A.; Mirkin, M. *Scanning Electrochemical Microscopy*, 2nd ed.; CRC Press: New York, 2012.
- (9) Edwards, M. A.; Martin, S.; Whitworth, A. L.; Macpherson, J. V.; Unwin, P. R. Scanning Electrochemical Microscopy: Principles and Applications to Biophysical Systems. *Physiol. Meas.* **2006**, *27*, R63–108.
- (10) Lefrou, C.; Cornut, R. Analytical Expressions for Quantitative Scanning Electrochemical Microscopy (SECM). *ChemPhysChem* **2010**, *11*, 547–556.
- (11) Zhou, F.; Unwin, P. R.; Bard, A. J. Scanning Electrochemical Microscopy. 16. Study of Second-Order Homogeneous Chemical Reactions via the Feedback and Generation/Collection Modes. *J. Phys. Chem.* **1992**, *96*, 4917–4924.
- (12) Eckhard, K.; Chen, X.; Turcu, F.; Schuhmann, W. Redox Competition Mode of Scanning Electrochemical Microscopy (RC-SECM) for Visualisation of Local Catalytic Activity. *Phys. Chem. Chem. Phys.* **2006**, *8*, 5359–5365.
- (13) Santana, J. J.; González-Guzmán, J.; Fernández-Mérida, L.; González, S.; Souto, R. M. Visualization of Local Degradation Processes in Coated Metals by Means of Scanning Electrochemical Microscopy in the Redox Competition Mode. *Electrochim. Acta* **2010**, *55*, 4488–4494.
- (14) Wittstock, G.; Schuhmann, W. Formation and Imaging of Microscopic Enzymatically Active Spots on an Alkanethiolate-covered Gold Electrode by Scanning Electrochemical Microscopy. *Anal. Chem.* **1997**, *69*, S059–S066.
- (15) Meltzer, S.; Mandler, D. Microwriting of Gold Patterns with the Scanning Electrochemical Microscope. *J. Electrochem. Soc.* **1995**, *142*, L82–L84.
- (16) Wu, Y.-M.; Fan, F.-R. F.; Bard, A. J. High Resolution Deposition of Polyaniline on Pt with the Scanning Electrochemical Microscope. *J. Electrochem. Soc.* **1989**, *136*, 885–886.
- (17) El-Giar, E. E. D. M.; Wipf, D. O. Microparticle-Based Iridium Oxide Ultramicroelectrodes for pH Sensing and Imaging. *J. Electroanal. Chem.* **2007**, *609*, 147–154.



- (18) Cai, C.; Liu, B.; Mirkin, M. V.; Frank, H. A.; Rusling, J. F. Scanning Electrochemical Microscopy of Living Cells. 3. Rhodobacter Sphaeroides. *Anal. Chem.* **2002**, *74*, 114–119.
- (19) Longobardi, F.; Cosma, P.; Milano, F.; Agostiano, A.; Mauzeroll, J.; Bard, A. J. Scanning Electrochemical Microscopy of the Photosynthetic Reaction Center of Rhodobacter Sphaeroides in Different Environmental Systems. *Anal. Chem.* **2006**, *78*, 5046–5051.
- (20) Zhang, J.; Barker, A. L.; Mandler, D.; Unwin, P. R. Effect of Surface Pressure on the Insulator to Metal Transition of a Langmuir Polyaniline Monolayer. *J. Am. Chem. Soc.* **2003**, *125*, 9312–9313.
- (21) Liljeroth, P.; Vanmaekelbergh, D.; Ruiz, V.; Kontturi, K.; Jiang, H.; Kauppinen, E.; Quinn, B. M. Electron Transport in Two-Dimensional Arrays of Gold Nanocrystals Investigated by Scanning Electrochemical Microscopy. *J. Am. Chem. Soc.* **2004**, *126*, 7126–7132.
- (22) Ruiz, V.; Nicholson, P. G.; Jollands, S.; Thomas, P. A.; Macpherson, J. V.; Unwin, P. R. Molecular Ordering and 2D Conductivity in Ultrathin Poly(3-hexylthiophene)/ Gold Nanoparticle Composite Films. *J. Phys. Chem. B* **2005**, *109*, 19335–19344.
- (23) O'Mullane, A. P.; Macpherson, J. V.; Unwin, P. R.; Cervera-Montesinos, J.; Manzanares, J. A.; Frehill, F.; Vos, J. G. Measurement of Lateral Charge Propagation in [Os(bpy)<sub>2</sub>(PVP) nCl]Cl Thin Films: A Scanning Electrochemical Microscopy Approach. *J. Phys. Chem. B* **2004**, *108*, 7219–7227.
- (24) Slevin, C. J.; Unwin, P. R. Lateral Proton Diffusion Rates along Stearic Acid Monolayers. *J. Am. Chem. Soc.* **2000**, *122*, 2597–2602.
- (25) Pust, S. E.; Salomo, M.; Oesterschulze, E.; Wittstock, G. Influence of Electrode Size and Geometry on Electrochemical Experiments with Combined SECM-SFM Probes. *Nanotechnology* **2010**, *21*, 105709.
- (26) Fortin, E.; Chane-Tune, J.; Mailley, P.; Szunerits, S.; Marcus, B.; Petit, J. P.; Mermoux, M.; Vieil, E. Nucleosides and ODN Electrochemical Detection onto Boron Doped Diamond Electrodes. *Bioelectrochemistry* **2004**, *63*, 303–306.
- (27) Nebel, M.; Neugebauer, S.; Eckhard, K.; Schuhmann, W. Ring-Disk Microelectrodes for Simultaneous Constant-Distance and Constant-Current Mode Scanning Electrochemical Microscopy. *Electrochem. Commun.* **2013**, *27*, 160–163.
- (28) Xiong, H.; Gross, D. A.; Guo, J.; Amemiya, S. Local Feedback Mode of Scanning Electrochemical Microscopy for Electrochemical Characterization of One-Dimensional Nanostructure: Theory and Experiment with Nanoband Electrode as Model Substrate. *Anal. Chem.* **2006**, *78*, 1946–1957.
- (29) Ghilane, J.; Guilloux-Viry, M.; Lagrost, C.; Simonet, J.; Hapiot, P. Reactivity of Platinum Metal with Organic Radical anions from Metal to Negative Oxidation States. *J. Am. Chem. Soc.* **2007**, *129*, 6654–6661.
- (30) Ghilane, J.; Martin, P.; Janin, M.; Randriamahazaka, H.; Hapiot, P.; Lacroix, J. C. Electrochemical Investigation of Thin PEDOT Film Above an Insulating Substrate Using Scanning Electrochemical Microscopy. *Electrochem. Commun.* **2009**, *11*, 2304–2307.
- (31) Fabre, B.; Bassani, D. M.; Liang, C. K.; Ray, D.; Hui, F.; Hapiot, P. Anthracene and Anthracene:C<sub>60</sub> Adduct-Terminated Monolayers Covalently Bound to Hydrogen-Terminated Silicon Surfaces. *J. Phys. Chem. C* **2011**, *115*, 14786–14796.
- (32) Fabre, B.; Bassani, D. M.; Liang, C. K.; Lhenry, S.; Hapiot, P. Photodimerization and Micropatterning of Anthracene-Appended Receptors Covalently Bound to Silicon Surfaces: En Route to Write-Read-Erase Molecular Print Board. *J. Phys. Chem. C* **2013**, *117*, 12725–12734.
- (33) Nogala, W.; Szot, K.; Burchardt, M.; Jonsson-Niedziolka, M.; Rogalski, J.; Wittstock, G.; Opallo, M. Scanning Electrochemical Microscopy Activity Mapping of Electrodes Modified with Laccase Encapsulated in Sol-Gel Processed Matrix. *Bioelectrochemistry* **2010**, *79*, 101–107.
- (34) Fave, C.; Noel, V.; Ghilane, J.; Trippé-Allard, G.; Randriamahazaka, H.; Lacroix, J. C. Electrochemical Switches Based on Ultrathin Organic Films: From Diode-like Behavior to Charge Transfer Transparency. *J. Phys. Chem. C* **2008**, *112*, 18638–18643.
- (35) Combellas, C.; Kanoufi, F.; Mazouzi, D. Surface Modification of Halogenated Polymers. 8. Local Reduction of Poly(tetrafluoroethylene) by the Scanning Electrochemical Microscope - Transient Investigation. *J. Phys. Chem. B* **2004**, *108*, 19260–19268.
- (36) Zigah, D.; Ghilane, J.; Lagrost, C.; Hapiot, P. Variations of Diffusion Coefficients of Redox Active Molecules in Room Temperature Ionic Liquids upon Electron Transfer. *J. Phys. Chem. B* **2008**, *112*, 14952–14958.
- (37) Lhenry, S.; Leroux, Y. R.; Hapiot, P. Chemically Irreversible Redox Mediator for SECM Kinetics Investigations: Determination of the Absolute Tip-Sample Distance. *Anal. Chem.* **2013**, *85*, 1840–1845.
- (38) Zhou, J.; Campbell, C.; Heller, A.; Bard, A. J. Scanning Electrochemical Microscopy. 44. Imaging of Horseradish Peroxidase Immobilized on Insulating Substrates. *Anal. Chem.* **2002**, *74*, 4007–4010.
- (39) Heß, C.; Borgwarth, K.; Ricken, C.; Ebling, D. G.; Heinze, J. Scanning Electrochemical Microscopy: Study of Silver Deposition on Non-Conducting Substrates. *Electrochim. Acta* **1997**, *42*, 3065–3073.
- (40) Li, X.; Geng, Q.; Wang, Y.; Si, Z.; Jiang, W.; Zhang, X.; Jin, W. Fabrication of Active Horseradish Peroxidase Micropatterns with a High Resolution by Scanning Electrochemical Microscopy. *Electroanalysis* **2007**, *19*, 1734–1740.
- (41) Nogala, W.; Szot, K.; Burchardt, M.; Roelfs, F.; Rogalski, J.; Opallo, M.; Wittstock, G. Feedback Mode SECM Study of Laccase and Bilirubin Oxidase Immobilised in a Sol-Gel Processed Silicate Film. *Analyst* **2010**, *135*, 2051–2058.
- (42) Valenti, G.; Bardini, L.; Bonazzi, D.; Rapino, S.; Marcaccio, M.; Paolucci, F. Creation of Reactive Micro Patterns on Silicon by Scanning Electrochemical Microscopy. *J. Phys. Chem. C* **2010**, *114*, 22165–22170.
- (43) Basame, S. B.; White, H. S. Scanning Electrochemical Microscopy of Native Titanium Oxide Films. Mapping the Potential Dependence of Spatially-Localized Electrochemical Reactions. *J. Phys. Chem.* **1995**, *99*, 16430–16435.
- (44) Macpherson, J. V.; Unwin, P. R.; Hillier, A. C.; Bard, A. J. In-Situ Imaging of Ionic Crystal Dissolution Using an Integrated Electrochemical/AFM Probe. *J. Am. Chem. Soc.* **1996**, *118*, 6445–6452.
- (45) Zhang, J.; Jia, J.; Han, L.; Yuan, Y.; Tian, Z. Q.; Tian, Z. W.; Zhan, D. Kinetic Investigation on the Confined Etching System of n-type Gallium Arsenide by Scanning Electrochemical Microscopy. *J. Phys. Chem. C* **2014**, *118*, 18604–18611.
- (46) Zhang, H.; Xiao, X.; Su, T.; Gu, X.; Jin, T.; Du, L.; Tang, J. A Novel Thermocouple Microelectrode for Applications in SECM and Variable Temperature Electrochemistry. *Electrochem. Commun.* **2014**, *47*, 71–74.
- (47) Han, L.; Yuan, Y.; Zhang, J.; Zhao, X.; Cao, Y.; Hu, Z.; Yan, Y.; Dong, S.; Tian, Z. Q.; Tian, Z. W.; et al. A Leveling Method Based on Current Feedback Mode of Scanning Electrochemical Microscopy. *Anal. Chem.* **2013**, *85*, 1322–1326.
- (48) Zhao, C.; Witte, I.; Wittstock, G. Switching on Cell Adhesion with Microelectrodes. *Angew. Chem., Int. Ed.* **2006**, *45*, 5469–5471.
- (49) Zhao, C.; Zawisza, I.; Nullmeier, M.; Burchardt, M.; Träuble, M.; Witte, I.; Wittstock, G. Microelectrochemical Modulation of Micropatterned Cellular Environments. *Langmuir* **2008**, *24*, 7605–7613.
- (50) Zhao, C.; Burchardt, M.; Brinkhoff, T.; Beardsley, C.; Simon, M.; Wittstock, G. Microfabrication of Patterns of Adherent Marine Bacterium *Phaeobacter Inhibens* Using Soft Lithography and Scanning Probe Lithography. *Langmuir* **2010**, *26*, 8641–8647.
- (51) Shao, Y.; Mirkin, M. V.; Rusling, J. F. Liquid/Liquid Interface as a Model System for Studying Electrochemical Catalysis in Microemulsions. Reduction of Trans-1,2-dibromocyclohexane with Vitamin B12. *J. Phys. Chem. B* **1997**, *101*, 3202–3208.
- (52) Mirkin, M. V.; Bulhoes, L. O. S.; Bard, A. J. Determination of the Kinetic Parameters for the Electroreduction of C60 by Scanning Electrochemical Microscopy and Fast Scan Cyclic Voltammetry. *J. Am. Chem. Soc.* **1993**, *115*, 201–204.
- (53) Cliffel, D. E.; Bard, A. J. Scanning Electrochemical Microscopy. 36. A Combined Scanning Electrochemical Microscope-Quartz Crystal Microbalance Instrument for Studying Thin Films. *Anal. Chem.* **1998**, *70*, 1993–1998.
- (54) Zhang, J.; Unwin, P. R. Investigation of the Kinetics of Electron Transfer Processes Involving Fullerenes at Liquid-Liquid Interfaces Using Scanning Electrochemical Microscopy: Evidence for Marcus

Inverted Region Behaviour. *J. Chem. Soc., Perkin Trans.* **2001**, 2, 1608–1612.

(55) Zeradjanin, A. R.; Menzel, N.; Schuhmann, W.; Strasser, P. On the Faradaic Selectivity and the Role of Surface Inhomogeneity During the Chlorine Evolution Reaction on Ternary Ti-Ru-Ir Mixed Metal Oxide Electrocatalysts. *Phys. Chem. Chem. Phys.* **2014**, 16, 13741–13747.

(56) Aouina, N.; Balbaud-Celier, F.; Huet, F.; Joiret, S.; Perrot, H.; Rouillard, F.; Vivier, V. Single Pit Initiation on 316L Austenitic Stainless Steel Using Scanning Electrochemical Microscopy. *Electrochim. Acta* **2011**, 56, 8589–8596.

(57) Still, J. W.; Wipf, D. O. Breakdown of the Iron Passive Layer by Use of the Scanning Electrochemical Microscope. *J. Electrochem. Soc.* **1997**, 144, 2657–2665.

(58) Mandler, D.; Bard, A. J. Hole Injection and Etching Studies of GaAs Using the Scanning Electrochemical Microscope. *Langmuir* **1990**, 6, 1489–1494.

(59) Lie, L. H.; Mirkin, M. V.; Hakkarainen, S.; Houlton, A.; Horrocks, B. R. Electrochemical Detection of Lateral Charge Transport in Metal Complex-DNA Monolayers Synthesized on Si(1 1 1) Electrodes. *J. Electroanal. Chem.* **2007**, 603, 67–80.

(60) Zhang, B.; Xu, X.; Zhang, X.; Huang, D.; Li, S.; Zhang, Y.; Zhan, F.; Deng, M.; He, Y.; Chen, W.; et al. Investigation of Dye Regeneration Kinetics in Sensitized Solar Cells by Scanning Electrochemical Microscopy. *ChemPhysChem* **2014**, 15, 1182–1189.

(61) Zhang, B.; Yuan, H.; Zhang, X.; Huang, D.; Li, S.; Wang, M.; Shen, Y. Investigation of Regeneration Kinetics in Quantum-Dots-Sensitized Solar Cells with Scanning Electrochemical Microscopy. *ACS Appl. Mater. Interfaces* **2014**, 6, 20913–20918.

(62) Ritzert, N. L.; Rodríguez-López, J.; Tan, C.; Abruña, H. D. Kinetics of Interfacial Electron Transfer at Single-Layer Graphene Electrodes in Aqueous and Nonaqueous Solutions. *Langmuir* **2013**, 29, 1683–1694.

(63) Xiong, H.; Guo, J.; Amemiya, S. Probing Heterogeneous Electron Transfer at an Unbiased Conductor by Scanning Electrochemical Microscopy in the Feedback Mode. *Anal. Chem.* **2007**, 79, 2735–2744.

(64) Pust, S. E.; Scharnweber, D.; Baunack, S.; Wittstock, G. Electron Transfer Kinetics at Oxide Films on Metallic Biomaterials: Scanning Electrochemical Microscopy Studies of  $\text{Ti}_6\text{Al}_4\text{V}$ . *J. Electrochem. Soc.* **2007**, 154, C508–C514.

(65) Tsionsky, M.; Bard, A. J.; Mirkin, M. V. Long-Range Electron Transfer Through a Lipid Monolayer at the Liquid/Liquid Interface. *J. Am. Chem. Soc.* **1997**, 119, 10785–10792.

(66) Ding, Z.; Quinn, B. M.; Bard, A. J. Kinetics of Heterogeneous Electron Transfer at Liquid/Liquid Interfaces as Studied by SECM. *J. Phys. Chem. B* **2001**, 105, 6367–6374.

(67) Lhenry, S.; Leroux, Y. R.; Hapiot, P. Use of Catechol as Selective Redox Mediator in Scanning Electrochemical Microscopy Investigations. *Anal. Chem.* **2012**, 84, 7518–7524.

(68) Zhan, D.; Mao, S.; Zhao, Q.; Chen, Z.; Hu, H.; Jing, P.; Zhang, M.; Zhu, Z.; Shao, Y. Electrochemical Investigation of Dopamine at the Water/1,2-Dichloroethane Interface. *Anal. Chem.* **2004**, 76, 4128–4136.

(69) Bulter, H.; Peters, F.; Schwenzel, J.; Wittstock, G. Spatiotemporal Changes of the Solid Electrolyte Interphase in Lithium-Ion Batteries Detected by Scanning Electrochemical Microscopy. *Angew. Chem., Int. Ed.* **2014**, 53, 10531–10535.

(70) Stockhausen, V.; Ghilane, J.; Martin, P.; Trippe-Allard, G.; Randriamahazaka, H.; Lacroix, J. C. Grafting Oligothiophenes on Surfaces by Diazonium Electroreduction: A Step toward Ultrathin Junction with Well-Defined Metal/Oligomer Interface. *J. Am. Chem. Soc.* **2009**, 131, 14920–14927.

(71) Zigah, D.; Noel, J. M.; Lagrost, C.; Hapiot, P. Charge Transfer Between Electroactive Species Immobilized on Carbon Surfaces by Aryl Diazonium Reduction. SECM Investigations. *J. Phys. Chem. C* **2010**, 114, 3075–3081.

(72) Zhang, J.; Barker, A. L.; Unwin, P. R. Microelectrochemical Studies of Charge Transfer at the Interface Between Two Immiscible Electrolyte Solutions: Electron Transfer from Decamethyl Ferrocene to Aqueous Oxidants. *J. Electroanal. Chem.* **2000**, 483, 95–107.

(73) Shul, G.; Nogala, W.; Zakorchemna, I.; Niedziolka, J.; Opallo, M. Scanning Electrochemical Microscopy Study of Ion Transfer Process Across Water/2-Nitrophenyloctylether Interface Supported by Hydrophobic Carbon Ceramic Electrode. *J. Solid State Electrochem.* **2008**, 12, 1285–1291.

(74) Adamiak, W.; Jedraszko, J.; Krysiak, O.; Nogala, W.; Hidalgo-Acosta, J. C.; Girault, H. H.; Opallo, M. Hydrogen and Hydrogen Peroxide Formation in Trifluorotoluene-Water Biphasic Systems. *J. Phys. Chem. C* **2014**, 118, 23154–23161.

(75) Lu, X. Q.; Ma, J. Y.; Liu, X. H.; Dong, C. W.; Wang, W. T. Kinetic Comparison Between Ferric Ion and Decamethylferrocene at the Liquid/Liquid Interface as Studied by Scanning Electrochemical Microscopy. *Chin. Chem. Lett.* **2010**, 21, 89–92.

(76) Liu, B.; Mirkin, M. V. Potential-Independent Electron Transfer Rate at the Liquid/Liquid Interface. *J. Am. Chem. Soc.* **1999**, 121, 8352–8355.

(77) Zigah, D.; Herrier, C.; Scheres, L.; Giesbers, M.; Fabre, B.; Hapiot, P.; Zuilhof, H. Tuning the Electronic Communication Between Redox Centers Bound to Insulating Surfaces. *Angew. Chem., Int. Ed.* **2010**, 49, 3157–3160.

(78) Georganopoulou, D. G.; Strutwolf, J.; Pereira, C. M.; Silva, F.; Unwin, P. R.; Williams, D. E. Effect of Nonionic Surfactants on Interfacial Electron Transfer at the Liquid/Liquid Interface. *Langmuir* **2001**, 17, 8348–8354.

(79) Shreve, G. A.; Karp, C. D.; Pomykal, K. E.; Lewis, N. S. Limits on the Corrosion Rate of Si Surfaces in Contact with  $\text{CH}_3\text{OH}$ -Ferrocene<sup>+/0</sup> and  $\text{CH}_3\text{OH}$ -1,1'-Dimethylferrocene<sup>+/0</sup> Solutions. *J. Phys. Chem.* **1995**, 99, 5575–5580.

(80) Xie, S.; Meng, X.; Liang, Z.; Li, B.; Chen, Z.; Zhu, Z.; Li, M.; Shao, Y. Kinetics of Heterogeneous Electron Transfer Reactions at the Externally Polarized Water/o-nitrophenyl Octyl Ether Interface. *J. Phys. Chem. C* **2008**, 112, 18117–18124.

(81) Seegmiller, J. C.; Buttry, D. A. A SECM Study of Heterogeneous Redox Activity at AA2024 Surfaces. *J. Electrochem. Soc.* **2003**, 150, B413–B418.

(82) Dufek, E. J.; Buttry, D. A. Characterization of Zr(IV)-Phosphonate Thin Films which Inhibit  $\text{O}_2$  Reduction on AA2024-T3. *J. Electrochem. Soc.* **2009**, 156, C322–C330.

(83) Seegmiller, J. C.; Pereira Da Silva, J. E.; Buttry, D. A.; Córdoba De Torresi, S. I.; Torresi, R. M. Mechanism of Action of Corrosion Protection Coating for AA2024-T3 Based on Poly(aniline)-Poly(methylmethacrylate) Blend. *J. Electrochem. Soc.* **2005**, 152, B45–B53.

(84) Wittstock, G.; Wilhelm, T.; Bahrs, S.; Steinrucke, P. SECM Feedback Imaging of Enzymatic Activity on Agglomerated Microbeads. *Electroanalysis* **2001**, 13, 669–675.

(85) Diaz-Ballote, L.; Alpuche-Aviles, M.; Wipf, D. O. Fast-Scan Cyclic Voltammetry-Scanning Electrochemical Microscopy. *J. Electroanal. Chem.* **2007**, 604, 17–25.

(86) Unwin, P. R.; Bard, A. J. Scanning Electrochemical Microscopy. 9. Theory and Application of the Feedback Mode to the Measurement of Following Chemical Reaction Rates in Electrode Processes. *J. Phys. Chem.* **1991**, 95, 7814–7824.

(87) Cristarella, T. C.; Chinderle, A. J.; Hui, J.; Rodriguez-Lopez, J. Single-Layer Graphene as a Stable and Transparent Electrode for Nonaqueous Radical Annihilation Electrogenenerated Chemiluminescence. *Langmuir* **2015**, 31, 3999–4007.

(88) Cao, F.; Kim, J.; Bard, A. J. Detection of the Short-Lived Cation Radical Intermediate in the Electrochemical Oxidation of N, N-dimethylaniline by Scanning Electrochemical Microscopy. *J. Am. Chem. Soc.* **2014**, 136, 18163–18169.

(89) Barton, Z. J.; Rodriguez-Lopez, J. Lithium Ion Quantification Using Mercury Amalgams as In Situ Electrochemical Probes in Nonaqueous Media. *Anal. Chem.* **2014**, 86, 10660–10667.

(90) Quinto, M.; Jenekhe, S. A.; Bard, A. J. Polymer Films on Electrodes. 30. Electrochemistry and Scanning Electrochemical Microscopy Characterization of Benimidazolebenzophenanthroline-type Ladder (BBL) and Semiladder (BBB) Polymer Films. *Chem. Mater.* **2001**, 13, 2824–2832.



- (91) Ghilane, J.; Hauquier, F.; Fabre, B.; Hapiot, P. Scanning Electrochemical Microscopy Investigations of Monolayers Bound to p-type Silicon Substrates. *Anal. Chem.* **2006**, *78*, 6019–6025.
- (92) Zampardi, G.; Ventosa, E.; La Mantia, F.; Schuhmann, W. In Situ Visualization of Li-Ion Intercalation and Formation of the Solid Electrolyte Interphase on TiO<sub>2</sub> Based Paste Electrodes Using Scanning Electrochemical Microscopy. *Chem. Commun.* **2013**, *49*, 9347–9349.
- (93) Nkuku, C. A.; LeSuer, R. J. Electrochemistry in Deep Eutectic Solvents. *J. Phys. Chem. B* **2007**, *111*, 13271–13277.
- (94) Selzer, Y.; Mandler, D. A Novel Approach for Studying Charge Transfer Across an Interface of Two Immiscible Solutions Using the Scanning Electrochemical Microscope (SECM). *J. Electroanal. Chem.* **1996**, *409*, 15–17.
- (95) Laforge, F. O.; Kakiuchi, T.; Shigematsu, F.; Mirkin, M. V. Comparative Study of Electron Transfer Reactions at the Ionic Liquid/Water and Organic/Water Interfaces. *J. Am. Chem. Soc.* **2004**, *126*, 15380–15381.
- (96) Semenikhin, O. A.; Stromberg, C.; Ehrenburg, M. R.; König, U.; Schultze, J. W. Photoelectrochemical Properties and Microstructuring of Polythiophenes. *Electrochim. Acta* **2001**, *47*, 171–180.
- (97) Bozic, B.; Figgemeier, E. Scanning Electrochemical Microscopy Under Illumination: An Elegant Tool to Directly Determine the Mobility of Charge Carriers within Dye-Sensitized Nanostructured Semiconductors. *Chem. Commun.* **2006**, 2268–2270.
- (98) Oliveira, E. M.; Beyer, S.; Heinze, J. SECM Characterization of Immobilised Enzymes by Self-Assembled Monolayers on Titanium Dioxide Surfaces. *Bioelectrochemistry* **2007**, *71*, 186–191.
- (99) Mirkin, M. V.; Richards, T. C.; Bard, A. J. Scanning Electrochemical Microscopy. 20. Steady-State Measurements of the Fast Heterogeneous Kinetics in the Ferrocene/Acetonitrile System. *J. Phys. Chem.* **1993**, *97*, 7672–7677.
- (100) Horrocks, B. R.; Mirkin, M. V.; Bard, A. J. Scanning Electrochemical Microscopy. 25. Application to Investigation of the Kinetics of Heterogeneous Electron Transfer at Semiconductor (WSe<sub>2</sub> and Si) Electrodes. *J. Phys. Chem.* **1994**, *98*, 9106–9114.
- (101) Kranz, C.; Lotzbeyer, T.; Schmidt, H. L.; Schuhmann, W. Lateral Visualization of Direct Electron Transfer Between Microperoxidase and Electrodes by Means of Scanning Electrochemical Microscopy. *Biosens. Bioelectron.* **1997**, *12*, 257–266.
- (102) Holmes, J. L.; Davis, F.; Collyer, S. D.; Higson, S. P. J. A New Application of Scanning Electrochemical Microscopy for the Label-Free Interrogation of Antibody-Antigen Interactions. *Anal. Chim. Acta* **2011**, *689*, 206–211.
- (103) Guo, J.; Amemiya, S. Permeability of the Nuclear Envelope at Isolated Xenopus Oocyte Nuclei Studied by Scanning Electrochemical Microscopy. *Anal. Chem.* **2005**, *77*, 2147–2156.
- (104) Malik, M. A.; Kulesza, P. J. Monitoring of Conductivity Changes in passive Layers by Scanning Electrochemical Microscopy in Feedback Mode: Localization of Pitting Precursor Sites on Surfaces of Multimetallic Phase Materials. *Anal. Chem.* **2007**, *79*, 3996–4005.
- (105) Malik, M. A.; Kulesza, P. J.; Pawlowska, G. Surface Analysis with Scanning Electrochemical Microscopy in the Feedback Mode: Monitoring of Reactivity and Pitting Precursor Sites on the Nd-Fe-B-Type Magnet. *Electrochim. Acta* **2009**, *54*, 5537–5543.
- (106) Hussien, E. M.; Erichsen, T.; Schuhmann, W.; Maciejewska, M. SECM Visualization of the Spatial Variability of Enzyme-Polymer Spots. 3. Enzymatic Feedback Mode. *Anal. Bioanal. Chem.* **2008**, *391*, 1773–1782.
- (107) Kranz, C.; Wittstock, G.; Wohlschläger, H.; Schuhmann, W. Imaging of Microstructured Biochemically Active Surfaces by Means of Scanning Electrochemical Microscopy. *Electrochim. Acta* **1997**, *42*, 3105–3111.
- (108) Wei, C.; Bard, A. J.; Mirkin, M. V. Scanning Electrochemical Microscopy. 31. Application of SECM to the Study of Charge Transfer Processes at the Liquid/Liquid Interface. *J. Phys. Chem.* **1995**, *99*, 16033–16042.
- (109) Khamis, D.; Mahe, E.; Dardoize, F.; Devilliers, D. Peroxodisulfate Generation on Boron-Doped Diamond Microelectrodes Array and Detection by Scanning Electrochemical Microscopy. *J. Appl. Electrochem.* **2010**, *40*, 1829–1838.
- (110) Ferreyra, N. F.; Bollo, S.; Rivas, G. A. Self-Assembled Multilayers of Polyethylenimine, DNA and Gold Nanoparticles. A Study of Electron Transfer Reaction. *J. Electroanal. Chem.* **2010**, *638*, 262–268.
- (111) Liu, B.; Cheng, W.; Rotenberg, S. A.; Mirkin, M. V. Scanning Electrochemical Microscopy of Living Cells - Part 2. Imaging Redox and Acid/Basic Reactivities. *J. Electroanal. Chem.* **2001**, *500*, S90–S97.
- (112) Tosar, J. P.; Holmes, J. L.; Collyer, S. D.; Davis, F.; Lai-z, J.; Higson, S. P. J. Template and Catalytic Effects of DNA in the Construction of Polypyrrole/DNA Composite Macro and Micro-electrodes. *Biosens. Bioelectron.* **2013**, *41*, 294–301.
- (113) Zhang, J.; Burt, D. P.; Whitworth, A. L.; Mandler, D.; Unwin, P. R. Polyaniline Langmuir-Blodgett Films: Formation and Properties. *Phys. Chem. Chem. Phys.* **2009**, *11*, 3490–3496.
- (114) Fontaine, O.; Lagrost, C.; Ghilane, J.; Martin, P.; Trippé, G.; Fave, C.; Lacroix, J. C.; Hapiot, P.; Randriamahazaka, H. N. Mass Transport and Heterogeneous Electron Transfer of a Ferrocene Derivative in a Room-Temperature Ionic Liquid. *J. Electroanal. Chem.* **2009**, *632*, 88–96.
- (115) Sanchez-Sanchez, C. M.; Rodriguez-Lopez, J.; Bard, A. J. Scanning Electrochemical Microscopy. 60. Quantitative Calibration of the SECM Substrate Generation/Tip Collection Mode and its Use for the Study of the Oxygen Reduction Mechanism. *Anal. Chem.* **2008**, *80*, 3254–3260.
- (116) Noel, J. M.; Zigah, D.; Simonet, J.; Hapiot, P. Synthesis and Immobilization of Ag<sup>0</sup> Nanoparticles on Diazonium Modified Electrodes: SECM and Cyclic Voltammetry Studies of the Modified Interfaces. *Langmuir* **2010**, *26*, 7638–7643.
- (117) Johnson, L.; Walsh, D. A. Tip Generation-Substrate Collection-Tip Collection Mode Scanning Electrochemical Microscopy of Oxygen Reduction Electrocatalysts. *J. Electroanal. Chem.* **2012**, *682*, 45–52.
- (118) Asmussen, R. M.; Binns, W. J.; Jakupi, P.; Dauphin-Ducharme, P.; Tefashe, U. M.; Mauzeroll, J.; Shoesmith, D. Reducing the Corrosion Rate of Magnesium Alloys Using Ethylene Glycol for Advanced Electrochemical Imaging. *Corros. Sci.* **2015**, *93*, 70–79.
- (119) He, H.; Qin, Z.; Shoesmith, D. W. Characterizing the Relationship Between Hyperstoichiometry, Defect Structure and Local Corrosion Kinetics of Uranium Dioxide. *Electrochim. Acta* **2010**, *56*, 53–60.
- (120) Oyamatsu, D.; Hirano, Y.; Kanaya, N.; Mase, Y.; Nishizawa, M.; Matsue, T. Imaging of Enzyme Activity by Scanning Electrochemical Microscope Equipped with a Feedback Control for Substrate-Probe Distance. *Bioelectrochemistry* **2003**, *60*, 115–121.
- (121) Wilhelm, T.; Wittstock, G. Generation of Periodic Enzyme Patterns by Soft Lithography and Activity Imaging by Scanning Electrochemical Microscopy. *Langmuir* **2002**, *18*, 9485–9493.
- (122) Miao, W.; Ding, Z.; Bard, A. J. Solution Viscosity Effects on the Heterogeneous Electron Transfer Kinetics of Ferrocenemethanol in Dimethyl Sulfoxide-Water Mixtures. *J. Phys. Chem. B* **2002**, *106*, 1392–1398.
- (123) Sun, P.; Mirkin, M. V. Kinetics of Electron-Transfer Reactions at Nanoelectrodes. *Anal. Chem.* **2006**, *78*, 6526–6534.
- (124) Fonder, G.; Volcke, C.; Csoka, B.; Delhalle, J.; Mekhalif, Z. Electrochemical and Spectroscopic Study of C<sub>12</sub>H<sub>25</sub>X Molecules Adsorption on Copper Sheets, X (-SH, -S-S-, -SeH and -Se-Se-). *Electrochim. Acta* **2010**, *55*, 1557–1567.
- (125) Izquierdo, J.; Santana, J. J.; Gonzalez, S.; Souto, R. M. Uses of Scanning Electrochemical Microscopy for the Characterization of Thin Inhibitor Films on Reactive Metals: The Protection of Copper Surfaces by Benzotriazole. *Electrochim. Acta* **2010**, *55*, 8791–8800.
- (126) Takahashi, Y.; Hirano, Y.; Yasukawa, T.; Shiku, H.; Yamada, H.; Matsue, T. Topographic, Electrochemical, and Optical Images Captured Using Standing Approach Mode Scanning Electrochemical/Optical Microscopy. *Langmuir* **2006**, *22*, 10299–10306.
- (127) Sun, P.; Laforge, F. O.; Abeyweera, T. P.; Rotenberg, S. A.; Carpino, J.; Mirkin, M. V. Nanoelectrochemistry of Mammalian Cells. *Proc. Natl. Acad. Sci. U. S. A.* **2008**, *105*, 443–448.

- (128) Ahn, H. S.; Bard, A. J. Surface Interrogation of CoPi Water Oxidation Catalyst by Scanning Electrochemical Microscopy. *J. Am. Chem. Soc.* **2015**, *137*, 612–615.
- (129) Kim, E.; Xiong, H.; Striemer, C. C.; Fang, D. Z.; Fauchet, P. M.; McGrath, J. L.; Amemiya, S. A Structure-Permeability Relationship of Ultrathin Nanoporous Silicon Membrane: A Comparison with the Nuclear Envelope. *J. Am. Chem. Soc.* **2008**, *130*, 4230–4231.
- (130) Yamashita, K.; Takagi, M.; Uchida, K.; Kondo, H.; Takenaka, S. Visualization of DNA Microarrays by Scanning Electrochemical Microscopy (SECM). *Analyst* **2001**, *126*, 1210–1211.
- (131) Bertonecello, P.; Ciani, I.; Li, F.; Unwin, P. R. Measurement of Apparent Diffusion Coefficients within Ultrathin Nation Langmuir-Schaefer Films: Comparison of a Novel Scanning Electrochemical Microscopy Approach with Cyclic Voltammetry. *Langmuir* **2006**, *22*, 10380–10388.
- (132) Bath, B. D.; Scott, E. R.; Phipps, J. B.; White, H. S. Scanning Electrochemical Microscopy of Iontophoretic Transport in Hairless Mouse Skin. Analysis of the Relative Contributions of Diffusion, Migration, and Electroosmosis to Transport in Hair Follicles. *J. Pharm. Sci.* **2000**, *89*, 1537–1549.
- (133) Zhan, W.; Bard, A. J. Scanning Electrochemical Microscopy. 56. Probing Outside and Inside Single Giant Liposomes Containing Ru(bpy)<sub>3</sub><sup>2+</sup>. *Anal. Chem.* **2006**, *78*, 726–733.
- (134) Kim, J.; Xiong, H.; Hofmann, M.; Kong, J.; Amemiya, S. Scanning Electrochemical Microscopy of Individual Single-Walled Carbon Nanotubes. *Anal. Chem.* **2010**, *82*, 1605–1607.
- (135) Gonzalez, S.; Santana, J. J.; Gonzalez-Garcia, Y.; Fernandez-Merida, L.; Souto, R. M. Scanning Electrochemical Microscopy for the Investigation of Localized Degradation Processes in Coated Metals: Effect of Oxygen. *Corros. Sci.* **2011**, *53*, 1910–1915.
- (136) Sauter, S.; Wittstock, G. Local Deposition and Characterisation of K<sub>2</sub>Co[Fe(CN)<sub>6</sub>] and K<sub>2</sub>Ni[Fe(CN)<sub>6</sub>] by Scanning Electrochemical Microscopy. *J. Solid State Electrochem.* **2001**, *5*, 205–211.
- (137) Molina, J.; Fernandez, J.; Garcia, C.; Del Rio, A. I.; Bonastre, J.; Cases, F. Electrochemical Characterization of Electrochemically Reduced Graphene Coatings on Platinum. Electrochemical Study of Dye Adsorption. *Electrochim. Acta* **2015**, *166*, 54–63.
- (138) Cornut, R.; Nunige, S.; Lefrou, C.; Kanoufi, F. Local Etching of Copper Films by the Scanning Electrochemical Microscope in the Feedback Mode: A Theoretical and Experimental Investigation. *Electrochim. Acta* **2011**, *56*, 10701–10707.
- (139) Lee, C.; Bard, A. J. Scanning Electrochemical Microscopy. Application to Polymer and Thin Metal Oxide Films. *Anal. Chem.* **1990**, *62*, 1906–1913.
- (140) Lee, C.; Kwak, J.; Bard, A. J. Application of Scanning Electrochemical Microscopy to Biological Samples. *Proc. Natl. Acad. Sci. U. S. A.* **1990**, *87*, 1740–1743.
- (141) Cannan, S.; Cervera, J.; Steliaros, R. J.; Bitziou, E.; Whitworth, A. L.; Unwin, P. R. Scanning Electrochemical Microscopy (SECM) Studies of Catalytic EC' Processes: Theory and Experiment for Feedback, Generation/Collection and Imaging Measurements. *Phys. Chem. Chem. Phys.* **2011**, *13*, 5403–5412.
- (142) Fushimi, K.; Lill, K. A.; Habazaki, H. Heterogeneous Hydrogen Evolution on Corroding Fe-3 at.% Si Surface Observed by Scanning Electrochemical Microscopy. *Electrochim. Acta* **2007**, *52*, 4246–4253.
- (143) Pust, S. E.; Scharnweber, D.; Nunes Kirchner, C.; Wittstock, G. Heterogeneous Distribution of Reactivity on Metallic Biomaterials: Scanning Probe Microscopy Studies of the Biphasic Ti Alloy Ti6Al4V. *Adv. Mater.* **2007**, *19*, 878–882.
- (144) Sidane, D.; Bousquet, E.; Devos, O.; Puiggali, M.; Touzet, M.; Vivier, V.; Poulon-Quintin, A. Local Electrochemical Study of Friction Stir Welded Aluminum Alloy Assembly. *J. Electroanal. Chem.* **2015**, *737*, 206–211.
- (145) Pierce, D. T.; Unwin, P. R.; Bard, A. J. Scanning Electrochemical Microscopy. 17. Studies of Enzyme-Mediator Kinetics for Membrane- and Surface-Immobilized Glucose Oxidase. *Anal. Chem.* **1992**, *64*, 1795–1804.
- (146) Solomon, T.; Bard, A. J. Scanning Electrochemical Microscopy. 30. Application of Glass Micropipet Tips and Electron Transfer at the Interface Between Two Immiscible Electrolyte Solutions for SECM Imaging. *Anal. Chem.* **1995**, *67*, 2787–2790.
- (147) Barker, A. L.; Unwin, P. R.; Amemiya, S.; Zhou, J.; Bard, A. J. Scanning Electrochemistry Microscopy (SECM) in the Study of Electron Transfer Kinetics at Liquid/Liquid Interfaces: Beyond the Constant Composition Approximation. *J. Phys. Chem. B* **1999**, *103*, 7260–7269.
- (148) Tsionsky, M.; Zhou, J.; Amemiya, S.; Fan, F. R. F.; Bard, A. J.; Dryfe, R. A. W. Scanning Electrochemical Microscopy. 38. Application of SECM to the Study of Charge Transfer Through Bilayer Lipid Membranes. *Anal. Chem.* **1999**, *71*, 4300–4305.
- (149) Liu, B.; Rotenberg, S. A.; Mirkin, M. V. Scanning Electrochemical Microscopy of Living Cells: Different Redox Activities of Nonmetastatic and Metastatic Human Breast Cells. *Proc. Natl. Acad. Sci. U. S. A.* **2000**, *97*, 9855–9860.
- (150) Koley, D.; Bard, A. J. Triton X-100 Concentration Effects on Membrane Permeability of a Single HeLa Cell by Scanning Electrochemical Microscopy (SECM). *Proc. Natl. Acad. Sci. U. S. A.* **2010**, *107*, 16783–16787.
- (151) Combella, C.; Kanoufi, F.; Mazouzi, D.; Thiebault, A. Surface Modification of Halogenated Polymers: 5. Localized Electroless Deposition of Metals on Poly(tetrafluoroethylene) Surfaces. *J. Electroanal. Chem.* **2003**, *556*, 43–52.
- (152) Marck, C.; Borgwarth, K.; Heinze, J. Generation of Polythiophene Micropatterns by Scanning Electrochemical Microscopy. *Chem. Mater.* **2001**, *13*, 747–752.
- (153) Rodriguez-Lopez, J.; Minguzzi, A.; Bard, A. J. Reaction of Various Reductants with Oxide Films on Pt Electrodes as Studied by the Surface Interrogation Mode of Scanning Electrochemical Microscopy (SI-SECM): Possible Validity of a Marcus Relationship. *J. Phys. Chem. C* **2010**, *114*, 18645–18655.
- (154) Liu, B.; Bard, A. J.; Li, C. Z.; Kraatz, H. B. Scanning Electrochemical Microscopy. 51. Studies of Self-Assembled Monolayers of DNA in the Absence and Presence of Metal Ions. *J. Phys. Chem. B* **2005**, *109*, 5193–5198.
- (155) Mandler, D.; Bard, A. J. Scanning Electrochemical Microscopy: The Application of the Feedback Mode for High Resolution Copper Etching. *J. Electrochem. Soc.* **1989**, *136*, 3143–3144.
- (156) Turyan, I.; Orel, B.; Reisfeld, R.; Mandler, D. Studying Electron Transfer at Electrochromic Tungsten Oxide Sol-Gel Films with Scanning Electrochemical Microscopy (SECM). *Phys. Chem. Chem. Phys.* **2003**, *5*, 3212–3219.
- (157) Lu, X.; Gu, W.; Sun, R.; Liu, X. Investigation of Electrochemical Properties of Metalloporphyrin Species at the Liquid/Liquid Interface by Switching Substitutes on the Porphyrin Ring. *Electroanalysis* **2012**, *24*, 2341–2347.
- (158) Bi, S.; Liu, B.; Fan, F. R. F.; Bard, A. J. Electrochemical Studies of Guanosine in DMF and Detection of its Radical Cation in a Scanning Electrochemical Microscopy Nanogap Experiment. *J. Am. Chem. Soc.* **2005**, *127*, 3690–3691.
- (159) Selzer, Y.; Turyan, I.; Mandler, D. Studying Heterogeneous Catalysis by the Scanning Electrochemical Microscope (SECM): The Reduction of Protons by Methyl Viologen Catalyzed by a Platinum Surface. *J. Phys. Chem. B* **1999**, *103*, 1509–1517.
- (160) Leblanc, G.; Chen, G.; Jennings, G. K.; Cliffel, D. E. Photoreduction of Catalytic Platinum Particles Using Immobilized Multilayers of Photosystem I. *Langmuir* **2012**, *28*, 7952–7956.
- (161) Nicholson, P. G.; Zhou, S.; Hinds, G.; Wain, A. J.; Turnbull, A. Electrocatalytic Activity Mapping of Model Fuel Cell Catalyst Films Using Scanning Electrochemical Microscopy. *Electrochim. Acta* **2009**, *54*, 4525–4533.
- (162) Bard, A. J.; Fan, F. R. F.; Pierce, D. T.; Unwin, P. R.; Wipf, D. O.; Zhou, F. Chemical Imaging of Surfaces with the Scanning Electrochemical Microscope. *Science* **1991**, *254*, 68–74.
- (163) Zoski, C. G. Scanning Electrochemical Microscopy: Investigation of Hydrogen Oxidation at Polycrystalline Noble Metal Electrodes. *J. Phys. Chem. B* **2003**, *107*, 6401–6405.
- (164) Zhou, J.; Zu, Y.; Bard, A. J. Scanning Electrochemical Microscopy - Part 39. The Proton/Hydrogen Mediator System and



its Application to the Study of the Electrocatalysis of Hydrogen Oxidation. *J. Electroanal. Chem.* **2000**, *491*, 22–29.

(165) Horrocks, B. R.; Schmidtke, D.; Heller, A.; Bard, A. J. Scanning Electrochemical Microscopy. 24. Enzyme Ultramicroelectrodes for the Measurement of Hydrogen Peroxide at Surfaces. *Anal. Chem.* **1993**, *65*, 3605–3614.

(166) Liu, X.; Ramsey, M. M.; Chen, X.; Koley, D.; Whiteley, M.; Bard, A. J. Real-Time Mapping of a Hydrogen Peroxide Concentration Profile Across a Polymicrobial Bacterial Biofilm Using Scanning Electrochemical Microscopy. *Proc. Natl. Acad. Sci. U. S. A.* **2011**, *108*, 2668–2673.

(167) Eckhard, K.; Schuhmann, W. Localised Visualisation of O<sub>2</sub> Consumption and H<sub>2</sub>O<sub>2</sub> Formation by Means of SECM for the Characterisation of Fuel Cell Catalyst Activity. *Electrochim. Acta* **2007**, *53*, 1164–1169.

(168) Kishi, A.; Inoue, M.; Umeda, M. Scanning Electrochemical Microscopy Study of H<sub>2</sub>O<sub>2</sub> byproduct During O<sub>2</sub> Reduction at Pt/C-Nafion Composite Cathode. *J. Phys. Chem. C* **2010**, *114*, 1110–1116.

(169) Li, F.; Su, B.; Salazar, F. C.; Nia, R. P.; Girault, H. H. Detection of Hydrogen Peroxide Produced at a Liquid/Liquid Interface Using Scanning Electrochemical Microscopy. *Electrochem. Commun.* **2009**, *11*, 473–476.

(170) Csoka, B.; Nagy, G. Determination of Diffusion Coefficient in Gel and in Aqueous Solutions Using Scanning Electrochemical Microscopy. *J. Biochem. Biophys. Methods* **2004**, *61*, 57–67.

(171) Zhao, X.; Diakowski, P. M.; Ding, Z. Deconvoluting Topography and Spatial Physiological Activity of Live Macrophage Cells by Scanning Electrochemical Microscopy in Constant-Distance Mode. *Anal. Chem.* **2010**, *82*, 8371–8373.

(172) Zhang, J.; Unwin, P. R. Proton Diffusion at Phospholipid Assemblies. *J. Am. Chem. Soc.* **2002**, *124*, 2379–2383.

(173) Basame, S. B.; White, H. S. Scanning Electrochemical Microscopy of Metal/Metal Oxide Electrodes. Analysis of Spatially Localized Electron-Transfer Reactions During Oxide Growth. *Anal. Chem.* **1999**, *71*, 3166–3170.

(174) Shen, Y.; Nonomura, K.; Schlettwein, D.; Zhao, C.; Wittstock, G. Photoelectrochemical Kinetics of Eosin Y-sensitized Zinc Oxide Films Investigated by Scanning Electrochemical Microscopy. *Chem. - Eur. J.* **2006**, *12*, 5832–5839.

(175) Paik, C. H.; White, H. S.; Alkire, R. C. Scanning Electrochemical Microscopy Detection of Dissolved Sulfur Species from Inclusions in Stainless Steel. *J. Electrochem. Soc.* **2000**, *147*, 4120–4124.

(176) Paik, C. H.; Alkire, R. C. Role of Sulfide Inclusions on Localized Corrosion of Ni200 in NaCl Solutions. *J. Electrochem. Soc.* **2001**, *148*, B276–B281.

(177) Shen, Y.; Tefashe, U. M.; Nonomura, K.; Loewenstein, T.; Schlettwein, D.; Wittstock, G. Photoelectrochemical Kinetics of Eosin Y-sensitized Zinc Oxide Films Investigated by Scanning Electrochemical Microscopy under Illumination with Different LED. *Electrochim. Acta* **2009**, *55*, 458–464.

(178) Ejigu, A.; Lovelock, K. R. J.; Licence, P.; Walsh, D. A. Iodide/Triiodide Electrochemistry in Ionic Liquids: Effect of Viscosity on Mass Transport, Voltammetry and Scanning Electrochemical Microscopy. *Electrochim. Acta* **2011**, *56*, 10313–10320.

(179) Liu, B.; Rotenberg, S. A.; Mirkin, M. V. Scanning Electrochemical Microscopy of Living Cells. 4. Mechanistic Study of Charge Transfer Reactions in Human Breast Cells. *Anal. Chem.* **2002**, *74*, 6340–6348.

(180) Lucas, M.; Stafiej, J.; Slim, C.; Delpech, S.; Di Caprio, D. Cellular Automata Modeling of Scanning Electrochemical Microscopy (SECM) Experiments. *Electrochim. Acta* **2014**, *145*, 314–318.

(181) Park, H. S.; Leonard, K. C.; Bard, A. J. Surface Interrogation Scanning Electrochemical Microscopy (SI-SECM) of Photoelectrochemistry at a W/Mo-BiVO<sub>4</sub> Semiconductor Electrode: Quantification of Hydroxyl Radicals During Water Oxidation. *J. Phys. Chem. C* **2013**, *117*, 12093–12102.

(182) Zhang, M.; Wittstock, G.; Shao, Y.; Girault, H. H. Scanning Electrochemical Microscopy as a Readout Tool for Protein Electrophoresis. *Anal. Chem.* **2007**, *79*, 4833–4839.

(183) Zhang, J.; Unwin, P. R. Kinetics of IrCl<sub>6</sub><sup>2-</sup> Ion Transfer Across the Water/1,2-Dichloroethane Interface and the Effect of a Phospholipid Monolayer. *Langmuir* **2002**, *18*, 2313–2318.

(184) Jeon, I. C.; Anson, F. C. Application of Scanning Electrochemical Microscopy to Studies of Charge Propagation within Polyelectrolyte Coatings on Electrodes. *Anal. Chem.* **1992**, *64*, 2021–2028.

(185) Slevin, C. J.; Gray, N. J.; MacPherson, J. V.; Webb, M. A.; Unwin, P. R. Fabrication and Characterisation of Nanometre-Sized Platinum Electrodes for Voltammetric Analysis and Imaging. *Electrochem. Commun.* **1999**, *1*, 282–288.

(186) Laforge, F. O.; Velmurugan, J.; Wang, Y.; Mirkin, M. V. Nanoscale Imaging of Surface Topography and Reactivity with the Scanning Electrochemical Microscope. *Anal. Chem.* **2009**, *81*, 3143–3150.

(187) Chen, Z.; Xie, S.; Shen, L.; Du, Y.; He, S.; Li, Q.; Liang, Z.; Meng, X.; Li, B.; Xu, X.; et al. Investigation of the Interactions Between Silver Nanoparticles and HeLa Cells by Scanning Electrochemical Microscopy. *Analyst* **2008**, *133*, 1221–1228.

(188) Morgenstern, T.; Schultze, J. W. Laser Deposition of Metals and Polymers in Si-Microstructures. *Electrochim. Acta* **1997**, *42*, 3057–3064.

(189) Grundig, B.; Wittstock, G.; Rudel, U.; Strehlitz, B. Mediator-Modified Electrodes for Electrocatalytic Oxidation of NADH. *J. Electroanal. Chem.* **1995**, *395*, 143–157.

(190) Pyo, M.; Bard, A. J. Scanning Electrochemical Microscopy. 35. Determination of Diffusion Coefficients and Concentrations of Ru(NH<sub>3</sub>)<sub>6</sub><sup>3+</sup> and Methylene Blue in Polyacrylamide Films by Chronoamperometry at Ultramicrodisk Electrodes. *Electrochim. Acta* **1997**, *42*, 3077–3083.

(191) Mauzeroll, J.; Bard, A. J. Scanning Electrochemical Microscopy of Menadione-Glutathione Conjugate Export from Yeast Cells. *Proc. Natl. Acad. Sci. U. S. A.* **2004**, *101*, 7862–7867.

(192) Sugimura, H.; Uchida, T.; Shimo, N.; Kitamura, N.; Masuhara, H. Fluorescent Micropattern Formation on Ionic Conductive Polymer Films by a Scanning Electrochemical Microscope. *Ultramicroscopy* **1992**, *42–44*, 468–474.

(193) Chen, G.; Hijazi, F. M.; LeBlanc, G.; Jennings, G. K.; Cliffl, D. E. Scanning Electrochemical Microscopy of Multilayer Photosystem I Photoelectrochemistry. *ECS Electrochem. Lett.* **2013**, *2*, H59–H62.

(194) Li, F.; Ciani, I.; Bertoncello, P.; Unwin, P. R.; Zhao, J.; Bradbury, C. R.; Fermin, D. J. Scanning Electrochemical Microscopy of Redox-Mediated Hydrogen Evolution Catalyzed by Two-Dimensional Assemblies of Palladium Nanoparticles. *J. Phys. Chem. C* **2008**, *112*, 9686–9694.

(195) Pierce, D. T.; Bard, A. J. Scanning Electrochemical Microscopy. 23. Reaction Localization of Artificially Patterned and Tissue-Bound Enzymes. *Anal. Chem.* **1993**, *65*, 3598–3604.

(196) Ragsdale, S. R.; White, H. S. Imaging Microscopic Magneto-hydrodynamic Flows. *Anal. Chem.* **1999**, *71*, 1923–1927.

(197) Pailleret, A.; Oni, J.; Reiter, S.; Isik, S.; Etienne, M.; Bedioui, F.; Schuhmann, W. In Situ Formation and Scanning Electrochemical Microscopy Assisted Positioning of NO-Sensors above Human Umbilical Vein Endothelial Cells for the Detection of Nitric Oxide Release. *Electrochem. Commun.* **2003**, *5*, 847–852.

(198) Borgmann, S.; Radtke, I.; Erichsen, T.; Blöchl, A.; Heumann, R.; Schuhmann, W. Electrochemical High-Content Screening of Nitric Oxide Release from Endothelial Cells. *ChemBioChem* **2006**, *7*, 662–668.

(199) Feng, W.; Rotenberg, S. A.; Mirkin, M. V. Scanning Electrochemical Microscopy of Living Cells. 5. Imaging of Fields of Normal and Metastatic Human Breast Cells. *Anal. Chem.* **2003**, *75*, 4148–4154.

(200) Volatron, F.; Noel, J. M.; Rinfray, C.; Decorse, P.; Combellas, C.; Kanoufi, F.; Proust, A. Electron Transfer Properties of a Monolayer of Hybrid Polyoxometalates on Silicon. *J. Mater. Chem. C* **2015**, *3*, 6266–6275.

(201) Tsionsky, M.; Cardon, Z. G.; Bard, A. J.; Jackson, R. B. Photosynthetic Electron Transport in Single Guard Cells as Measured by Scanning Electrochemical Microscopy. *Plant Physiol.* **1997**, *113*, 895–901.

- (202) Bollo, S.; Jara-Ulloa, P.; Finger, S.; Núñez Vergara, L. J.; Squella, J. A. Scanning Electrochemical Microscopy (SECM) Study of Superoxide Generation and its Reactivity with 1,4-Dihydropyridines. *J. Electroanal. Chem.* **2005**, *577*, 235–242.
- (203) Latus, A.; Noel, J. M.; Volanschi, E.; Lagrost, C.; Hapiot, P. Scanning Electrochemical Microscopy Studies of Glutathione-Modified Surfaces. An Erasable and Sensitive-to-Reactive Oxygen Species Surface. *Langmuir* **2011**, *27*, 11206–11211.
- (204) Ghilane, J.; Lagrost, C.; Hapiot, P. Scanning Electrochemical Microscopy in Nonusual Solvents: Inequality of Diffusion Coefficients Problem. *Anal. Chem.* **2007**, *79*, 7383–7391.
- (205) Gonsalves, M.; Barker, A. L.; Macpherson, J. V.; Unwin, P. R.; O'Hare, D.; Winlove, C. P. Scanning Electrochemical Microscopy as a Local Probe of Oxygen Permeability in Cartilage. *Biophys. J.* **2000**, *78*, 1578–1588.
- (206) Kueng, A.; Kranz, C.; Mizaikoff, B. Imaging of ATP Membrane Transport with Dual Micro-disk Electrodes and Scanning Electrochemical Microscopy. *Biosens. Bioelectron.* **2005**, *21*, 346–353.
- (207) Souto, R. M.; González-García, Y.; González, S. In Situ Monitoring of Electroactive Species by Using the Scanning Electrochemical Microscope. Application to the Investigation of Degradation Processes at Defective Coated Metals. *Corros. Sci.* **2005**, *47*, 3312–3323.
- (208) Strutwolf, J.; Zhang, J.; Barker, A. L.; Unwin, P. R. Effect of Phospholipids on the Kinetics of Dioxygen Transfer Across a 1,2-Dichloroethane/Water Interface. *Phys. Chem. Chem. Phys.* **2001**, *3*, 5553–5558.
- (209) Shiku, H.; Shiraishi, T.; Ohya, H.; Matsue, T.; Abe, H.; Hoshi, H.; Kobayashi, M. Oxygen Consumption of Single Bovine Embryos Probed by Scanning Electrochemical Microscopy. *Anal. Chem.* **2001**, *73*, 3751–3758.
- (210) Carano, M.; Lion, N.; Abid, J. P.; Girault, H. H. Detection of Proteins on Poly(vinylidene difluoride) Membranes by Scanning Electrochemical Microscopy. *Electrochem. Commun.* **2004**, *6*, 1217–1221.
- (211) Arca, M.; Mirkin, M. V.; Bard, A. J. Polymer Films on Electrodes. 26. Study of Ion Transport and Electron Transfer at Polypyrrole Films by Scanning Electrochemical Microscopy. *J. Phys. Chem.* **1995**, *99*, 5040–5050.
- (212) Hauquier, F.; Matrab, T.; Kanoufi, F.; Combellas, C. Local Direct and Indirect Reduction of Electrografted Aryldiazonium/Gold Surfaces for Polymer Brushes Patterning. *Electrochim. Acta* **2009**, *54*, 5127–5136.
- (213) Koley, D.; Ramsey, M. M.; Bard, A. J.; Whiteley, M. Discovery of a Biofilm Electroline Using Real-Time 3D Metabolite Analysis. *Proc. Natl. Acad. Sci. U. S. A.* **2011**, *108*, 19996–20001.
- (214) Emons, H.; Wittstock, G. Analytical In Situ Characterization of Chemical Reactivities at Interfaces in Aqueous Systems. *Mar. Chem.* **1996**, *53*, 17–23.
- (215) Bollo, S.; Finger, S.; Sturm, J. C.; Nunez-Vergara, L. J.; Squella, J. A. Cyclic Voltammetry and Scanning Electrochemical Microscopy Studies of the Heterogeneous Electron Transfer Reaction of Some Nitrosoaromatic Compounds. *Electrochim. Acta* **2007**, *52*, 4892–4898.
- (216) Fan, F. R. F.; Cliffl, D.; Bard, A. J. Scanning Electrochemical Microscopy. 37. Light Emission by Electrogenerated Chemiluminescence at SECM Tips and Their Application to Scanning Optical Microscopy. *Anal. Chem.* **1998**, *70*, 2941–2948.
- (217) Choi, J. P.; Bard, A. J. Electrogenerated Chemiluminescence (ECL) 79. Reductive-Oxidation ECL of Tris(2,2-bipyridine)ruthenium(II) Using Hydrogen Peroxide as a Coreactant in pH 7.5 Phosphate Buffer Solution. *Anal. Chim. Acta* **2005**, *541*, 141–148.
- (218) Li, F.; Whitworth, A. L.; Unwin, P. R. Measurement of Rapid Electron Transfer Across a Liquid/Liquid Interface from 7,7,8,8-Tetracyanoquinodimethane Radical Anion in 1,2-Dichloroethane to Aqueous Tris(2,2-bipyridyl)-ruthenium (III). *J. Electroanal. Chem.* **2007**, *602*, 70–76.
- (219) Macpherson, J. V.; Slevin, C. J.; Unwin, P. R. Probing the Oxidative Etching Kinetics of Metals with the Feedback Mode of the Scanning Electrochemical Microscope. *J. Chem. Soc., Faraday Trans.* **1996**, *92*, 3799–3805.
- (220) Tsionsky, M.; Bard, A. J.; Mirkin, M. V. Scanning Electrochemical Microscopy. 34. Potential Dependence of the Electron-Transfer Rate and Film Formation at the Liquid/Liquid Interface. *J. Phys. Chem.* **1996**, *100*, 17881–17888.
- (221) Neufeld, A. K.; O'Mullane, A. P. Effect of the Mediator in Feedback Mode-Based SECM Interrogation of Indium Tin-Oxide and Boron-Doped Diamond Electrodes. *J. Solid State Electrochem.* **2006**, *10*, 808–816.
- (222) Mandler, D.; Bard, A. J. New Approach to the High Resolution Electrodeposition of Metals via the Feedback Mode of the Scanning Electrochemical Microscope. *J. Electrochem. Soc.* **1990**, *137*, 1079–1086.
- (223) Macpherson, J. V.; O'Hare, D.; Unwin, P. R.; Winlove, C. P. Quantitative Spatially Resolved Measurements of Mass Transfer Through Laryngeal Cartilage. *Biophys. J.* **1997**, *73*, 2771–2781.
- (224) Basame, S. B.; White, H. S. Chemically-Selective and Spatially-Localized Redox Activity at Ta/Ta<sub>2</sub>O<sub>5</sub> Electrodes. *Langmuir* **1999**, *15*, 819–825.
- (225) Battistel, D.; Daniele, S.; Gerbasi, R.; Baldo, M. A. Characterization of Metal-Supported Al<sub>2</sub>O<sub>3</sub> Thin Films by Scanning Electrochemical Microscopy. *Thin Solid Films* **2010**, *518*, 3625–3631.
- (226) Zhang, J.; Unwin, P. R. Effect of Triton X-100 on Electron Transfer Kinetics at the Interface Between Two Immiscible Electrolyte Solutions: A Scanning Electrochemical Microscopy Study. *J. Electroanal. Chem.* **2000**, *494*, 47–52.
- (227) Mandler, D.; Bard, A. J. High Resolution Etching of Semiconductors by the Feedback Mode of the Scanning Electrochemical Microscope. *J. Electrochem. Soc.* **1990**, *137*, 2468–2472.
- (228) Calhoun, R. L.; Bard, A. J. Study of the Catalytic Following Reaction by Scanning Electrochemical Microscopy (SECM). *J. Electrochem. Soc.* **2012**, *159*, F42–F47.
- (229) Alemu, G.; Cui, J.; Cao, K.; Li, J.; Shen, Y.; Wang, M. Investigation of the Regeneration Kinetics of Organic Dyes with Pyridine Ring Anchoring Groups by Scanning Electrochemical Microscopy. *RSC Adv.* **2014**, *4*, 51374–51380.
- (230) O'Mullane, A. P.; Neufeld, A. K.; Bond, A. M. Scanning Electrochemical Microscopy Study of the Solid-Solid Interconversion of TCNQ to Phase I and Phase II CuTCNQ. *Electrochem. Commun.* **2012**, *22*, 21–24.
- (231) Zhang, J.; Unwin, P. R. Microelectrochemical Measurements of Electron Transfer Rates at the Interface Between Two Immiscible Electrolyte Solutions: Potential Dependence of the Ferro/Ferricyanide-7,7,8,8-tetracyanoquinodimethane (TCNQ)/TCNQ<sup>•−</sup> System. *Phys. Chem. Chem. Phys.* **2002**, *4*, 3820–3827.
- (232) Velmurugan, J.; Sun, P.; Mirkin, M. V. Scanning Electrochemical Microscopy with Gold Nanotips: The Effect of Electrode Material on Electron Transfer Rates. *J. Phys. Chem. C* **2009**, *113*, 459–464.
- (233) Wang, X. L.; Shi, Y. X.; Bai, Z. L.; Jin, W. R. Imaging of Activity of Horseradish Peroxidase at  $\beta$ -Cyclodextrin Polymer by Scanning Electrochemical Microscopy. *Chin. Chem. Lett.* **2004**, *15*, 214–215.
- (234) Rotenberg, S. A.; Mirkin, M. V. Scanning Electrochemical Microscopy: Detection of Human Breast Cancer Cells by Redox Environment. *J. Mammary Gland Biol. Neoplasia* **2004**, *9*, 375–382.
- (235) Leroux, Y.; Schaming, D.; Ruhlmann, L.; Hapiot, P. SECM Investigations of Immobilized Porphyrins Films. *Langmuir* **2010**, *26*, 14983–14989.
- (236) Neufeld, A. K.; O'Mullane, A. P.; Bond, A. M. Control of Localized Nanorod Formation and Patterns of Semiconducting CuTCNQ Phase I Crystals by Scanning Electrochemical Microscopy. *J. Am. Chem. Soc.* **2005**, *127*, 13846–13853.
- (237) Liu, B.; Mirkin, M. V. Electron Transfer at Liquid/Liquid Interfaces. The Effects of Ionic Adsorption, Electrolyte Concentration, and Spacer Length on the Reaction Rate. *J. Phys. Chem. B* **2002**, *106*, 3933–3940.
- (238) Demaille, C.; Bard, A. J. Kinetics and Mechanism of the Anodic Dimerization of Trans-Anethole Studied by Cyclic Voltammetry and Scanning Electrochemical Microscopy. *Acta Chem. Scand.* **1999**, *53*, 842–848.



- (239) Nogala, W.; Burchardt, M.; Opallo, M.; Rogalski, J.; Wittstock, G. Scanning Electrochemical Microscopy Study of Laccase Within a Sol-Gel Processed Silicate Film. *Bioelectrochemistry* **2008**, *72*, 174–182.
- (240) Jensen, M. B.; Guerard, A.; Tallman, D. E.; Bierwagen, G. P. Studies of Electron Transfer at Aluminum Alloy Surfaces by Scanning Electrochemical Microscopy. *J. Electrochem. Soc.* **2008**, *155*, C324–C332.
- (241) Treichel, D. A.; Mirkin, M. V.; Bard, A. J. Scanning Electrochemical Microscopy. 27. Application of a Simplified Treatment of an Irreversible Homogeneous Reaction Following Electron Transfer to the Oxidative Dimerization of 4-Nitrophenolate in Acetonitrile. *J. Phys. Chem.* **1994**, *98*, 5751–5757.
- (242) Mirkin, M. V.; Yang, H.; Bard, A. J. Borohydride Oxidation at a Gold Electrode. *J. Electrochem. Soc.* **1992**, *139*, 2212–2216.
- (243) Zhang, X.; Peng, X.; Jin, W. Scanning Electrochemical Microscopy with Enzyme Immunoassay of the Cancer-Related Antigen CA15–3. *Anal. Chim. Acta* **2006**, *558*, 110–114.
- (244) Fan, H.; Jiao, F.; Chen, H.; Zhang, F.; Wang, Q.; He, P.; Fang, Y. Qualitative and Quantitative Detection of DNA Amplified with HRP-Modified SiO<sub>2</sub> Nanoparticles Using Scanning Electrochemical Microscopy. *Biosens. Bioelectron.* **2013**, *47*, 373–378.
- (245) Conzuelo, F.; Stratmann, L.; Grütze, S.; Pingarrón, J. M.; Schuhmann, W. Detection and Quantification of Sulfonamide Antibiotic Residues in Milk Using Scanning Electrochemical Microscopy. *Electroanalysis* **2014**, *26*, 481–487.
- (246) Roberts, W. S.; Davis, F.; Collyer, S. D.; Higson, S. P. J. Construction and Interrogation of Enzyme Microarrays Using Scanning Electrochemical Microscopy - Optimisation of Adsorption and Determination of Enzymatic Activity. *Analyst* **2011**, *136*, 5287–5293.
- (247) Casillas, N.; Charlebois, S. J.; Smyrl, W. H. Scanning Electrochemical Microscopy of Precursor Sites for Pitting Corrosion on Titanium. *J. Electrochem. Soc.* **1993**, *140*, L142–L145.
- (248) Zeradjanin, A. R.; Schilling, T.; Seisel, S.; Bron, M.; Schuhmann, W. Visualization of Chlorine Evolution at Dimensionally Stable Anodes by Means of Scanning Electrochemical Microscopy. *Anal. Chem.* **2011**, *83*, 7645–7650.
- (249) Jung, C.; Sánchez-Sánchez, C. M.; Lin, C. L.; Rodríguez-López, J.; Bard, A. J. Electrocatalytic Activity of Pd-Co Bimetallic Mixtures for Formic Acid Oxidation Studied by Scanning Electrochemical Microscopy. *Anal. Chem.* **2009**, *81*, 7003–7008.
- (250) Frank, A.; Bard, A. J. The Decomposition of the Sulfonate Additive Sulfopropyl Sulfonate in Acid Copper Electroplating Chemistries. *J. Electrochem. Soc.* **2003**, *150*, C244–C250.
- (251) Janin, M.; Ghilane, J.; Lacroix, J. C. Scanning Electrochemical Microscopy for the Fabrication of Copper Nanowires: Atomic Contacts with Quantized Conductance, and Molecular Adsorption Effect. *Electrochim. Acta* **2012**, *83*, 7–12.
- (252) Quinton, D.; Maringa, A.; Griveau, S.; Nyokong, T.; Bedioui, F. Surface Patterning Using Scanning Electrochemical Microscopy to Locally Trigger a "Click" Chemistry Reaction. *Electrochem. Commun.* **2013**, *31*, 112–115.
- (253) Roach, D. M.; Hooper, S. E.; Anderson, M. R. Optimization of Electrode Alignment for Electrochemical Detection in Capillary Electrophoresis Using a Scanning Electrochemical Microscope. *Electroanalysis* **2005**, *17*, 2254–2259.
- (254) Martin, R. D.; Unwin, P. R. Scanning Electrochemical Microscopy: Kinetics of Chemical Reactions Following Electron-Transfer Measured with the Substrate-Generation-Tip-Collection Mode. *J. Chem. Soc., Faraday Trans.* **1998**, *94*, 753–759.
- (255) McKay, L.; LeSuer, R. J. A Mechanistic Investigation of Di-tert-butyl Nitroxide Using Scanning Electrochemical Microscopy (SECM). *Electrochim. Acta* **2008**, *53*, 8305–8309.
- (256) Engstrom, R. C.; Small, B.; Kattan, L. Observation of Microscopically Local Electron-Transfer Kinetics with Scanning Electrochemical Microscopy. *Anal. Chem.* **1992**, *64*, 241–244.
- (257) Yogeswaran, U.; Thiagarajan, S.; Chen, S. M. Nanocomposite of Functionalized Multiwall Carbon Nanotubes with Nafion, Nano Platinum, and Nano Gold Biosensing Film for Simultaneous Determination of Ascorbic Acid, Epinephrine, and Uric Acid. *Anal. Biochem.* **2007**, *365*, 122–131.
- (258) Martin, R. D.; Unwin, P. R. Theory and Experiment for the Substrate Generation/Tip Collection Mode of the Scanning Electrochemical Microscope: Application as an Approach for Measuring the Diffusion Coefficient Ratio of a Redox Couple. *Anal. Chem.* **1998**, *70*, 276–284.
- (259) Zhao, C.; Wittstock, G. Scanning Electrochemical Microscopy of Quinoprotein Glucose Dehydrogenase. *Anal. Chem.* **2004**, *76*, 3145–3154.
- (260) Williams, M. E.; Stevenson, K. J.; Massari, A. M.; Hupp, J. T. Imaging Size-Selective Permeation Through Micropatterned Thin Films Using Scanning Electrochemical Microscopy. *Anal. Chem.* **2000**, *72*, 3122–3128.
- (261) Takahashi, Y.; Shevchuk, A. I.; Novak, P.; Murakami, Y.; Shiku, H.; Korchev, Y. E.; Matsue, T. Simultaneous Noncontact Topography and Electrochemical Imaging by SECM/SICM Featuring Ion Current Feedback Regulation. *J. Am. Chem. Soc.* **2010**, *132*, 10118–10126.
- (262) Zhou, H.; Shiku, H.; Kasai, S.; Noda, H.; Matsue, T.; Ohya-Nishiguchi, H.; Kamada, H. Mapping Peroxidase in Plant Tissues by Scanning Electrochemical Microscopy. *Bioelectrochemistry* **2001**, *54*, 151–156.
- (263) Shiku, H.; Kumagai, A.; Luo, H. Q.; Takahashi, Y.; Yasukawa, T.; Yamada, H.; Matsue, T. Electrochemical Characterization of Enzyme and Immunoglobulin G Patterned Using Microcontact Printing. *Electrochemistry* **2010**, *78*, 122–125.
- (264) Xue, Y.; Ding, L.; Lei, J.; Yan, F.; Ju, H. In Situ Electrochemical Imaging of Membrane Glycan Expression on Micropatterned Adherent Single Cells. *Anal. Chem.* **2010**, *82*, 7112–7118.
- (265) Dumitrescu, I.; Dudin, P. V.; Edgeworth, J. P.; Macpherson, J. V.; Unwin, P. R. Electron Transfer Kinetics at Single-Walled Carbon Nanotube Electrodes Using Scanning Electrochemical Microscopy. *J. Phys. Chem. C* **2010**, *114*, 2633–2639.
- (266) Radtke, V.; Heß, C.; Souto, R.; Heinze, J. Electroless, Electrolytic and Galvanic Copper Deposition with the Scanning Electrochemical Microscope (SECM). *Z. Phys. Chem.* **2006**, *220*, 393–406.
- (267) Bastos, A. C.; Simões, A. M.; González, S.; González-García, Y.; Souto, R. M. Imaging Concentration Profiles of Redox-Active Species in Open-Circuit Corrosion Processes with the Scanning Electrochemical Microscope. *Electrochem. Commun.* **2004**, *6*, 1212–1215.
- (268) Gonzalez-Garcia, Y.; Burstein, G. T.; Gonzalez, S.; Souto, R. M. Imaging Metastable Pits on Austenitic Stainless Steel In Situ at the Open-Circuit Corrosion Potential. *Electrochem. Commun.* **2004**, *6*, 637–642.
- (269) Tel-Vered, R.; Bard, A. J. Generation and Detection of Single Metal Nanoparticles Using Scanning Electrochemical Microscopy Techniques. *J. Phys. Chem. B* **2006**, *110*, 25279–25287.
- (270) Williams, M. E.; Hupp, J. T. Scanning Electrochemical Microscopy Assessment of Rates of Molecular Transport Through Mesoporous Thin-Films of Porphyrinic "Molecular Squares". *J. Phys. Chem. B* **2001**, *105*, 8944–8950.
- (271) Tefashe, U. M.; Snowden, M. E.; Ducharme, P. D.; Danaie, M.; Botton, G. A.; Mauzeroll, J. Local Flux of Hydrogen from Magnesium Alloy Corrosion Investigated by Scanning Electrochemical Microscopy. *J. Electroanal. Chem.* **2014**, *720*–721, 121–127.
- (272) Jamali, S. S.; Moulton, S. E.; Tallman, D. E.; Forsyth, M.; Weber, J.; Wallace, G. G. Evaluating the Corrosion Behaviour of Magnesium Alloy in Simulated Biological Fluid by Using SECM to Detect Hydrogen Evolution. *Electrochim. Acta* **2015**, *152*, 294–301.
- (273) Sun, T.; Yu, Y.; Zacher, B. J.; Mirkin, M. V. Scanning Electrochemical Microscopy of Individual Catalytic Nanoparticles. *Angew. Chem., Int. Ed.* **2014**, *53*, 14120–3.
- (274) Abad, J. M.; Tesio, A. Y.; Pariente, F.; Lorenzo, E. Patterning Gold Nanoparticle Using Scanning Electrochemical Microscopy. *J. Phys. Chem. C* **2013**, *117*, 22087–22093.
- (275) Husser, O. E.; Craston, D. H.; Bard, A. J. Scanning Electrochemical Microscopy. *J. Electrochem. Soc.* **1989**, *136*, 3222–3229.
- (276) O'Mullane, A. P.; Ippolito, S. J.; Bond, A. M.; Bhargava, S. K. A Study of Localised Galvanic Replacement of Copper and Silver Films

with Gold Using Scanning Electrochemical Microscopy. *Electrochem. Commun.* **2010**, *12*, 611–615.

(277) Turyan, I.; Matsue, T.; Mandler, D. Patterning and Characterization of Surfaces with Organic and Biological Molecules by the Scanning Electrochemical Microscope. *Anal. Chem.* **2000**, *72*, 3431–3435.

(278) Fernandez, J. L.; Hurth, C.; Bard, A. J. Scanning Electrochemical Microscopy 54. Application to the Study of Heterogeneous Catalytic Reactions - Hydrogen Peroxide Decomposition. *J. Phys. Chem. B* **2005**, *109*, 9532–9539.

(279) Shen, Y.; Trauble, M.; Wittstock, G. Detection of Hydrogen Peroxide Produced During Electrochemical Oxygen Reduction Using Scanning Electrochemical Microscopy. *Anal. Chem.* **2008**, *80*, 750–759.

(280) Xu, F.; Beak, B.; Jung, C. In Situ Electrochemical Studies for Li<sup>+</sup> Ions Dissociation from the LiCoO<sub>2</sub> Electrode by the Substrate-Generation/Tip-Collection Mode in SECM. *J. Solid State Electrochem.* **2012**, *16*, 305–311.

(281) Cannes, C.; Kanoufi, F.; Bard, A. J. Cyclic Voltammetric and Scanning Electrochemical Microscopic Study of Menadione Permeability Through a Self-Assembled Monolayer on a Gold Electrode. *Langmuir* **2002**, *18*, 8134–8141.

(282) Nagamine, K.; Takahashi, Y.; Ino, K.; Shiku, H.; Matsue, T. Influence of Tip Size on Single Yeast Cell Imaging Using Scanning Electrochemical Microscopy. *Electroanalysis* **2011**, *23*, 1168–1174.

(283) Bollo, S.; Nunez-Vergara, L.; Squella, J. A. Electrogenerated Nitro Radical Anions a Comparative Kinetic Study Using Scanning Electrochemical Microscopy. *J. Electrochem. Soc.* **2004**, *151*, E322–E325.

(284) Fernandez, J. L.; Bard, A. J. Scanning Electrochemical Microscopy. 47. Imaging Electrocatalytic Activity for Oxygen Reduction in an Acidic Medium by the Tip Generation - Substrate Collection Mode. *Anal. Chem.* **2003**, *75*, 2967–2974.

(285) Wilhelm, T.; Wittstock, G. Analysis of Interaction in Patterned Multienzyme Layers by Using Scanning Electrochemical Microscopy. *Angew. Chem., Int. Ed.* **2003**, *42*, 2248–2250.

(286) Fernandez, J. L.; Bard, A. J. Scanning Electrochemical Microscopy 50. Kinetic Study of Electrode Reactions by the Tip Generation-Substrate Collection Mode. *Anal. Chem.* **2004**, *76*, 2281–2289.

(287) Nebel, M.; Grutze, S.; Diab, N.; Schulte, A.; Schuhmann, W. Microelectrochemical Visualization of Oxygen Consumption of Single Living Cells. *Faraday Discuss.* **2013**, *164*, 19–32.

(288) Wittstock, G.; Yu, K. J.; Halsall, H. B.; Ridgway, T. H.; Heineman, W. R. Imaging of Immobilized Antibody Layers with Scanning Electrochemical Microscopy. *Anal. Chem.* **1995**, *67*, 3578–3582.

(289) Wijayawardhana, A. C.; Wittstock, G.; Halsall, H. B.; Heineman, W. R. Electrochemical Immunoassay with Microscopic Immunomagnetic Bead Domains and Scanning Electrochemical Microscopy. *Electroanalysis* **2000**, *12*, 640–644.

(290) Zhao, C.; Wittstock, G. An SECM Detection Scheme with Improved Sensitivity and Lateral Resolution: Detection of Galactosidase Activity with Signal Amplification by Glucose Dehydrogenase. *Angew. Chem., Int. Ed.* **2004**, *43*, 4170–4172.

(291) Torisawa, Y. S.; Ohara, N.; Nagamine, K.; Kasai, S.; Yasukawa, T.; Shiku, H.; Matsue, T. Electrochemical Monitoring of Cellular Signal Transduction with a Secreted Alkaline Phosphatase Reporter System. *Anal. Chem.* **2006**, *78*, 7625–7631.

(292) Takahashi, Y.; Miyamoto, T.; Shiku, H.; Asano, R.; Yasukawa, T.; Kumagai, I.; Matsue, T. Electrochemical Detection of Epidermal Growth Factor Receptors on a Single Living Cell Surface by Scanning Electrochemical Microscopy. *Anal. Chem.* **2009**, *81*, 2785–2790.

(293) Saez, A.; Sanchez-Sanchez, C. M.; Solla-Gullon, J.; Exposito, E.; Montiel, V. Electrosynthesis of L-Cysteine on a Dispersed Pb/Carbon Black Electrode. *J. Electrochem. Soc.* **2009**, *156*, E154–E160.

(294) Chang, J.; Bard, A. J. Detection of the Sn(III) Intermediate and the Mechanism of the Sn(IV)/Sn(II) Electroreduction Reaction in Bromide Media by Cyclic Voltammetry and Scanning Electrochemical Microscopy. *J. Am. Chem. Soc.* **2014**, *136*, 311–320.

(295) Serebrennikova, I.; Lee, S.; White, H. S. Visualization and Characterization of Electroactive Defects in the Native Oxide Film on Aluminium. *Faraday Discuss.* **2002**, *121*, 199–210.

(296) Koley, D.; Bard, A. J. Inhibition of the MRP1-Mediated Transport of the Menadione-Glutathione Conjugate (Thiodione) in HeLa Cells as Studied by SECM. *Proc. Natl. Acad. Sci. U. S. A.* **2012**, *109*, 11522–11527.

(297) Mauzeroll, J.; Bard, A. J.; Owhadian, O.; Monks, T. J. Menadione Metabolism to Thiodione in Hepatoblastoma by Scanning Electrochemical Microscopy. *Proc. Natl. Acad. Sci. U. S. A.* **2004**, *101*, 17582–17587.

(298) Mauzeroll, J.; Buda, M.; Bard, A. J.; Prieto, F.; Rueda, M. Detection of Tl(I) Transport Through a Gramicidin-Dioleoylphosphatidylcholine Monolayer Using the Substrate Generation-Tip Collection Mode of Scanning Electrochemical Microscopy. *Langmuir* **2002**, *18*, 9453–9461.

(299) Guadagnini, L.; Maljusch, A.; Chen, X.; Neugebauer, S.; Tonelli, D.; Schuhmann, W. Visualization of Electrocatalytic Activity of Microstructured Metal Hexacyanoferrates by Means of Redox Competition Mode of Scanning Electrochemical Microscopy (RC-SECM). *Electrochim. Acta* **2009**, *54*, 3753–3758.

(300) Szot, K.; Nogala, W.; Niedziolka-Jonsson, J.; Jonsson-Niedziolka, M.; Marken, F.; Rogalski, J.; Kirchner, C. N.; Wittstock, G.; Opallo, M. Hydrophilic Carbon Nanoparticle-Laccase Thin Film Electrode for Mediatorless Dioxygen Reduction. SECM Activity Mapping and Application in Zinc-Dioxygen Battery. *Electrochim. Acta* **2009**, *54*, 4620–4625.

(301) Schaller, R. F.; Thomas, S.; Birbilis, N.; Scully, J. R. Spatially Resolved Mapping of the Relative Concentration of Dissolved Hydrogen Using the Scanning Electrochemical Microscope. *Electrochem. Commun.* **2015**, *51*, 54–58.

(302) Jiang, M. Y.; Wu, L. K.; Hu, J. M.; Zhang, J. Q. Silane-Incorporated Epoxy Coatings on Aluminum Alloy (AA2024). Part 1: Improved Corrosion Performance. *Corros. Sci.* **2015**, *92*, 118–126.

(303) Marques, A. G.; Izquierdo, J.; Souto, R. M.; Simões, A. M. SECM Imaging of the Cut Edge Corrosion of Galvanized Steel as a Function of pH. *Electrochim. Acta* **2015**, *153*, 238–245.

(304) Karnicka, K.; Eckhard, K.; Guschin, D. A.; Stoica, L.; Kulesza, P. J.; Schuhmann, W. Visualisation of the Local Bio-Electrocatalytic Activity in Biofuel Cell Cathodes by Means of Redox Competition Scanning Electrochemical Microscopy (RC-SECM). *Electrochem. Commun.* **2007**, *9*, 1998–2002.

(305) Nagaiah, T. C.; Maljusch, A.; Chen, X.; Bron, M.; Schuhmann, W. Visualization of the Local Catalytic Activity of Electrodeposited Pt-Ag Catalysts for Oxygen Reduction by Means of SECM. *ChemPhysChem* **2009**, *10*, 2711–2718.

(306) Li, F.; Edwards, M.; Guo, J.; Unwin, P. R. Silver Particle Nucleation and Growth at Liquid/Liquid Interfaces: A Scanning Electrochemical Microscopy Approach. *J. Phys. Chem. C* **2009**, *113*, 3553–3565.

(307) Holt, K. B.; Bard, A. J. Interaction of Silver(I) Ions with the Respiratory Chain of Escherichia Coli: An Electrochemical and Scanning Electrochemical Microscopy Study of the Antimicrobial Mechanism of Micromolar Ag. *Biochemistry* **2005**, *44*, 13214–13223.

(308) Lima, A. S.; Meloni, G. N.; Bertotti, M. Determination of Paracetamol in Presence of Ascorbic Acid in Pharmaceutical Products by Scanning Electrochemical Microscopy. *Electroanalysis* **2013**, *25*, 1395–1399.

(309) Uitto, O. D.; White, H. S. Scanning Electrochemical Microscopy of Membrane Transport in the Reverse Imaging Mode. *Anal. Chem.* **2001**, *73*, 533–539.

(310) Alpuche-Aviles, M. A.; Baur, J. E.; Wipf, D. O. Imaging of Metal Ion Dissolution and Electrodeposition by Anodic Stripping Voltammetry-Scanning Electrochemical Microscopy. *Anal. Chem.* **2008**, *80*, 3612–3621.

(311) Kapui, I.; Gyurcsanyi, R. E.; Nagy, G.; Toth, K.; Arca, M.; Arca, E. Investigation of Styrene-Methacrylic Acid Block Copolymer Micelle Doped Polypyrrole Films by Scanning Electrochemical Microscopy. *J. Phys. Chem. B* **1998**, *102*, 9934–9939.



- (312) Daniele, S.; Ciani, I.; Baldo, M. A.; Bragato, C. Application of Sphere Cap Mercury Microelectrodes and Scanning Electrochemical Microscopy (SECM) for Heavy Metal Monitoring at Solid/Solution Interfaces. *Electroanalysis* **2007**, *19*, 2067–2076.
- (313) Lin, C. L.; Rodriguez-Lopez, J.; Bard, A. J. Micropipet Delivery-Substrate Collection Mode of Scanning Electrochemical Microscopy for the Imaging of Electrochemical Reactions and the Screening of Methanol Oxidation Electrocatalysts. *Anal. Chem.* **2009**, *81*, 8868–8877.
- (314) Etienne, M.; Lhenry, S.; Cornut, R.; Lefrou, C. Optimization of the Shearforce Signal for Scanning Electrochemical Microscopy and Application for Kinetic Analysis. *Electrochim. Acta* **2013**, *88*, 877–884.
- (315) Sugimura, H.; Shimo, N.; Kitamura, N.; Masuhara, H.; Itaya, K. Topographical Imaging of Prussian Blue Surfaces by Direct-Mode Scanning Electrochemical Microscopy. *J. Electroanal. Chem.* **1993**, *346*, 147–160.
- (316) Tenent, R. C.; Wipf, D. O. Patterning and Imaging of Oxides on Glassy Carbon Electrode Surfaces by Scanning Electrochemical Microscopy. *J. Electrochem. Soc.* **2003**, *150*, E131–E139.
- (317) Unwin, P. R.; Bard, A. J. Scanning Electrochemical Microscopy. 14. Scanning Electrochemical Microscope Induced Desorption: A New Technique for the Measurement of Adsorption/Desorption Kinetics and Surface Diffusion Rates at the Solid/Liquid Interface. *J. Phys. Chem.* **1992**, *96*, 5035–5045.
- (318) Zigah, D.; Rodriguez-Lopez, J.; Bard, A. J. Quantification of Photoelectrogenerated Hydroxyl Radical on TiO<sub>2</sub> by Surface Interrogation Scanning Electrochemical Microscopy. *Phys. Chem. Chem. Phys.* **2012**, *14*, 12764–12772.
- (319) Xin, N.; Xin, Y.; Gao, Y.; Xiang, J. Interaction of Mercury(II) Ions with Immobilized Apo-Metlothioneins Studied by Scanning Electrochemical Microscopy Combined with Surface Plasmon Resonance. *Microchim. Acta* **2011**, *174*, 81–87.
- (320) Gonsalves, M.; Macpherson, J. V.; O'Hare, D.; Winlove, C. P.; Unwin, P. R. High Resolution Imaging of the Distribution and Permeability of Methyl Viologen Dication in Bovine Articular Cartilage Using Scanning Electrochemical Microscopy. *Biochim. Biophys. Acta, Gen. Subj.* **2000**, *1524*, 66–74.
- (321) Ruhlig, D.; Gugel, H.; Schulte, A.; Theisen, W.; Schuhmann, W. Visualization of Local Electrochemical Activity and Local Nickel Ion Release on Laser-Welded NiTi/Steel Joints Using Combined Alternating Current Mode and Stripping Mode SECM. *Analyst* **2008**, *133*, 1700–1706.
- (322) Ciani, I.; Daniele, S.; Bragato, C.; Baldo, M. A. Stability of Mercury-Coated Platinum Microelectrodes upon Touching a Solid Surface in Scanning Electrochemical Microscopy (SECM) Experiments. *Electrochem. Commun.* **2003**, *5*, 354–358.
- (323) Rodriguez-Lopez, J.; Bard, A. J. Scanning Electrochemical Microscopy: Surface Interrogation of Adsorbed Hydrogen and the Open Circuit Catalytic Decomposition of Formic Acid at Platinum. *J. Am. Chem. Soc.* **2010**, *132*, 5121–5129.
- (324) Schrock, D. S.; Baur, J. E. Chemical Imaging with Combined Fast-Scan Cyclic Voltammetry-Scanning Electrochemical Microscopy. *Anal. Chem.* **2007**, *79*, 7053–7061.
- (325) Souto, R. M.; Gonzalez-Garcia, Y.; Battistel, D.; Daniele, S. On the Use of Mercury-Coated Tips in Scanning Electrochemical Microscopy to Investigate Galvanic Corrosion Processes Involving Zinc and Iron. *Corros. Sci.* **2012**, *55*, 401–406.
- (326) Dickinson, E.; Limon-Petersen, J.; Rees, N.; Compton, R. How Much Supporting Electrolyte is Required to Make a Cyclic Voltammetry Experiment Quantitatively "Diffusional"? A Theoretical and Experimental Investigation. *J. Phys. Chem. C* **2009**, *113*, 11157–11171.
- (327) Fang, P. P.; Chen, S.; Deng, H.; Scanlon, M. D.; Guffy, F.; Lee, H. J.; Momotenko, D.; Amstutz, V.; Cortes-Salazar, F.; Pereira, C. M.; et al. Conductive Gold Nanoparticle Mirrors at Liquid/Liquid Interfaces. *ACS Nano* **2013**, *7*, 9241–9248.
- (328) Walsh, D. A.; Lovelock, K. R. J.; Licence, P. Ultramicroelectrode Voltammetry and Scanning Electrochemical Microscopy in Room-Temperature Ionic Liquid Electrolytes. *Chem. Soc. Rev.* **2010**, *39*, 4185–4194.
- (329) Zhang, J.; Strutwolf, J.; Cannan, S.; Unwin, P. R. Combined Scanning Electrochemical Microscopy-Langmuir Trough Technique for Investigating Phase Transfer Kinetics Across Liquid/Liquid Interfaces Modified by a Molecular Monolayer. *Electrochem. Commun.* **2003**, *5*, 105–110.
- (330) Osakai, T.; Okamoto, M.; Sugihara, T.; Nakatani, K. Bimolecular-Reaction Effect on the Rate Constant of Electron Transfer at the Oil/Water Interface as Studied by Scanning Electrochemical Microscopy. *J. Electroanal. Chem.* **2009**, *628*, 27–34.
- (331) Zoski, C. G. Ultramicroelectrodes: Design, Fabrication, and Characterization. *Electroanalysis* **2002**, *14*, 1041–1051.
- (332) Fu-Ren, F. F.; Christophe, D. *Scanning Electrochemical Microscopy*, 2nd ed.; CRC Press: New York, 2012; pp 25–52.
- (333) Bard, A.; Faulkner, L. *Electrochemical Methods: Fundamentals and Applications*; Wiley: New York, 2001; p 169.
- (334) Katemann, B. B.; Schuhmann, W. Fabrication and Characterization of Needle-Type Pt-Disk Nanoelectrodes. *Electroanalysis* **2002**, *14*, 22–28.
- (335) Danis, L.; Snowden, M. E.; Tefashe, U. M.; Heinemann, C. N.; Mauzeroll, J. Development of Nano-Disc Electrodes for Application as Shear Force Sensitive Electrochemical Probes. *Electrochim. Acta* **2014**, *136*, 121–129.
- (336) Kranz, C. Recent Advancements in Nanoelectrodes and Nanopipettes Used in Combined Scanning Electrochemical Microscopy Techniques. *Analyst* **2014**, *139*, 336–352.
- (337) Matsui, N.; Kaya, T.; Nagamine, K.; Yasukawa, T.; Shiku, H.; Matsue, T. Electrochemical Mutagen Screening Using Microbial Chip. *Biosens. Bioelectron.* **2006**, *21*, 1202–1209.
- (338) Mauzeroll, J.; Hueske, E. A.; Bard, A. J. Scanning Electrochemical Microscopy. 48. Hg/Pt Hemispherical Ultramicroelectrodes: Fabrication and Characterization. *Anal. Chem.* **2003**, *75*, 3880–3889.
- (339) Lee, Y.; Amemiya, S.; Bard, A. J. Scanning Electrochemical Microscopy. 41. Theory and Characterization of Ring Electrodes. *Anal. Chem.* **2001**, *73*, 2261–2267.
- (340) Danis, L.; Polcari, D.; Kwan, A.; Gateman, S. M.; Mauzeroll, J. Fabrication of Carbon, Gold, Platinum, Silver, and Mercury Ultramicroelectrodes with Controlled Geometry. *Anal. Chem.* **2015**, *87*, 2565–2569.
- (341) Mirkin, M. V. High Resolution Studies of Heterogeneous Processes with the Scanning Electrochemical Microscope. *Microchim. Acta* **1999**, *130*, 127–153.
- (342) Leonhardt, K.; Avdic, A.; Lugstein, A.; Pobelov, I.; Wandlowski, T.; Wu, M.; Gollas, B.; Denuault, G. Atomic Force Microscopy-Scanning Electrochemical Microscopy: Influence of Tip Geometry and Insulation Defects on Diffusion Controlled Currents at Conical Electrodes. *Anal. Chem.* **2011**, *83*, 2971–2977.
- (343) Cornut, R.; Poirier, S.; Mauzeroll, J. Forced Convection During Feedback Approach Curve Measurements in Scanning Electrochemical Microscopy: Maximal Displacement Velocity with a Microdisk. *Anal. Chem.* **2012**, *84*, 3531–3537.
- (344) Xiong, H.; Guo, J.; Kurihara, K.; Amemiya, S. Fabrication and Characterization of Conical Microelectrode Probes Templated by Selectively Etched Optical Fibers for Scanning Electrochemical Microscopy. *Electrochem. Commun.* **2004**, *6*, 615–620.
- (345) Walsh, D. A.; Fernandez, J. L.; Mauzeroll, J.; Bard, A. J. Scanning Electrochemical Microscopy. 55. Fabrication and Characterization of Micropipet Probes. *Anal. Chem.* **2005**, *77*, 5182–5188.
- (346) Kranz, C.; Friedbacher, G.; Mizakoff, B.; Lugstein, A.; Smoliner, J.; Bertagnolli, E. Integrating an Ultramicroelectrode in an AFM Cantilever: Combined Technology for Enhanced Information. *Anal. Chem.* **2001**, *73*, 2491–2500.
- (347) Blanc, C.; Pebere, N.; Tribollet, B.; Vivier, V. Galvanic Coupling Between Copper and Aluminium in a Thin-layer Cell. *Corros. Sci.* **2010**, *52*, 991–995.
- (348) Wei, C.; Bard, A. J.; Kapui, I.; Nagy, G.; Toth, K. Scanning Electrochemical Microscopy. 32. Gallium Ultramicroelectrodes and Their Application in Ion-Selective Probes. *Anal. Chem.* **1996**, *68*, 2651–2655.

- (349) Leonard, K. C.; Bard, A. J. The Study of Multireactional Electrochemical Interfaces via a Tip Generation/Substrate Collection Mode of Scanning Electrochemical Microscopy: The Hydrogen Evolution Reaction for Mn in Acidic Solution. *J. Am. Chem. Soc.* **2013**, *135*, 15890–15896.
- (350) Ge, F.; Tenent, R. C.; Wipf, D. O. Fabricating and Imaging Carbon-Fiber Immobilized Enzyme Ultramicroelectrodes with Scanning Electrochemical Microscopy. *Anal. Sci.* **2001**, *17*, 27–35.
- (351) Deng, C.; Li, M.; Xie, Q.; Liu, M.; Yang, Q.; Xiang, C.; Yao, S. Construction as well as EQCM and SECM Characterizations of a Novel Nafion/Glucose Oxidase-Glutaraldehyde/Poly(thionine)/Au Enzyme Electrode for Glucose Sensing. *Sens. Actuators, B* **2007**, *122*, 148–157.
- (352) Ciobanu, M.; Taylor, D. E., Jr; Wilburn, J. P.; Cliffel, D. E. Glucose and Lactate Biosensors for Scanning Electrochemical Microscopy Imaging of Single Live Cells. *Anal. Chem.* **2008**, *80*, 2717–2727.
- (353) Izquierdo, J.; Nagy, L.; Varga, A.; Bitter, I.; Nagy, G.; Souto, R. M. Scanning Electrochemical Microscopy for the Investigation of Corrosion Processes: Measurement of  $Zn^{2+}$  Spatial Distribution with Ion Selective Microelectrodes. *Electrochim. Acta* **2012**, *59*, 398–403.
- (354) Nazarov, V. A.; Taryba, M. G.; Zdrachek, E. A.; Andronchyk, K. A.; Egorov, V. V.; Lamaka, S. V. Sodium- and Chloride-Selective Microelectrodes Optimized for Corrosion Studies. *J. Electroanal. Chem.* **2013**, *706*, 13–24.
- (355) Csoka, B.; Mekhalif, Z. Carbon Paste-Based Ion-Selective Dual Function Microelectrodes for SECM Measurements. *Electrochim. Acta* **2009**, *54*, 3225–3232.
- (356) Amemiya, S.; Bard, A. J. Scanning Electrochemical Microscopy. 40. Voltammetric Ion-Selective Micropipet Electrodes for Probing Ion Transfer at Bilayer Lipid Membranes. *Anal. Chem.* **2000**, *72*, 4940–4948.
- (357) Berger, C. E. M.; Rathod, H.; Gillespie, J. I.; Horrocks, B. R.; Datta, H. K. Scanning Electrochemical Microscopy at the Surface of Bone-Resorbing Osteoclasts: Evidence for Steady-State Disposal and Intracellular Functional Compartmentalization of Calcium. *J. Bone Miner. Res.* **2001**, *16*, 2092–2102.
- (358) Wei, C.; Bard, A. J.; Nagy, G.; Toth, K. Scanning Electrochemical Microscopy. 28. Ion-Selective Neutral Carrier-Based Microelectrode Potentiometry. *Anal. Chem.* **1995**, *67*, 1346–1356.
- (359) Etienne, M.; Schulte, A.; Mann, S.; Jordan, G.; Dietzel, I. D.; Schuhmann, W. Constant-Distance Mode Scanning Potentiometry. 1. Visualization of Calcium Carbonate Dissolution in Aqueous Solution. *Anal. Chem.* **2004**, *76*, 3682–3688.
- (360) Kiss, A.; Kiss, L.; Kovács, B.; Nagy, G. Air Gap Microcell for Scanning Electrochemical Microscopic Imaging of Carbon Dioxide Output. Model Calculation and Gas Phase SECM Measurements for Estimation of Carbon Dioxide Producing Activity of Microbial Sources. *Electroanalysis* **2011**, *23*, 2320–2326.
- (361) Gray, N. J.; Unwin, P. R. Simple Procedure for the Fabrication of Silver/silver Chloride Potentiometric Electrodes with Micrometre and Smaller Dimensions: Application to Scanning Electrochemical Microscopy. *Analyst* **2000**, *125*, 889–893.
- (362) Horrocks, B. R.; Mirkin, M. V.; Pierce, D. T.; Bard, A. J.; Nagy, G.; Toth, K. Scanning Electrochemical Microscopy. 19. Ion-Selective Potentiometric Microscopy. *Anal. Chem.* **1993**, *65*, 1213–1224.
- (363) Klusmann, E.; Schultze, J. W. pH-Microscopy - Theoretical and Experimental Investigations. *Electrochim. Acta* **1997**, *42*, 3123–3134.
- (364) Kang, J.; Yang, Y.; Jiang, F.; Shao, H. Study on the Anodic Reaction of Ni in an Alkaline Solution by Transient pH Detection Based on Scanning Electrochemical Microscopy (SECM). *Surf. Interface Anal.* **2007**, *39*, 877–884.
- (365) Izquierdo, J.; Kiss, A.; Santana, J. J.; Nagy, L.; Bitter, I.; Isaacs, H. S.; Nagy, G.; Souto, R. M. Development of  $Mg^{2+}$  Ion-Selective Microelectrodes for Potentiometric Scanning Electrochemical Microscopy Monitoring of Galvanic Corrosion Processes. *J. Electrochem. Soc.* **2013**, *160*, C451–C459.
- (366) Yamada, H.; Ikuta, Y.; Koike, T.; Matsue, T. Fabrication of a Shear Force-Based Ion-Selective Capillary Probe for Scanning Electrochemical Microscopy. *Chem. Lett.* **2008**, *37*, 392–393.
- (367) Shao, Y.; Mirkin, M. V.; Fish, G.; Kokotov, S.; Palanker, D.; Lewis, A. Nanometer-Sized Electrochemical Sensors. *Anal. Chem.* **1997**, *69*, 1627–1634.
- (368) Schafer, D.; Puschhof, A.; Schuhmann, W. Scanning Electrochemical Microscopy at Variable Temperatures. *Phys. Chem. Chem. Phys.* **2013**, *15*, S215–S223.
- (369) O'Connell, M. A.; Wain, A. J. Combined Electrochemical-Topographical Imaging: A Critical Review. *Anal. Methods* **2015**, *7*, 6983–6999.
- (370) McKelvey, K.; Edwards, M. A.; Unwin, P. R. Intermittent Contact-Scanning Electrochemical Microscopy (IC-SECM): A New Approach for Tip Positioning and Simultaneous Imaging of Interfacial Topography and Activity. *Anal. Chem.* **2010**, *82*, 6334–6337.
- (371) Lazenby, R. A.; McKelvey, K.; Unwin, P. R. Hopping Intermittent Contact-Scanning Electrochemical Microscopy (HIC-SECM): Visualizing Interfacial Reactions and Fluxes from Surfaces to Bulk Solution. *Anal. Chem.* **2013**, *85*, 2937–2944.
- (372) Gebala, M.; Schuhmann, W.; La Mantia, F. A New AC-SECM Mode: On the Way to High-Resolution Local Impedance Measurements in SECM. *Electrochem. Commun.* **2011**, *13*, 689–693.
- (373) Koch, J. A.; Baur, M. B.; Woodall, E. L.; Baur, J. E. Alternating Current Scanning Electrochemical Microscopy with Simultaneous Fast-Scan Cyclic Voltammetry. *Anal. Chem.* **2012**, *84*, 9537–9543.
- (374) Cougnon, C.; Bauer-Espindola, K.; Fabre, D. S.; Mauzeroll, J. Development of a Phase-Controlled Constant-Distance Scanning Electrochemical Microscope. *Anal. Chem.* **2009**, *81*, 3654–3659.
- (375) Hussien, E. M.; Schuhmann, W.; Schulte, A. Shearforce-Based Constant-Distance Scanning Electrochemical Microscopy as Fabrication Tool for Needle-Type Carbon-Fiber Nanoelectrodes. *Anal. Chem.* **2010**, *82*, 5900–5905.
- (376) Nebel, M.; Eckhard, K.; Erichsen, T.; Schulte, A.; Schuhmann, W. 4D Shearforce-Based Constant-Distance Mode Scanning Electrochemical Microscopy. *Anal. Chem.* **2010**, *82*, 7842–7848.
- (377) Dincer, C.; Laubender, E.; Hees, J.; Nebel, C. E.; Urban, G.; Heinze, J. SECM Detection of Single Boron Doped Diamond Nanodes and Nanoelectrode Arrays Using Phase-Operated Shear Force Technique. *Electrochem. Commun.* **2012**, *24*, 123–127.
- (378) Etienne, M.; Layoussifi, B.; Giornelli, T.; Jacquet, D. SECM-Based Automate Equipped with a Shearforce Detection for the Characterization of Large and Complex Samples. *Electrochem. Commun.* **2012**, *15*, 70–73.
- (379) Nebel, M.; Erichsen, T.; Schuhmann, W. Constant-Distance Mode SECM as a Tool to Visualize Local Electrocatalytic Activity of Oxygen Reduction Catalysts. *Beilstein J. Nanotechnol.* **2014**, *5*, 141–151.
- (380) Ludwig, M.; Kranz, C.; Schuhmann, W.; Gaub, H. Topography Feedback Mechanism for the Scanning Electrochemical Microscope Based on Hydrodynamic Forces Between Tip and Sample. *Rev. Sci. Instrum.* **1995**, *66*, 2857–2860.
- (381) Hengstenberg, A.; Kranz, C.; Schuhmann, W. Facilitated Tip-Positioning and Applications of Non-Electrode Tips in Scanning Electrochemical Microscopy Using a Shear Force Based Constant-Distance Mode. *Chem. - Eur. J.* **2000**, *6*, 1547–1554.
- (382) Wang, L.; Kowalik, J.; Mizaikoff, B.; Kranz, C. Combining Scanning Electrochemical Microscopy with Infrared Attenuated Total Reflection Spectroscopy for In Situ Studies of Electrochemically Induced Processes. *Anal. Chem.* **2010**, *82*, 3139–3145.
- (383) Wang, L.; Kranz, C.; Mizaikoff, B. Monitoring Scanning Electrochemical Microscopy Approach Curves with Mid-Infrared Spectroscopy: Toward a Novel Current-independent Positioning Mode. *Anal. Chem.* **2010**, *82*, 3132–3138.
- (384) Pähler, M.; Schuhmann, W.; Gratzl, M. Simultaneous Visualization of Surface Topography and Concentration Field by Means of Scanning Electrochemical Microscopy Using a Single Electrochemical Probe and Impedance Spectroscopy. *ChemPhysChem* **2011**, *12*, 2798–2805.
- (385) Hou, Y.; Xin, N.; Chen, S.; Deng, C.; Xiang, J. Controllable Release and High-Efficiency Collection of Hydrogen Peroxide: Application on the Quantitative Investigation of Biomolecule Oxidation



Induced by Reactive Oxygen Species. *Electroanalysis* **2014**, *26*, 1497–1503.

(386) Maljusch, A.; Senoz, C.; Rohwerder, M.; Schuhmann, W. Combined High Resolution Scanning Kelvin Probe - Scanning Electrochemical Microscopy Investigations for the Visualization of Local Corrosion Processes. *Electrochim. Acta* **2012**, *82*, 339–348.

(387) Senoz, C.; Maljusch, A.; Rohwerder, M.; Schuhmann, W. SECM and SKPFM Studies of the Local Corrosion Mechanism of Al Alloys - A Pathway to an Integrated SKP-SECM System. *Electroanalysis* **2012**, *24*, 239–245.

(388) Comstock, D. J.; Elam, J. W.; Pellin, M. J.; Hersam, M. C. Integrated Ultramicroelectrode-Nanopipet Probe for Concurrent Scanning Electrochemical Microscopy and Scanning Ion Conductance Microscopy. *Anal. Chem.* **2010**, *82*, 1270–1276.

(389) Morris, C. A.; Chen, C. C.; Baker, L. A. Transport of Redox Probes Through Single Pores Measured by Scanning Electrochemical-Scanning Ion Conductance Microscopy (SECM-SICM). *Analyst* **2012**, *137*, 2933–2938.

(390) O'Connell, M. A.; Wain, A. J. Mapping Electroactivity at Individual Catalytic Nanostructures Using High-Resolution Scanning Electrochemical-Scanning Ion Conductance Microscopy. *Anal. Chem.* **2014**, *86*, 12100–12107.

(391) Sen, M.; Takahashi, Y.; Matsumae, Y.; Horiguchi, Y.; Kumatani, A.; Ino, K.; Shiku, H.; Matsue, T. Improving the Electrochemical Imaging Sensitivity of Scanning Electrochemical Microscopy-Scanning Ion Conductance Microscopy by Using Electrochemical Pt Deposition. *Anal. Chem.* **2015**, *87*, 3484–3489.

(392) Salamifar, S. E.; Lai, R. Y. Use of Combined Scanning Electrochemical and Fluorescence Microscopy for Detection of Reactive Oxygen Species in Prostate Cancer Cells. *Anal. Chem.* **2013**, *85*, 9417–9421.

(393) Renault, C.; Marchuk, K.; Ahn, H. S.; Titus, E. J.; Kim, J.; Willets, K. A.; Bard, A. J. Observation of Nanometer-Sized Electro-Active Defects in Insulating Layers by Fluorescence Microscopy and Electrochemistry. *Anal. Chem.* **2015**, *87*, 5730–5737.

(394) Salomo, M.; Pust, S. E.; Wittstock, G.; Oesterschulze, E. Integrated Cantilever Probes for SECM/AFM Characterization of Surfaces. *Microelectron. Eng.* **2010**, *87*, 1537–1539.

(395) Wiedemair, J.; Moon, J. S.; Reinauer, F.; Mizaikoff, B.; Kranz, C. Ion Beam Induced Deposition of Platinum Carbon Composite Electrodes for Combined Atomic Force Microscopy-Scanning Electrochemical Microscopy. *Electrochem. Commun.* **2010**, *12*, 989–991.

(396) Avdic, A.; Lugstein, A.; Wu, M.; Gollas, B.; Pobelov, I.; Wandlowski, T.; Leonhardt, K.; Denuault, G.; Bertagnolli, E. Fabrication of Cone-Shaped Boron Doped Diamond and Gold Nanoelectrodes for AFM-SECM. *Nanotechnology* **2011**, *22*, 145306.

(397) Derylo, M. A.; Morton, K. C.; Baker, L. A. Parylene Insulated Probes for Scanning Electrochemical-Atomic Force Microscopy. *Langmuir* **2011**, *27*, 13925–13930.

(398) Wain, A. J.; Cox, D.; Zhou, S.; Turnbull, A. High-Aspect Ratio Needle Probes for Combined Scanning Electrochemical Microscopy - Atomic Force Microscopy. *Electrochem. Commun.* **2011**, *13*, 78–81.

(399) Eifert, A.; Mizaikoff, B.; Kranz, C. Advanced Fabrication Process for Combined Atomic Force-Scanning Electrochemical Microscopy (AFM-SECM) Probes. *Micron* **2015**, *68*, 27–35.

(400) Nault, L.; Taoufenua, C.; Anne, A.; Chovin, A.; Demaille, C.; Besong-Ndika, J.; Cardinale, D.; Carrette, N.; Michon, T.; Walter, J. Electrochemical Atomic Force Microscopy Imaging of Redox-Immunomarked Proteins on Native Potyviruses: From Subparticle to Single-Protein Resolution. *ACS Nano* **2015**, *9*, 4911–4924.

(401) Paulose Nadappuram, B.; McKelvey, K.; Byers, J. C.; Guell, A. G.; Colburn, A. W.; Lazenby, R. A.; Unwin, P. R. Quad-Barrel Multifunctional Electrochemical and Ion Conductance Probe for Voltammetric Analysis and Imaging. *Anal. Chem.* **2015**, *87*, 3566–3573.

(402) Li, L.; Bu, C.; Zhang, Y.; Du, J.; Lu, X.; Liu, X. Composite System Based on Biomolecules-Functionalized Multiwalled Carbon Nanotube and Ionic Liquid: Electrochemistry and Electrocatalysis of Tryptophane. *Electrochim. Acta* **2011**, *58*, 105–111.

(403) Abdelhamid, M. E.; Piantavigna, S.; Bond, A. M.; Graham, B.; Spiccia, L.; Martin, L. L.; O'Mullane, A. P. An SECM Study on the Influence of Cationic, Membrane-Active Peptides on a Gold-Supported Self-Assembled Monolayer. *Electrochem. Commun.* **2015**, *51*, 11–14.

(404) Hamzehloei, A.; Zahra Bathaie, S.; Mousavi, M. F. Probing Redox Reaction of Azurin Protein Immobilized on Hydroxyl-Terminated Self-Assembled Monolayers with Different Lengths. *J. Electroanal. Chem.* **2015**, *755*, 27–38.

(405) She, Z.; Topping, K.; Shamsi, M. H.; Wang, N.; Chan, N. W. C.; Kraatz, H. B. Investigation of the Utility of Complementary Electrochemical Detection Techniques to Examine the In Vitro Affinity of Bacterial Flagellins for a Toll-like Receptor 5 Biosensor. *Anal. Chem.* **2015**, *87*, 4218–4224.

(406) Alizadeh, V.; Mousavi, M. F.; Mehrgardi, M. A.; Kazemi, S. H.; Sharghi, H. Electron Transfer Kinetics of Cytochrome C Immobilized on a Phenolic Terminated Thiol Self Assembled Monolayer Determined by Scanning Electrochemical Microscopy. *Electrochim. Acta* **2011**, *56*, 6224–6229.

(407) Sciutto, G.; Prati, S.; Mazzeo, R.; Zangheri, M.; Roda, A.; Bardini, L.; Valenti, G.; Rapino, S.; Marcaccio, M. Localization of Proteins in Paint Cross-Sections by Scanning Electrochemical Microscopy as an Alternative Immunochemical Detection Technique. *Anal. Chim. Acta* **2014**, *831*, 31–37.

(408) Cortes-Salazar, F.; Trauble, M.; Li, F.; Busnel, J. M.; Gassner, A. L.; Hojeij, M.; Wittstock, G.; Girault, H. H. Soft Stylus Probes for Scanning Electrochemical Microscopy. *Anal. Chem.* **2009**, *81*, 6889–6896.

(409) Qin, G.; Zhang, M.; Zhang, T.; Zhang, Y.; McIntosh, M.; Li, X.; Zhang, X. Label-Free Electrochemical Imaging of Latent Fingerprints on Metal Surfaces. *Electroanalysis* **2012**, *24*, 1027–1032.

(410) Lin, T. E.; Cortes-Salazar, F.; Lesch, A.; Qiao, L.; Bondarenko, A.; Girault, H. H. Multiple Scanning Electrochemical Microscopy Mapping of Tyrosinase in Micro-Contact Printed Fruit Samples on Polyvinylidene Fluoride Membrane. *Electrochim. Acta* **2015**, *179*, 57–64.

(411) Zhang, M.; Qin, G.; Zuo, Y.; Zhang, T.; Zhang, Y.; Su, L.; Qiu, H.; Zhang, X. SECM Imaging of Latent Fingerprints Developed by Deposition of Al-doped ZnO Thin Film. *Electrochim. Acta* **2012**, *78*, 412–416.

(412) Turcu, F.; Schulte, A.; Hartwich, G.; Schuhmann, W. Label-Free Electrochemical Recognition of DNA Hybridization by Means of Modulation of the Feedback Current in SECM. *Angew. Chem., Int. Ed.* **2004**, *43*, 3482–3485.

(413) Nakano, K.; Nakamura, K.; Iwamoto, K.; Soh, N.; Imato, T. Positive-Feedback-Mode Scanning Electrochemical Microscopy Imaging of Redox-Active DNA-Poly(1,4-benzoquinone) Conjugate Film Deposited on Carbon Fiber Electrode for Micrometer-Sized Hybridization Biosensor Applications. *J. Electroanal. Chem.* **2009**, *628*, 113–118.

(414) Roberts, W. S.; Davis, F.; Higson, S. P. J. Scanning Electrochemical Microscopy of Genomic DNA Microarrays - Study of Adsorption and Subsequent Interactions. *Analyst* **2009**, *134*, 1302–1308.

(415) Shamsi, M. H.; Kraatz, H. B. Probing Nucleobase Mismatch Variations by Electrochemical Techniques: Exploring the Effects of Position and Nature of the Single-nucleotide Mismatch. *Analyst* **2010**, *135*, 2280–2285.

(416) Zhang, Z.; Zhou, J.; Tang, A.; Wu, Z.; Shen, G.; Yu, R. Scanning Electrochemical Microscopy Assay of DNA Based on Hairpin Probe and Enzymatic Amplification Biosensor. *Biosens. Bioelectron.* **2010**, *25*, 1953–1957.

(417) Luque, G. L.; Ferreyra, N. F.; Granero, A.; Bollo, S.; Rivas, G. A. Electrooxidation of DNA at Glassy Carbon Electrodes Modified with Multiwall Carbon Nanotubes Dispersed in Polyethylenimine. *Electrochim. Acta* **2011**, *56*, 9121–9126.

(418) Shamsi, M. H.; Kraatz, H. B. Electrochemical Identification of Artificial Oligonucleotides Related to Bovine Species. Potential for Identification of Species Based on Mismatches in the Mitochondrial Cytochrome C<sub>1</sub> Oxidase Gene. *Analyst* **2011**, *136*, 4724–4731.



- (419) Diakowski, P. M.; Kraatz, H. B. Detection of Single-Nucleotide Mismatches Using Scanning Electrochemical Microscopy. *Chem. Commun.* **2009**, 1189–1191.
- (420) Souto, D. E. P.; Silva, J. V.; Martins, H. R.; Reis, A. B.; Luz, R. C. S.; Kubota, L. T.; Damos, F. S. Development of a Label-Free Immunosensor Based on Surface Plasmon Resonance Technique for the Detection of Anti-Leishmania Infantum Antibodies in Canine Serum. *Biosens. Bioelectron.* **2013**, *46*, 22–29.
- (421) Song, W.; Yan, Z.; Hu, K. Electrochemical Immunoassay for CD10 Antigen Using Scanning Electrochemical Microscopy. *Biosens. Bioelectron.* **2012**, *38*, 425–429.
- (422) Wittstock, G. Modification and Characterization of Artificially Patterned Enzymatically Active Surfaces by Scanning Electrochemical Microscopy. *Fresenius' J. Anal. Chem.* **2001**, *370*, 303–315.
- (423) Zigah, D.; Pellissier, M.; Fabre, B.; Barriere, F.; Hapiot, P. Covalent Immobilization and SECM Analysis in Feedback Mode of Glucose Oxidase on a Modified Oxidized Silicon Surface. *J. Electroanal. Chem.* **2009**, *628*, 144–147.
- (424) Matysiak, E.; Botz, A. J. R.; Clausmeyer, J.; Wagner, B.; Schuhmann, W.; Stojek, Z.; Nowicka, A. M. Assembling Paramagnetic Ceruloplasmin at Electrode Surfaces Covered with Ferromagnetic Nanoparticles. Scanning Electrochemical Microscopy in the Presence of a Magnetic Field. *Langmuir* **2015**, *31*, 8176–8183.
- (425) Yang, S.; Jia, W. Z.; Qian, Q. Y.; Zhou, Y. G.; Xia, X. H. Simple Approach for Efficient Encapsulation of Enzyme in Silica Matrix with Retained Bioactivity. *Anal. Chem.* **2009**, *81*, 3478–3484.
- (426) Muresan, L.; Nistor, M.; Gaspar, S.; Popescu, I. C.; Csoregi, E. Monitoring of Glucose and Glutamate Using Enzyme Microstructures and Scanning Electrochemical Microscopy. *Bioelectrochemistry* **2009**, *76*, 81–86.
- (427) Nunes Kirchner, C.; Träuble, M.; Wittstock, G. Diffusion and Reaction in Microbead Agglomerates. *Anal. Chem.* **2010**, *82*, 2626–2635.
- (428) Pitta Bauermann, L.; Schuhmann, W.; Schulte, A. An Advanced Biological Scanning Electrochemical Microscope (Bio-SECM) for Studying Individual Living Cells. *Phys. Chem. Chem. Phys.* **2004**, *6*, 4003–4008.
- (429) Beaulieu, I.; Kuss, S.; Mauzeroll, J.; Geissler, M. Biological Scanning Electrochemical Microscopy and its Application to Live Cell Studies. *Anal. Chem.* **2011**, *83*, 1485–1492.
- (430) Yasukawa, T.; Kondo, Y.; Uchida, I.; Matsue, T. Imaging of Cellular Activity of Single Cultured Cells by Scanning Electrochemical Microscopy. *Chem. Lett.* **1998**, *27*, 767–768.
- (431) Yasukawa, T.; Kaya, T.; Matsue, T. Characterization and Imaging of Single Cells with Scanning Electrochemical Microscopy. *Electroanalysis* **2000**, *12*, 653–659.
- (432) Bard, A. J.; Li, X.; Zhan, W. Chemically Imaging Living Cells by Scanning Electrochemical Microscopy. *Biosens. Bioelectron.* **2006**, *22*, 461–472.
- (433) Navratil, M.; Mabbott, G. A.; Arriaga, E. A. Chemical Microscopy Applied to Biological Systems. *Anal. Chem.* **2006**, *78*, 4005–4019.
- (434) Roberts, W. S.; Lonsdale, D. J.; Griffiths, J.; Higson, S. P. J. Advances in the Application of Scanning Electrochemical Microscopy to Bioanalytical Systems. *Biosens. Bioelectron.* **2007**, *23*, 301–318.
- (435) Mauzeroll, J.; Schougaard, S. B. *Scanning Electrochemical Microscopy*, 2nd ed.; CRC Press: New York, 2012; pp 379–416.
- (436) Bergner, S.; Vatsyayan, P.; Matysik, F. M. Recent Advances in High Resolution Scanning Electrochemical Microscopy of Living Cells - A Review. *Anal. Chim. Acta* **2013**, *775*, 1–13.
- (437) Li, X.; Bard, A. J. Scanning Electrochemical Microscopy of HeLa Cells - Effects of Ferrocene Methanol and Silver Ion. *J. Electroanal. Chem.* **2009**, *628*, 35–42.
- (438) Bergner, S.; Wegener, J.; Matysik, F. M. Monitoring Passive Transport of Redox Mediators Across a Confluent Cell Monolayer with Single-Cell Resolution by Means of Scanning Electrochemical Microscopy. *Anal. Methods* **2012**, *4*, 623–629.
- (439) Connell, J. L.; Kim, J.; Shear, J. B.; Bard, A. J.; Whiteley, M. Real-Time Monitoring of Quorum Sensing in 3D-Printed Bacterial Aggregates Using Scanning Electrochemical Microscopy. *Proc. Natl. Acad. Sci. U. S. A.* **2014**, *111*, 18255–18260.
- (440) Takahashi, Y.; Shevchuk, A. I.; Novak, P.; Babakinejad, B.; Macpherson, J.; Unwin, P. R.; Shiku, H.; Gorelik, J.; Klennerman, D.; Korchev, Y. E.; et al. Topographical and Electrochemical Nanoscale Imaging of Living Cells Using Voltage-Switching Mode Scanning Electrochemical Microscopy. *Proc. Natl. Acad. Sci. U. S. A.* **2012**, *109*, 11540–11545.
- (441) Bergner, S.; Palatzky, P.; Wegener, J.; Matysik, F. M. High-Resolution Imaging of Nanostructured Si/SiO<sub>2</sub> Substrates and Cell Monolayers Using Scanning Electrochemical Microscopy. *Electroanalysis* **2011**, *23*, 196–200.
- (442) Obregon, R.; Horiguchi, Y.; Arai, T.; Abe, S.; Zhou, Y.; Takahashi, R.; Hisada, A.; Ino, K.; Shiku, H.; Matsue, T. A Pt Layer/Pt Disk Electrode Configuration to Evaluate Respiration and Alkaline Phosphatase Activities of Mouse Embryoid Bodies. *Talanta* **2012**, *94*, 30–35.
- (443) McKelvey, K.; Martin, S.; Robinson, C.; Unwin, P. R. Quantitative Local Photosynthetic Flux Measurements at Isolated Chloroplasts and Thylakoid Membranes Using Scanning Electrochemical Microscopy (SECM). *J. Phys. Chem. B* **2013**, *117*, 7878–7888.
- (444) Hirano, Y.; Kodama, M.; Shibuya, M.; Maki, Y.; Komatsu, Y. Analysis of Beat Fluctuations and Oxygen Consumption in Cardiomyocytes by Scanning Electrochemical Microscopy. *Anal. Biochem.* **2014**, *447*, 39–42.
- (445) Shiku, H.; Takeda, M.; Murata, T.; Akiba, U.; Hamada, F.; Matsue, T. Development of Electrochemical Reporter Assay Using HeLa Cells Transfected with Vector Plasmids Encoding Various Responsive Elements. *Anal. Chim. Acta* **2009**, *640*, 87–92.
- (446) Arai, T.; Nishijo, T.; Matsumae, Y.; Zhou, Y.; Ino, K.; Shiku, H.; Matsue, T. Noninvasive Measurement of Alkaline Phosphatase Activity in Embryoid Bodies and Coculture Spheroids with Scanning Electrochemical Microscopy. *Anal. Chem.* **2013**, *85*, 9647–9654.
- (447) Roberts, W. S.; Davis, F.; Holmes, J. L.; Collyer, S. D.; Larcombe, L. D.; Morgan, S. L.; Higson, S. P. J. Detection and Imaging the Expression of the Trans-Membrane Protein CD44 in RT112 Cells by Use of Enzyme-Labeled Antibodies and SECM. *Biosens. Bioelectron.* **2013**, *41*, 282–288.
- (448) Takahashi, Y.; Shiku, H.; Murata, T.; Yasukawa, T.; Matsue, T. Transfected Single-Cell Imaging by Scanning Electrochemical Optical Microscopy with Shear Force Feedback Regulation. *Anal. Chem.* **2009**, *81*, 9674–9681.
- (449) Zhan, D.; Li, X.; Nepomnyashchii, A. B.; Alpuche-Aviles, M. A.; Fan, F. R. F.; Bard, A. J. Characterization of Ag<sup>+</sup> Toxicity on Living Fibroblast Cells by the Ferrocenemethanol and Oxygen Response with the Scanning Electrochemical Microscope. *J. Electroanal. Chem.* **2013**, *688*, 61–68.
- (450) Li, M. S. M.; Filice, F. P.; Ding, Z. A Time Course Study of Cadmium Effect on Membrane Permeability of Single Human Bladder Cancer Cells Using Scanning Electrochemical Microscopy. *J. Inorg. Biochem.* **2014**, *136*, 177–183.
- (451) Zhang, M. M. N.; Long, Y. T.; Ding, Z. Cisplatin Effects on Evolution of Reactive Oxygen Species from Single Human Bladder Cancer Cells Investigated by Scanning Electrochemical Microscopy. *J. Inorg. Biochem.* **2012**, *108*, 115–122.
- (452) Bergner, S.; Wegener, J.; Matysik, F. M. Simultaneous Imaging and Chemical Attack of a Single Living Cell Within a Confluent Cell Monolayer by Means of Scanning Electrochemical Microscopy. *Anal. Chem.* **2011**, *83*, 169–174.
- (453) Prasanth, R.; Gopinath, D. Effect of ZnO Nanoparticles on Nasopharyngeal Cancer Cells Viability and Respiration. *Appl. Phys. Lett.* **2013**, *102*, 113702.
- (454) Zhao, X.; Lam, S.; Jass, J.; Ding, Z. Scanning Electrochemical Microscopy of Single Human Urinary Bladder Cells Using Reactive Oxygen Species as Probe of Inflammatory Response. *Electrochem. Commun.* **2010**, *12*, 773–776.
- (455) Kuss, S.; Polcari, D.; Geissler, M.; Brassard, D.; Mauzeroll, J. Assessment of Multidrug Resistance on Cell Coculture Patterns Using

Scanning Electrochemical Microscopy. *Proc. Natl. Acad. Sci. U. S. A.* **2013**, *110*, 9249–9254.

(456) Wipf, D. Initiation and Study of Localized Corrosion by Scanning Electrochemical Microscopy. *Colloids Surf., A* **1994**, *93*, 251–261.

(457) Eckhard, K.; Etienne, M.; Schulte, A.; Schuhmann, W. Constant-Distance Mode ACSECM for the Visualisation of Corrosion Pits. *Electrochem. Commun.* **2007**, *9*, 1793–1797.

(458) Niu, L.; Yin, Y.; Guo, W.; Lu, M.; Qin, R.; Chen, S. Application of Scanning Electrochemical Microscope in the Study of Corrosion of Metals. *J. Mater. Sci.* **2009**, *44*, 4511–4521.

(459) Dennis, E. T.; Mark, B. J. *Scanning Electrochemical Microscopy*, 2nd ed.; CRC Press: New York, 2012; pp 51–488.

(460) Dauphin-Ducharme, P.; Mauzeroll, J. Surface Analytical Methods Applied to Magnesium Corrosion. *Anal. Chem.* **2015**, *87*, 7499–7509.

(461) Nowierski, C.; Noel, J. J.; Shoesmith, D. W.; Ding, Z. Correlating Surface Microstructures with Reactivity on Commercially Pure Zirconium Using Scanning Electrochemical Microscopy and Scanning Electrochemical Microscopy. *Electrochem. Commun.* **2009**, *11*, 1234–1236.

(462) Gonzalez-Garcia, Y.; Santana, J. J.; Gonzalez-Guzman, J.; Izquierdo, J.; Gonzalez, S.; Souto, R. M. Scanning Electrochemical Microscopy for the Investigation of Localized Degradation Processes in Coated Metals. *Prog. Org. Coat.* **2010**, *69*, 110–117.

(463) Souto, R. M.; Gonzalez-Garcia, Y.; Battistel, D.; Daniele, S. In Situ Scanning Electrochemical Microscopy (SECM) Detection of Metal Dissolution During Zinc Corrosion by Means of Mercury Sphere-Cap Microelectrode Tips. *Chem. - Eur. J.* **2012**, *18*, 230–236.

(464) Sorriano, C.; Oltra, R.; Zimmer, A.; Vuillemin, B.; Borkowski, C. Microstructural Corrosion of Aluminium Alloys: A Predictive Finite Element Model Based on Corrosion-Mimicking Experiments. *Surf. Interface Anal.* **2013**, *45*, 1649–1653.

(465) Xia, D. H.; Zhu, R. K.; Behnamian, Y.; Luo, J. L.; Lin, C. J.; Klimas, S. Understanding the Interaction of Thiosulfate with Alloy 800 in Aqueous Chloride Solutions Using SECM. *J. Electroanal. Chem.* **2015**, *744*, 77–84.

(466) Sidane, D.; Devos, O.; Puiggali, M.; Touzet, M.; Tribollet, B.; Vivier, V. Electrochemical Characterization of a Mechanically Stressed Passive Layer. *Electrochem. Commun.* **2011**, *13*, 1361–1364.

(467) Tefashe, U. M.; Dauphin-Ducharme, P.; Danaie, M.; Cano, Z. P.; Kish, J. R.; Botton, G. A.; Mauzeroll, J. Localized Corrosion Behavior of AZ31B Magnesium Alloy with an Electrodeposited Poly(3,4-Ethylene-dioxythiophene) Coating. *J. Electrochem. Soc.* **2015**, *162*, C536–C544.

(468) Moreira, R.; Schutz, M. K.; Libert, M.; Tribollet, B.; Vivier, V. Influence of Hydrogen-Oxidizing Bacteria on the Corrosion of Low Carbon Steel: Local Electrochemical Investigations. *Bioelectrochemistry* **2014**, *97*, 69–75.

(469) Bertoncello, P. Advances on Scanning Electrochemical Microscopy (SECM) for Energy. *Energy Environ. Sci.* **2010**, *3*, 1620–1633.

(470) Li, H.; Liu, R.; Kong, W.; Liu, J.; Liu, Y.; Zhou, L.; Zhang, X.; Lee, S. T.; Kang, Z. Carbon Quantum Dots with Photo-Generated Proton Property as Efficient Visible Light Controlled Acid Catalyst. *Nanoscale* **2014**, *6*, 867–873.

(471) Huang, K. C.; Huang, J. H.; Wu, C. H.; Liu, C. Y.; Chen, H. W.; Chu, C. W.; Lin, J. T.; Lin, C. L.; Ho, K. C. Nanographite/Polyaniline Composite Films as the Counter Electrodes for Dye-Sensitized Solar Cells. *J. Mater. Chem.* **2011**, *21*, 10384–10389.

(472) Sumboja, A.; Tefashe, U. M.; Wittstock, G.; Lee, P. S. Monitoring Electroactive Ions at Manganese Dioxide Pseudocapacitive Electrodes with Scanning Electrochemical Microscope for Supercapacitor Electrodes. *J. Power Sources* **2012**, *207*, 205–211.

(473) Scodeller, P.; Carballo, R.; Szamocki, R.; Levin, L.; Forchiasin, F.; Calvo, E. J. Layer-by-Layer Self-Assembled Osmium Polymer-Mediated Laccase Oxygen Cathodes for Biofuel Cells: The Role of Hydrogen Peroxide. *J. Am. Chem. Soc.* **2010**, *132*, 11132–11140.

(474) Sanchez-Sanchez, C. M.; Bard, A. J. Hydrogen Peroxide Production in the Oxygen Reduction Reaction at Different Electro-

catalysts as Quantified by Scanning Electrochemical Microscopy. *Anal. Chem.* **2009**, *81*, 8094–8100.

(475) Umeda, M.; Shironita, S.; Sakai, T.; Ide, M.; Ikeda, H. Ex Situ Microelectrode Study of Cathode Catalyst Degraded by Long-Term Endurance Test in Polymer Electrolyte Fuel Cell. *Electrochim. Acta* **2014**, *128*, 259–264.

(476) Li, W.; Fan, F. R. F.; Bard, A. J. The Application of Scanning Electrochemical Microscopy to the Discovery of Pd-W electrocatalysts for the Oxygen Reduction Reaction that Demonstrate High Activity, Stability, and Methanol Tolerance. *J. Solid State Electrochem.* **2012**, *16*, 2563–2568.

(477) Kylberg, W.; Wain, A. J.; Castro, F. A. Screening of Photoactive Dyes on TiO<sub>2</sub> Surfaces Using Scanning Electrochemical Microscopy. *J. Phys. Chem. C* **2012**, *116*, 17384–17392.

(478) Alemu, G.; Zhang, B.; Li, J.; Xu, X.; Cui, J.; Shen, Y.; Wang, M. Investigation of Dye-Regeneration Kinetics at Dye-Sensitized p-type CuCrO<sub>2</sub> Film/Electrolytes Interface with Scanning Electrochemical Microscopy. *Nano* **2014**, *09*, 1440008.

(479) Martin, C. J.; Bozic-Weber, B.; Constable, E. C.; Glatzel, T.; Housecroft, C. E.; Wright, I. A. Development of Scanning Electrochemical Microscopy (SECM) Techniques for the Optimization of Dye Sensitized Solar Cells. *Electrochim. Acta* **2014**, *119*, 86–91.

(480) Tefashe, U. M.; Loewenstein, T.; Miura, H.; Schlettwein, D.; Wittstock, G. Scanning Electrochemical Microscope Studies of Dye Regeneration in Indoline (D149)-sensitized ZnO Photoelectrochemical Cells. *J. Electroanal. Chem.* **2010**, *650*, 24–30.

(481) Snook, G. A.; Huynh, T. D.; Hollenkamp, A. F.; Best, A. S. Rapid SECM Probing of Dissolution of LiCoO<sub>2</sub> Battery Materials in an Ionic Liquid. *J. Electroanal. Chem.* **2012**, *687*, 30–34.

(482) Rodriguez-Lopez, J.; Alpuche-Aviles, M. A.; Bard, A. J. Selective Insulation with Poly(tetrafluoroethylene) of Substrate Electrodes for Electrochemical Background Reduction in Scanning Electrochemical Microscopy. *Anal. Chem.* **2008**, *80*, 1813–1818.

(483) Ktari, N.; Combellas, C.; Kanoufi, F. Local Oxidation of Polystyrene by Scanning Electrochemical Microscopy. *J. Phys. Chem. C* **2011**, *115*, 17891–17897.

(484) Tang, J.; Zheng, J. J.; Yu, Y. T.; Chen, L.; Zhang, N.; Tian, Z. Selective Etching of ZnO Films on an ITO Substrate Using a Scanning Electrochemical Microscope. *Electrochim. Acta* **2012**, *83*, 247–252.

(485) Battistel, D.; Daniele, S.; Fratter, D. A Scanning Electrochemical Microscopy Procedure for Micropatterning Al<sub>2</sub>O<sub>3</sub>-Thin Films Deposited on a Platinum Substrate. *Electrochim. Acta* **2012**, *78*, 557–562.

(486) Chen, P. C.; Chen, R. L. C.; Cheng, T. J.; Wittstock, G. Localized Deposition of Chitosan as Matrix for Enzyme Immobilization. *Electroanalysis* **2009**, *21*, 804–810.

(487) Malel, E.; Ludwig, R.; Gorton, L.; Mandler, D. Localized Deposition of Au Nanoparticles by Direct Electron Transfer Through Cellobiose dehydrogenase. *Chem. - Eur. J.* **2010**, *16*, 11697–11706.

(488) Danieli, T.; Colleran, J.; Mandler, D. Deposition of Au and Ag Nanoparticles on PEDOT. *Phys. Chem. Chem. Phys.* **2011**, *13*, 20345–20353.

(489) Fedorov, R. G.; Mandler, D. Local Deposition of Anisotropic Nanoparticles Using Scanning Electrochemical Microscopy (SECM). *Phys. Chem. Chem. Phys.* **2013**, *15*, 2725–2732.

(490) Malel, E.; Colleran, J.; Mandler, D. Studying the Localized Deposition of Ag Nanoparticles on Self-Assembled Monolayers by Scanning Electrochemical Microscopy (SECM). *Electrochim. Acta* **2011**, *56*, 6954–6961.

(491) Grisotto, F.; Ghorbal, A.; Goyer, C.; Charlier, J.; Palacin, S. Direct SECM Localized Electrografting of Vinylic Monomers on a Conducting Substrate. *Chem. Mater.* **2011**, *23*, 1396–1405.

(492) Cougnon, C.; Gohier, F.; Belanger, D.; Mauzeroll, J. In Situ Formation of Diazonium Salts from Nitro Precursors for Scanning Electrochemical Microscopy Patterning of Surfaces. *Angew. Chem., Int. Ed.* **2009**, *48*, 4006–4008.

(493) Ghorbal, A.; Grisotto, F.; Charlier, J.; Palacin, S.; Goyer, C.; Demaille, C. Localized Electrografting of Vinylic Monomers on a Conducting Substrate by Means of an Integrated Electrochemical AFM Probe. *ChemPhysChem* **2009**, *10*, 1053–1057.



- (494) Cougnon, C.; Mauzeroll, J.; Belanger, D. Patterning of Surfaces by Oxidation of Amine-Containing Compounds Using Scanning Electrochemical Microscopy. *Angew. Chem., Int. Ed.* **2009**, *48*, 7395–7397.
- (495) Radtke, V.; Heß, C.; Heinze, J. Generation of Platinum Microstructures on Non-Conducting Surfaces by Means of the Scanning Electrochemical Microscope (SECM). *Electrochim. Acta* **2009**, *55*, 416–422.
- (496) Guo, S. X.; Unwin, P. R.; Whitworth, A. L.; Zhang, T. Microelectrochemical Techniques for Probing Kinetics at Liquid/Liquid Interfaces. *Prog. React. Kinet. Mech.* **2004**, *29*, 43–166.
- (497) Zigah, D.; Wang, A.; Lagrost, C.; Hapiot, P. Diffusion of Molecules in Ionic Liquids/Organic Solvent Mixtures. Example of the Reversible Reduction of O<sub>2</sub> to Superoxide. *J. Phys. Chem. B* **2009**, *113*, 2019–2023.
- (498) Jedraszko, J.; Nogala, W.; Adamiak, W.; Rozniecka, E.; Lubarska-Radziejewska, I.; Girault, H. H.; Opallo, M. Hydrogen Peroxide Generation at Liquid Liquid Interface under Conditions Unfavorable for Proton Transfer from Aqueous to Organic Phase. *J. Phys. Chem. C* **2013**, *117*, 20681–20688.
- (499) Deng, H.; Peljo, P.; Momotenko, D.; Cortes-Salazar, F.; Jane Stockmann, T.; Kontturi, K.; Opallo, M.; Girault, H. H. Kinetic Differentiation of Bulk/Interfacial Oxygen Reduction Mechanisms at/near Liquid/Liquid Interfaces Using Scanning Electrochemical Microscopy. *J. Electroanal. Chem.* **2014**, *732*, 101–109.
- (500) Zhou, M.; Yu, Y.; Hu, K.; Mirkin, M. V. Nanoelectrochemical Approach To Detecting Short-Lived Intermediates of Electrocatalytic Oxygen Reduction. *J. Am. Chem. Soc.* **2015**, *137*, 6517–6523.
- (501) Wain, A. J. Imaging Size Effects on the Electrocatalytic Activity of Gold Nanoparticles Using Scanning Electrochemical Microscopy. *Electrochim. Acta* **2013**, *92*, 383–391.
- (502) Fernandez, J. L.; Imaduwa, K. P.; Zoski, C. G. Carbon Supported Noble Metal (Pd and Au) Catalysts Synthesized by an Oxide Route with High Performance for Oxygen Reduction in Acidic Media. *Electrochim. Acta* **2015**, *180*, 460–470.
- (503) Ma, L.; Zhou, H.; Xin, S.; Xiao, C.; Li, F.; Ding, S. Characterization of Local Electrocatalytic Activity of Nanosheet-Structured ZnCo<sub>2</sub>O<sub>4</sub>/Carbon Nanotubes Composite for Oxygen Reduction Reaction with Scanning Electrochemical Microscopy. *Electrochim. Acta* **2015**, *178*, 767–777.
- (504) Maljusch, A.; Ventosa, E.; Rincon, R. A.; Bandarenka, A. S.; Schuhmann, W. Revealing Onset Potentials Using Electrochemical Microscopy to Assess the Catalytic Activity of Gas-Evolving Electrodes. *Electrochem. Commun.* **2014**, *38*, 142–145.
- (505) Sanchez-Sanchez, C. M.; Solla-Gullon, J.; Vidal-Iglesias, F. J.; Aldaz, A.; Montiel, V.; Herrero, E. Imaging Structure Sensitive Catalysis on Different Shape-Controlled Platinum Nanoparticles. *J. Am. Chem. Soc.* **2010**, *132*, 5622–5624.
- (506) Zhong, J. H.; Zhang, J.; Jin, X.; Liu, J. Y.; Li, Q.; Li, M. H.; Cai, W.; Wu, D. Y.; Zhan, D.; Ren, B. Quantitative Correlation Between Defect Density and Heterogeneous Electron Transfer Rate of Single Layer Graphene. *J. Am. Chem. Soc.* **2014**, *136*, 16609–16617.
- (507) Patten, H. V.; Meadows, K. E.; Hutton, L. A.; Iacobini, J. G.; Battistel, D.; McKelvey, K.; Colburn, A. W.; Newton, M. E.; MacPherson, J. V.; Unwin, P. R. Electrochemical Mapping Reveals Direct Correlation Between Heterogeneous Electron-Transfer Kinetics and Local Density of States in Diamond Electrodes. *Angew. Chem., Int. Ed.* **2012**, *51*, 7002–7006.
- (508) Spaine, T. W.; Baur, J. E. A Positionable Microcell for Electrochemistry and Scanning Electrochemical Microscopy in Subnanoliter Volumes. *Anal. Chem.* **2001**, *73*, 930–938.
- (509) Sun, P.; Mirkin, M. V. Electrochemistry of Individual Molecules in Zeptoliter Volumes. *J. Am. Chem. Soc.* **2008**, *130*, 8241–8250.
- (510) Hengstenberg, A.; Blochl, A.; Dietzel, I. D.; Schuhmann, W. Spatially Resolved Detection of Neurotransmitter Secretion from Individual Cells by Means of Scanning Electrochemical Microscopy. *Angew. Chem., Int. Ed.* **2001**, *40*, 905–908.
- (511) Kim, J.; Shen, M.; Nioradze, N.; Amemiya, S. Stabilizing Nanometer Scale Tip-to-Substrate Gaps in Scanning Electrochemical Microscopy Using an Isothermal Chamber for Thermal Drift Suppression. *Anal. Chem.* **2012**, *84*, 3489–3492.
- (512) Amatore, C.; Deakin, M.; Wightman, R. Electrochemical Kinetics at Microelectrodes. Part IV. Electrochemistry in Media of Low Ionic Strength. *J. Electroanal. Chem. Interfacial Electrochem.* **1987**, *225*, 49–63.
- (513) Amatore, C.; Fosset, B.; Bartelt, J.; Deakin, M.; Wightman, R. Electrochemical Kinetics at Microelectrodes. Part V. Migrational Effects on Steady or Quasi-Steady-State Voltammograms. *J. Electroanal. Chem. Interfacial Electrochem.* **1988**, *256*, 255–268.
- (514) Oja, S.; Wood, M.; Zhang, B. Nanoscale Electrochemistry. *Anal. Chem.* **2013**, *85*, 473–486.
- (515) Adam, C.; Kanoufi, F.; Sojic, N.; Etienne, M. Shearforce Positioning of Nanoprobe Electrode Arrays for Scanning Electrochemical Microscopy Experiments. *Electrochim. Acta* **2015**, *179*, 45–56.
- (516) Filice, F. P.; Li, M. S. M.; Henderson, J. D.; Ding, Z. Three-Dimensional Electrochemical Functionality of an Interdigitated Array Electrode by Scanning Electrochemical Microscopy. *J. Phys. Chem. C* **2015**, *119*, 21473–21482.
- (517) Kanno, Y.; Ino, K.; Inoue, K. Y.; Sen, M.; Suda, A.; Kunikata, R.; Matsudaira, M.; Abe, H.; Li, C.-Z.; Shiku, H.; et al. Feedback Mode-Based Electrochemical Imaging of Conductivity and Topography for Large Substrate Surfaces Using an LSI-Based Amperometric Chip Device with 400 Sensors. *J. Electroanal. Chem.* **2015**, *741*, 109–113.
- (518) Meyer, H.; Drewer, H.; Grundig, B.; Cammann, K.; Kakerow, R.; Manoli, Y.; Mokwa, W.; Rospert, M. Two-Dimensional Imaging of O<sub>2</sub>, H<sub>2</sub>O<sub>2</sub>, and Glucose Distributions by an Array of 400 Individually Addressable Microelectrodes. *Anal. Chem.* **1995**, *67*, 1164–1170.
- (519) Lister, T. E.; Pinhero, P. J. Microelectrode Array Microscopy: Investigation of Dynamic Behavior of Localized Corrosion at Type 304 Stainless Steel Surfaces. *Anal. Chem.* **2005**, *77*, 2601–2607.
- (520) Barker, A. L.; Unwin, P. R.; Gardner, J. W.; Rieley, H. A Multi-Electrode Probe for Parallel Imaging in Scanning Electrochemical Microscopy. *Electrochem. Commun.* **2004**, *6*, 91–97.
- (521) Momotenko, D.; Byers, J. C.; McKelvey, K.; Kang, M.; Unwin, P. R. High-Speed Electrochemical Imaging. *ACS Nano* **2015**, *9*, 8942–8952.
- (522) Kuss, S.; Trinh, D.; Danis, L.; Mauzeroll, J. High-Speed Scanning Electrochemical Microscopy Method for Substrate Kinetic Determination: Method and Theory. *Anal. Chem.* **2015**, *87*, 8096–8101.
- (523) Kuss, S.; Trinh, D.; Mauzeroll, J. High-Speed Scanning Electrochemical Microscopy Method for Substrate Kinetic Determination: Application to Live Cell Imaging in Human Cancer. *Anal. Chem.* **2015**, *87*, 8102–8106.
- (524) He, H.; Ding, Z.; Shoesmith, D. W. The Determination of Electrochemical Reactivity and Sustainability on Individual Hyper-Stoichiometric UO<sub>2+x</sub> Grains by Raman Microspectroscopy and Scanning Electrochemical Microscopy. *Electrochem. Commun.* **2009**, *11*, 1724–1727.
- (525) Macpherson, J. V.; Unwin, P. R. Combined Scanning Electrochemical-Atomic Force Microscopy. *Anal. Chem.* **2000**, *72*, 276–285.
- (526) Szunerits, S.; Knorr, N.; Calemczuk, R.; Livache, T. New Approach to Writing and Simultaneous Reading of Micropatterns: Combining Surface Plasmon Resonance Imaging with Scanning Electrochemical Microscopy (SECM). *Langmuir* **2004**, *20*, 9236–9241.
- (527) Li, F.; Unwin, P. Scanning Electrochemical Microscopy (SECM) of Photoinduced Electron Transfer Kinetics at Liquid/Liquid Interfaces. *J. Phys. Chem. C* **2015**, *119*, 4031–4043.